Investigating the *Predictive Code* of Predictive Coding Theory via Face Identity Expectation in a Learning Task

Dem Fachbereich Biologie der Technischen Universität Darmstadt
zur Erlangung des akademischen Grades *Doctor rerum naturalium (Dr. rer. nat.)*
Dissertation von Dipl. Biol. Georg-Friedrich Paasch aus Schwerin

Erstgutachter: Prof. Dr. Ralf Galuske, Technische Universität Darmstadt
Zweitgutachter: Prof. Dr. Bodo Laube, Technische Universität Darmstadt
Externer Gutachter: Prof. Dr. Michael Wibral, Goethe-Universität, Frankfurt am Main

Darmstadt 2018

Paasch, Georg-Friedrich: Investigating the Predictive Code of Predictive Coding Theory via Face Identity Expectation in a and Learning Task
Darmstadt, Technischen Universität Darmstadt,
Jahr der Veröffentlichung der Dissertation auf TUprints: 2018
URN: urn:nbn:de:tuda-tuprints-78208
Tag der mündlichen Prüfung: 31.08.2018

Abstract

Human behaviour is based on a reliable recognition of its environment. The predictive coding theory (PCT) provides an explanation of how recognition becomes reliable by integrating prior experience about the environment. The PCT suggests that the brain provides a prediction based on prior experience which is compared with the sensory information. The sensory information that cannot be explained by the prediction causes the prediction to be updated.

An established view is that the brain is organised in a hierarchical manner and the sensory information is transferred bottom-up the hierarchy. Within the hierarchical organisation, the PCT proposes that the prediction is sent top-down to be compared to the sensory information and that the unexplained information, the prediction error (PE), is sent bottom-up to update the prediction (Friston, 2003, 2005; Rao and Ballard, 1999). Accordingly, the information flow circulates: PEs drives *Prediction* updates, and *Predictions* drive PE minimization.

The predictive coding concept is compelling, but the neurophysiological implementation still remains unknown. However, Bastos and colleagues (Bastos et al., 2012) suggest that high frequency band activity (>30Hz) reflects PEs and low frequency band activity (<30Hz) reflects *Predictions*. This variant of the implementation of the PCT is testable with neurophysiological methods like the magnetoencephalography (MEG).

The present thesis investigated the representation of the Prediction within the framework of the PCT with a new learning paradigm using two-tone stimuli. In this paradigm, the participants expected a target face identity (TFID) at a predefined position in a trial to gain reliable visual information of the TFID. Furthermore, the participants were supposed to test their recognition ability with a test stimulus as well at a predefined position in a trial.

First, our understanding is that to solve this task sensory evidences of the TFID must be integrated into a coherent internal model (IM). Second, according to Bubic (Bubic, 2010), we can assume that the IM should become the predictive information when expecting an upcoming stimulus of the TFID. Third, we suppose that the IM should increase in detail

through learning and accordingly we assume that this refinement of the IM can be associated with the increasing precision of predictions.

Indeed, an increase in the discrimination performance of the TFID with increasing refinement of the IM could be verified when analysing the behaviour of 41 participants. At the neurophysiological level, this was accompanied by an enhancement of the well-known familiarity ERF component M250 (Olivares et al., 2015; Schweinberger and Neumann, 2016).

Recent proposals of the PCT claim a distinction of the low frequency band activity in alpha and beta frequency band activity (ABA, BBA). It is proposed that the ABA signals the precision of predictions and the BBA signals the update of predictions (Sedley et al., 2016). In our MEG data, we observed a change in the ABA in the expectation interval which had a positive relationship to the increasing discriminability of the participants. Three brain sources of major importance were identified for this effect in the expectation interval and in the ABA by a beamformer source localization approach. These were the occipital face area (OFA), the precuneus (PreC) and the lateral occipital cortex (LOC). These brain areas (and two others) were supposed to constitute a face-identity-predictive (FIP) network. Further, we tested for effects of ABA in the post-stimulus interval and found an increase in ABA in primarily early visual areas and the PreC. Thus, we assign the PreC a key role in the representation of the IM of faces.

It stands to reason that the ABA in the expectation interval and the post-stimulus interval are related to the same IM. Thus, we propose the ABA in the expectation interval to reflect an abstract representation and the ABA in the post-stimulus interval to reflect a more detailed internal model representation. This interpretation is in line with a tentatively proposed implementation of the PE minimization by Kwisthout and colleagues (Kwisthout et al., 2017).

Acknowledgement

This research is part of a cooperation between the Faculty of Biology of the Technical University of Darmstadt and the Brain Imaging Center (BIC) of the Goethe University Frankfurt. Prof. R. Galuske from the TU Darmstadt has agreed that this research project can be carried out at the BIC under the supervision of Prof. M. Wibral and he supports the project from the TU Darmstadt.

I am grateful to Prof. M. Wibral for supervising my research project. I thank him for all the important research support and research environment. After all, the project was possible, because he was confident that my approach to investigate the *predictive brain* would work. Equally important, I am grateful to Prof. R. Galuske, who supervised the work from the TU Darmstadt. Equally, I thank Prof. B. Laube that he agreed to the co-supervision from the TU-Darmstadt.

The first years of implementation of the design, data collection and data analysis I spent at the MEG and MRI laboratories of the BIC. I thank Alla Brodski-Guerniero, Susanne Eisenhauer, Patricia Wollstadt, Anja Pflug, Cerisa Stawowski, Michael Schaum and Ivo Peres for all the support regarding the MEG measurements and analyses, but also for the shared coffee and pizza. Further, I want to thank Prof. R. Deichmann and his group from the MRI laboratories for every technical support regarding the MRI.

The last year of the work, I spent at the MPI for empirical aesthetics. Here I finalized the analysis, visualized results and wrote up the thesis. I am grateful to Prof. D. Poeppel for giving me the opportunity to be a part of his group. I thank the whole Neuroscience Department for an enriching scientific and a delightful ambiance. Especially, I like to thank Tina Röske, Johanna Rimmele, Yue Sun, Pauline Larrouy-Maestri, Alessandro Tavano, Ilky Isik, Ed Vessel, Cordulla Ullah for any kind of support and fruitful discussion. Pauline, thanks for letting me play your grand piano after work.

Finally, I would like to mention the Foundation Villigst for the three-year scholarship which supported my independence as well as the Foundation Schoenebeck for financial support for equipment.

Last but not least, my biggest thanks go to my Julia, who had to endure all ups and downs accompanying the project work. Julia said that when I submit the thesis she will be happier than I will be – we will see. I thank my parents for a support only the family can give. Thank you, dad, for all the animal photos in times when PC work became more and more. Thank you, mum, for updates about the home during these times. I also thank my sister and Sebastian for all the distractions associated with the education of a one-year-old boy, which indeed can be as interesting as research. Thank you, Ingrid, for reading my thesis.

Table of Contents

Figures and Tables

Abbreviations

ABA	alpha frequency band activity
A&BBA	alpha- and beta frequency band activity
BBA	beta frequency band activity
BOLD	blood oxygenation level dependent
cITG	caudal inferio-temporal gyrus
CoD	Cohen's D
CSD	spectral density matrix
DICS	dynamic imaging of coherent source algorithm
ERF	event related field(s)
ES	effect size/s
FFA	fusiform face area
GBA	gamma frequency band activity
HR	hit rates
IS	incremental sequence
ITI	inter stimulus interval
JHA	Juelich Histological atlas
LOC	lateral occipital cortex
LOD	level of detail
MEG	magnetoencephalography
MRI	magnet resonance imaging
MTL	medial temporal lobe
OFA	occipital face area
OFG	occipital fusiform gyrus
PC	predictive coding
PCT	predictive coding theory
PE	prediction error
PHC	para-hippocampal cortex
PK	prior knowledge
PreC	precuneus
PM	processing model
RHT	reverse hierarchy theory
RS	randomized sequence
RT	reaction times
RR	response rate
SCA	sequential classification approach
SOA	stimulus onset asynchrony
V1 V2 V3	primary, secondary, tertiary visual cortex
VSTM	visual short-term memory
WM	working memory

1 Introduction

1.1 Foundation and Derivation of Current Predictive Coding Theories

Our external world is full of redundant information in time and space. This redundant information constitutes reliable aspects of our environment like, for example, buildings, trees and other objects or organisms we meet in our daily routines. Our brain extracts and stores the statistical regularities from redundant information to make use of it when sensory information is limited. Regarding these situations, the predictive coding theory (PCT) proposes that our brain uses such probabilistic knowledge to generate predictions to facilitate and enhance recognition. Approximately 150 years ago, Helmholtz already gave a nice example of this: When we act in a familiar environment like our personal room, and it is dawn, so only few light comes through the window, it is still possible to move and act in the room, because the insufficient visual information is interpretable by *prior knowledge* (Von Helmholtz, 1867) (for an illustration of the example, see Figure 1.1). Helmholtz was picturing highly uncertain sensory data about our outer world and points out that past experiences (prior knowledge & statistical regularities) reduce these sensory uncertainties to complete a reliable internal environment that matches the reliable outer environment. These examples illustrate also that the time window is narrow when we receive optimally reliable information (e.g., vision during daylight). These narrow time frames are used to extract the reliable sensory information and its statistical regularities. These regularities are stored in memory as parameters (estimates) and their variances with the result to enable behaviour in a known environment with bad sensory information.

Helmholtz' theory of *perceptual inference* has inspired modern theories of perception claiming that the brain is an *inference machine* (Ballard et al., 1983; Gregory, 1997; Dayan et al., 1995; Friston, 2003). During the last two decades, PCT has become popular (Clark, 2013; Hohwy, 2013; 2011). PCT, in general, claims that the brain predicts its future state, including how this state is changed by the environment, and many psychophysical, neurobiological and computational studies support this perspective (Clark, 2013).

Figure 1-1: *Example of the use of prior knowledge when sensory information is limited.* Only few light is illuminating the living room, but with prior knowledge, it is possible to act. The white lines indicate prior knowledge and complete the sensory percept, e.g., how far the couch reaches into the room and where the door is located when one wants to leave the room.

Seminal work had been done by Rao and Ballard (Rao and Ballard, 1997) who introduced a computational model to explain extracellular recordings from brain areas like V1, V2 and V4 in a monkey, who performed a free viewing experiment. Within their computation model, they introduced the *extended Kalman filter* embedded in a cortical-like architecture. That means they respected the hierarchical organization of modules in the brain that are reciprocally connected (Felleman et al., 1991; Maunsell and Essen, 1983).

The authors said, "The model acknowledges the fact that vision is an active, dynamic process," and the results were impressive. The visual object in an output stimulus, given an input stimulus with an occluded part of the object, is fully completed, that means the occluded part is completed from knowledge about the object (Rao and Ballard, 1997). The authors successfully continued their work on artificial neural networks by explaining the end-stopping effect of receptive field neurons in V1 by *predictive coding* (Rao and Ballard, 1999) and therefore provide for the first time a link between a predictive coding algorithm and neurophysiological evidence.

Since then, PCT proposes how top-down and bottom-up information is integrated (Rao and Ballard, 1999; Friston, 2003, 2005; Spratling, 2008). It is agreed that the prediction (or the brains inference of the world) is sent top-down via feedback connections to meet the sensory signal which is sent bottom-up via feedforward connections within the

cortical hierarchy. But still it is a matter of debate what happens when the prediction meets the sensory input. One interpretation is that the resulting match leads to silencing the predicted and enhancing the unpredicted content of the sensory information (Friston, 2005).

For this interpretation, it is proposed that unpredicted content, which is named the prediction error (PE), is sent further bottom-up the hierarchy to update the prediction. This updated prediction then explains away the unpredicted content. A neurophysiological implementation of this was proposed by Bastos and colleagues (Bastos et al., 2012) by respecting recently described micro-circuitry on the cellular level and layer-resolved electrophysiological evidence. The authors proposed distinct frequency channels for messages passing up and down the cortical hierarchy (Figure 1-2). In short, they point out that the feedforward connections mainly project into the granular (intermediate) layer (layer 4) and originate in superficial layers (layer 2/3). Because these superficial layers mainly produce high gamma rhythms (> 30 Hz), they conclude that high-frequency neuronal activity indicates the bottom-up flow of information, which is the PE. In contrast, the feedback connections that project back into superficial (layer 2/3) and infragranular layers (layer 5/6) originate in deeper (infragranular) layers. The infragranular layer was mainly reported to produce low rhythms (< 30 Hz). Thus, the authors concluded low frequencies indicate the top-down flow of information, which is the prediction. Preceding and similar work of Wang (Wang, 2010) emphasized the importance of laminar anatomy and of laminar electrophysiology for cortico-cortical communication. Accordingly, it has been recently demonstrated that low and high frequencies indicate information transfer in opposite directions across feedback and feedforward connections (Bastos et al., 2015; van Kerkoerle et al., 2014; Michalareas et al., 2016) irrespective of what is transferred.

Again, the crucial aspect of Bastos and colleagues is to link the frequency distinction in top-down and bottom-up messages passing with PCT. At the end, it is this link that makes PCT testable with electrophysiological measures, and since then there is a growing number of evidence in support of this implementation. According to experimental manipulations and applied methods, it was tested separately whether high frequencies

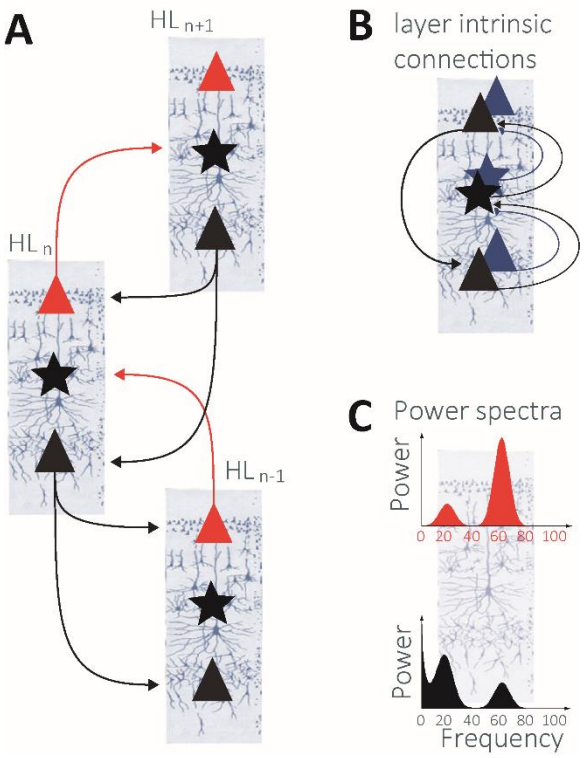

Figure 1-2: *Predictive coding: Its intra and extra-laminar micro-circuitry and its spectral asymmetries*. **A**: Hierarchical message passing in PCT according to Bastos (2012). Ascending and descending fibres are shown for hierarchical level HL_n. Predictions are conveyed via descending feedback connections originating in deep layers (5/6) and projecting into superficial layers (2/3). They are suggested to be mediated by excitatory fibres (black arrow) and transposed via interneurons into inhibitory function (the latter not shown). The predictions are also transmitted directly to the layer 5/6, in that the dendrites of the layer 5/6 protrude into the layer 1. In contrast, prediction errors are conveyed via feedforward connections (red arrows) originating in superficial layers and projecting in intermediate layer 4 (illustrated by a star for stellar cells). **B**: Interlaminar connections illustrate the suggestion of how predictions and PE are conveyed. The schematic representation was slightly adapted from Bastos (2012). **C**: The asymmetric power spectra of superficial and deep layers show a preference for superficial layers to produce high frequency band activity and deep layers to produce low frequency band activity.

signal PE when violating predications (Arnal et al., 2011; Brodski and Paasch et al., 2015; Dürschmid et al., 2016) or whether low frequencies signal predictions when altering the prediction (Brodski-Guerniero et al., 2017; Mayer et al., 2016).

However, when an experimental design intervenes in the prediction updating or the PE minimization process, the signal of the counterpart should be able to be measured as well. Indeed, it had been shown simultaneously that 1) changes in low

frequencies were associated with the prediction, and 2) changes in high frequencies were associated with PE simultaneously (Engel and Fries, 2010; Bauer et al., 2014; Fontolan et

al., 2014; Lewis et al., 2015; van Pelt et al., 2016) (Figure 1-2-C). We here assume that the micro-circuitry theory of Bastos and colleagues is largely correct.

1.2 Distinctions of Low Frequency in Top-Down Predictions

Recent attempts to investigate the top-down predictions have focussed on frequency changes in the pre- and post-stimulus intervals to disentangle the representation of the prediction from the process of PE-minimization in post-stimulus interval. However, it remains open which of the classical low-frequency bands, namely the alpha and beta frequency band activity (A&BBA), refer to the prediction and if there is a distinction between these frequencies in the pre-stimulus interval. Brodski and colleagues (Brodski-Guerniero et al., 2017) provide evidence that both ABA and BBA are equally associated with predictions in the pre-stimulus interval in a *house versus face* detection task in which they elicited expectation of either category. Mayer and colleagues (Mayer et al., 2016) provide evidences for changes in the ABA exclusively when manipulating the expectation to see a letter in a stimulus degradation experiment with an ascending and descending signal to noise ratio. Nevertheless, regarding low-frequency activation in the pre-stimulus interval, suggestions for distinct functions of A&BBA exist in the framework of PCT. For instance, Spaak and colleagues (Spaak et al., 2016) proposed that (1) predictions of a target (which is the orientation of a letter) are associated with changes in the BBA and (2) predictions of the target location are associated with changes in the ABA via expectation, which guides attention.

Independently of PCT, low frequency band activity (notably ABA) in the pre-stimulus interval was reported to be tightly linked to excitability changes in neural populations (Jensen and Mazaheri, 2010; Thut et al., 2012; Weisz et al., 2011). Thus, pre-stimulus excitability changes in neural populations presumably accomplishes gain control for the post-stimulus processing. Regarding this, Cao and colleagues (Cao et al., 2017) hypothesized that changes in low frequency band activity in the pre-stimulus interval might correspond to the implementation of the suppression of post-stimulus responses, i.e., sensory attenuation. Further, the authors provide evidence that changes in pre-

stimulus ABA are associated with the representational activity of context-specific predictions (Cao et al., 2017).

In contrast, Sedley and colleagues (Sedley et al., 2016) proposed distinct functions of the low frequencies in the post-stimulus interval. The authors proposed that (1) changes in the BBA are associated with the changes of a prediction and that (2) changes in the ABA are associated with the precision of a prediction. The precision of prediction was defined as the inverse variance of a likelihood function connecting sensory input with parameters of states of the world, and on the biophysical implementation level as being implemented by synaptic gain modulation (post-synaptic responsiveness) of units reporting prediction error (Feldman and Friston, 2010). This is in line with the here previously reported influence of pre-stimulus ABA on post-stimulus processing. Seminal work has been done by Bauer and colleagues (2014) who demonstrated that the strength of pre-stimulus alpha frequency modulations increased with the predictability of the anticipated sensory target, regardless of current afferent drive (Bauer et al., 2014). Even though evidence exists, it is still debated how the precision and the representation of the prediction are associated and how this association is linked when considering pre- and post-stimulus activity. The most promising proposal is that changes in the ABA represent the precision of prediction in the post-stimulus interval (Bauer et al., 2014; Sedley et al., 2016) as introduced above. However, we acknowledge that others have linked ABA to representational content (Cao et al., 2017; Mayer et al., 2016) and target location (Spaak et al., 2016) in the pre-stimulus interval.

Further insights regarding the discussion about the precision of prediction on a theoretical and abstract level are given by the work of Kwisthout and colleagues (Kwisthout and van Rooij, 2015; Kwisthout et al., 2017). The authors propose a mathematical model of how PE minimization is realized under the assumption of a categorical probability distribution. This assumption has consequences for formalizing the minimization of the PE. The authors introduce the concept of *level of detail* (LOD), which captures the state space granularity and can increase or decrease, depending on the LOD. An idea for the implementation level has not been formulated yet. Here, we tentatively propose how the concept of increasing the LOD could be implemented when a more detailed prediction is formulated.

1.3 Aim of the Study and Study Design

According to the recent literature, there is a debate about how precision is implemented in PCT. The aim of this study is to investigate changes in the deep frequencies while the brain makes predictions that vary in detail. In particular, we test which of the two frequency bands (A&BBA) are associated with precision in predictive coding. To accomplish that, we introduce a new paradigm that enables us to monitor the brain activity during making predictions. We provide verification of the paradigm by expected response behaviour and recent predicted changes in the event-related field (ERF) of face recognition components.

The experimental design primarily conforms to a face learning paradigm with two-tone stimuli. Participants had to learn previously unknown face identities and to test their recognition ability from the beginning. A trial comprised the presentation of two face stimuli separated by the interval of a blank screen (for a detail display of the paradigm, see Figure 2-1 in Methods). Participants knew that the first (sample) stimulus always presented the target face identity (TFID) and the second (test) stimulus presented a target or a non-target face identity by chance. Importantly, the sample stimulus always revealed some new visual information about the TFID, which was realized by the stimuli of the TFID differing in illumination condition and camera position. Thus, the sample stimulus enabled the participants to learn about a TFID by seeing different stimuli of this TFID. In addition to that, the instruction to the participant always was to expect the TFID in the sample stimulus, which was supported by new stimuli of the target. Consequently, we call the sample pre-stimulus interval the expectation interval, and it is the focus of neurophysiological investigations. In contrast, the test stimulus required a response of the participants and was implemented to measure the discriminability (as proposed by the signal detection theory (SDT) (Green, 1966; Macmillan and Creelman, 2005) of the TFID from other faces from the beginning.

While the participant completed the task, magneto-encephalographic (MEG) responses were collected. The MEG data were analysed by a beamformer source localization of deep frequencies (A&BBA) in the expectation interval. We assumed that the increase of visual knowledge and, thus, of the precision of predictions about the TFID is behaviourally

captured by the discriminability index. Thus, we investigated the precision of the prediction by testing which frequency had a relationship with the discriminability index d-prime. After that, we investigated changes in this frequency in the sample post-stimulus interval.

To validate the position of sources found with the MEG beamformer, we conducted an fMRI study. We assume to gain insights into the precision of prediction by the BOLD responses, in the expectation interval by parametrical modulation, which is motivated by the behavioural discriminability.

1.4 Results and Conclusions

The behavioural response analysis verified that participants learned to discriminate the target face identity by an increase in hit rates and discriminability (d-prime) in both the MEG and the fMRI studies. The source localization of the low frequencies and the relationship with the discriminability revealed ABA to be associated with the prediction. This is in line with the recent predictive coding account according to which low frequencies mediate top-down predictions. However, we further discuss our results in the light of the recent evidence by Bauer and colleagues (Bauer et al., 2014) and the proposal by Sedley and colleagues (Sedley et al., 2016) that ABA is associated with the precision of prediction.

The five functional brain areas identified were summarize in a Face-identity-predictive (FIP) network (Figure 4-2). Three of the five functional brain areas were more or less verified by the BOLD response. Furthermore, the analysis of the BOLD responses additionally revealed activity in early visual areas in the expectation interval. An adjacent test of ABA in post-stimulus interval revealed similar early visual brain areas that are associated with low-level visual function. Also, the BOLD response in the expectation interval revealed increased precuneus (PreC) activity. As PreC activity was observed in all measures and investigated time intervals, thus, we agree with the proposal by Land (Land, 2014) that the PreC plays a key role in the representation of the internal model.

Further, we suggest that ABA measured in the pre- and post-stimulus intervals indicates two distinct processes. We argue for two different interpretations. First, we propose that

changes in the ABA could be associated with the representation of the precision of prediction in the pre-stimulus interval and with the refinement of the prediction in the post-stimulus interval. We argue that the refinement could refer to a process underlying short-term inference, and the representation of the precision of prediction could be due to long-term prediction.

Second, with regard to the above-mentioned theory of Kwisthout (Kwisthout et al., 2017), an alternative interpretation of the increased ABA in pre- and post-stimulus intervals in a varying network could be explained by the fact that each interval represents a different *level of detail (LOD)*. According to Kwisthout, we propose that in the post-stimulus interval the PE minimization is executed on a high *LOD* when the precision of prediction is high. And further, when PE minimization is absent, the representation of the prediction (in the pre-stimulus interval) is executed on a lower LOD. This can be accomplished by an increasing pre-stimulus ABA in representational units higher in the cortical hierarchy, which modulate the gain of PE-units of hierarchical lower brain areas. Here, we argue that the consequence of this modulation of units reporting PE is not only the related decrease in high frequency band activity (> 30 Hz) (Bauer et al., 2014; Feldman and Friston, 2010) but also an increase in ABA. This, in turn, enables the reduction of the PE in hierarchically even lower brain areas. Thus, we speculate that the observed ABA in the pre-stimulus interval that involves higher cortical brain areas (OFA, LOC, V2) and that ABA in the post-stimulus interval (V1/V2; V3; cITG) could be explained by processes on two different LODs.

In sum, by introducing a paradigm suited to investigate PCT, we provide evidence that ABA is related to the precision of prediction. Specifically, we could show a distinct ABA network in pre- and post-stimulus time intervals and, therefore, we could propose two alternative interpretations.

2 Methods

2.1 Experimental Setting

Our paradigm is a face learning paradigm with two-tone stimuli of faces (Figure 2-1). The paradigm included three tasks on different time scales. The short task was a perceptual closure task in which the participants had to recognize an identity by a face presented in a two-tone stimulus (200 ms). The intermediate time-scale task was a matching operation: The participants were asked to reply if the second stimulus was a target or not (~4 s). For the long time-scale task, we refer to the learning task. The participants had to learn a predefined unfamiliar face identity across 25 trials constituting a series (~4 min). In the following, each task and additional parameters of the paradigm are described in detail.

We used highly degraded natural images of faces as stimuli. These stimuli contained only black and white patches. Between these patches, it is the edges that carry the remaining information. These edges make the stimuli ambiguous, because they can be object borders or light/shadow borders. How these borders are classified as object or shadow borders is explained by a model of two-tone image processing proposed by Cavanagh (Cavanagh, 1991). Cavanagh's recognition model considers the estimation of the illumination direction to identify the cast shadow borders and to validate object recognition. Cavanagh's recognition model motivated our stimulus manipulation, which mainly involved variations in illumination direction. Thus, we can assume that the (short) perceptual closure task involves estimations of illumination direction to validate identity recognition. In the following, the sequence of the two-tone stimuli in our paradigm is described.

The trial structure in our paradigm was similar to a *match-to-sample* working memory task. The first *sample* stimulus was presented for 200ms, followed by a 1,5s delay, and then a second *test* stimulus. A subsequent question mark on the screen indicated the observer to answer the question whether the second stimulus represented the same identity as the sample stimulus. During the inter-trial-interval (ITI), a red fixation circle was presented. A colour change of the red fixation circle to a black fixation circle cued

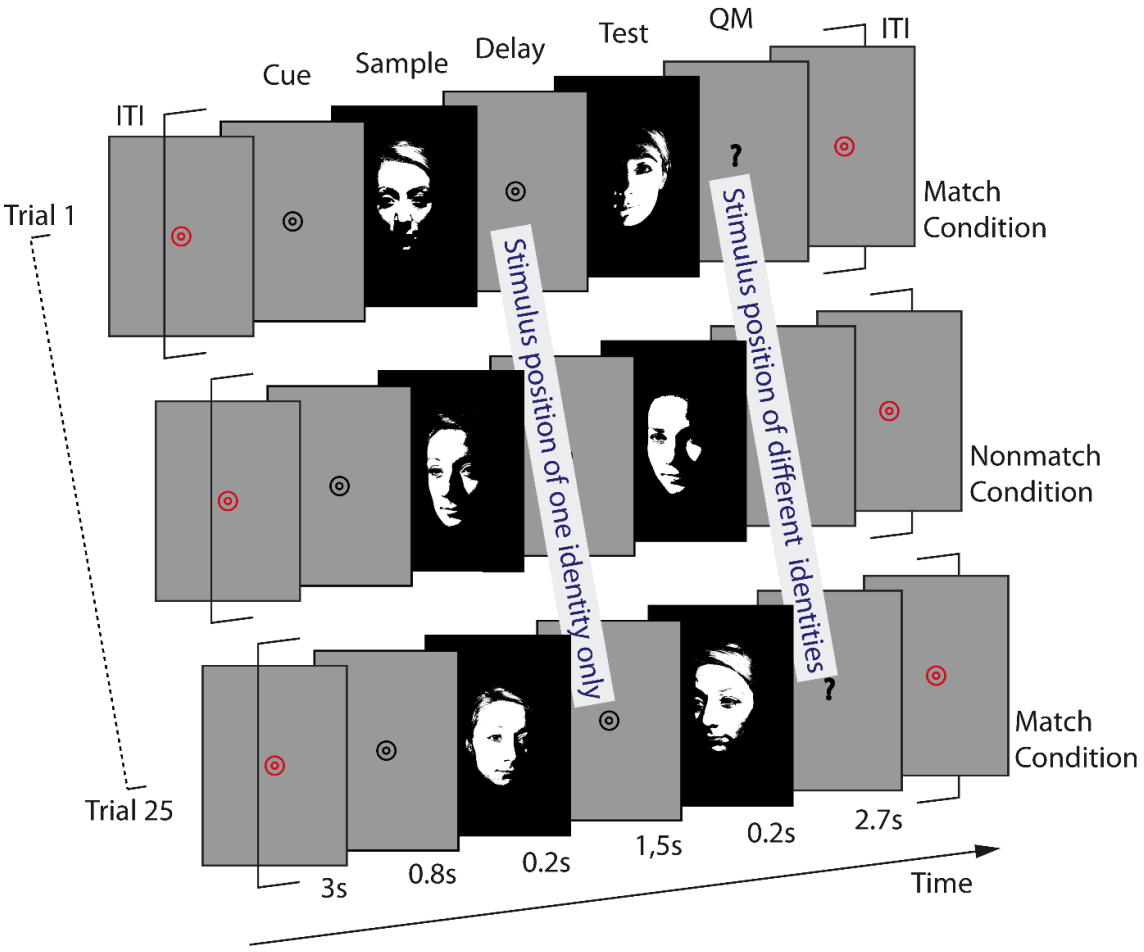

Figure 2-1: *The face learning paradigm with two-tone stimuli.* One trial consists of two two-tone stimuli with a short delay in between and a question mark right after. The question mark reminded the participants to reply to the question 'Have you recognized the target identity in the test stimulus?'. During the inter-trial interval (ITI) a red fixation circle was shown. A colour change of the fixation circle from red to black cued the sample stimulus arising next. Participants were told to expect a new stimulus of the target face identity during this period. Right to the example trials, the labels of the trial condition are displayed. Both stimuli in the first and third trial belong to the same identity. The test stimulus of the second trial does not belong to the target identity. MEG timings are shown below the graph. QM, question mark

the start of the next trial, but the presentation of the sample stimulus was always delayed by 800ms with respect to the cue. This 'delay' interval was defined as the expectation interval.

The third task for the participant was to learn the visual appearance of a (previously) unfamiliar face identity (in the following termed *target face identity, TFID*) across 25 trials. These 25 trials defined a series. Each series was separated from the next series with an information screen of individual duration. To ensure that the participants learned the correct TFID, we formulated a rule. The rule was that the TFID appeared always at the

sample position, while the test stimulus showed the TFID in 50% of the cases. This means that the observer can be 100% confident in receiving (new) visual information of the TFID from the sample stimulus. This rule enables the participants to learn the visual appearance of the TFID from the beginning of each series. This rule alternates the *match-to-sample* working memory task to a "matching to an internal model of the TFID" task. The participants were informed about all conditions and were explicitly told to use the *sample stimuli* to learn the appearance of the TFID to improve their performance in the matching task.

2.1.1 Subseries-related pseudo-randomization

With respect to the analysis of the expectation interval, we repeated the first trial again at the end of a series and skipped the first trial for neurophysiological analysis (for behavioural analysis, we skipped the responses of the last trial). The resulting series of 24 consecutive trials was split into four equal and consecutive sub-series (four times six trials). The first sub-series comprised the first to the sixth trials when analysing the response behaviour and the second to the seventh trials when analysing the neurophysiological brain response in the expectation interval. The second sub-series comprised the seventh to the twelfth trials when analysing response behaviour and the eighth to the thirteenth when analysing the neurophysiological brain response in the expectation interval. This continued until subseries four to the twenty-fifth trial.

This four subseries restricted the randomization: First, three match and non-match conditions appeared in each subseries. Second, for each subseries the illumination

conditions for the test stimuli were balanced: Three stimuli were close to (max difference 90°) and three were far from (illumination differences between 100° and 260°) the illumination condition given by the prior stimulus at the sample position.

These illumination angles in the test stimulus were balanced for match and non-match conditions. Third, in a series the presentation of stranger identities was balanced in sex: Three different stimuli of two males and three stimuli of two females were selected. Across 15 series, we did not have enough stranger identities (for the non-match condition) for none of the identities to be repeated across the series. However, we had

enough stimuli to show no stimulus of a stranger identity twice. To rule out that participants implicitly learned the stranger identities, we defined a distance rule: The use of stimuli of the same stranger identity was not allowed in the two following series.

In the MEG experiment, we showed 15 distinct series, which were grouped into five single recordings. The break between each series within a recording was of individual length: This means that participants decided on their own when to continue with the presentation of the next series. In the fMRI experiment, we showed six series arranged in three single recordings, each containing two series. Here no individual length was enabled because of scanner timings. Across the two experiments, no series was used twice.

2.1.2 fMRI-specific Paradigm Amendments

In the fMRI experiment, we included two additional stimulus conditions: 1.) Scrambled faces stimuli and 2.) black and white animal stimuli (Figure 2-2). Animal stimuli were included to disentangle stimulus match processes from internal model match processes. Therefore, the task instruction regarding the animal stimuli was to answer the question “Have you seen the same image or not?”. For the animals, only match trials were presented. Participants were not informed about this. However, most participants realized that only match condition were presented and mentioned it in the post-measure interview. The animal stimuli were also used to disentangle the time confound across the sequential positions by presenting a pair of animal stimuli in each series within another subseries across the six series.

Scrambled faces stimuli are face stimuli in which the white patches are shuffled on the black background. This shuffling procedure ensured the same ratio of black and white pixels and edge information compared to face stimuli but destroyed the configuration of patches necessary for face perception. Four scrambled faces were presented in between two series in one recording session to cause a break between two series, which could not be individualized as in the MEG experiment due to scanner timings. The scrambled faces were introduced by an information screen and were viewed passively without any specific task. Every series was introduced by a countdown of three seconds visualized in numbers.

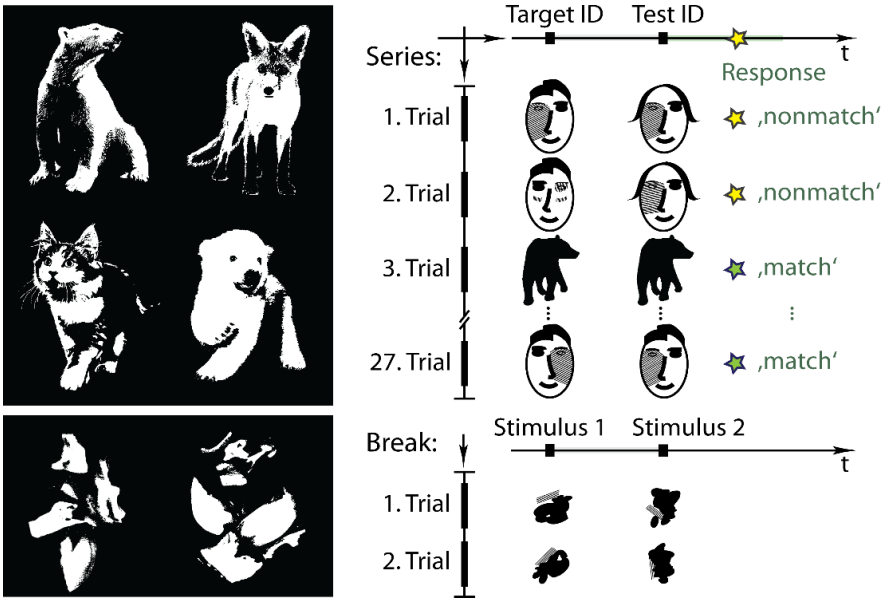

Figure 2-2: *Additional conditions in the fMRI paradigm.* Examples of animal stimuli and scrambled faces are seen in the left panel. The right panel illustrates how the two additional conditions fit in the paradigm. Two animal trials were placed in between the face trials of a series. Participants indicated by pressing the button whether they recognized the same stimuli or not. The star next to the two icons indicates the response match or non-match. A break between two series was defined by passively viewing scrambled faces. However, the presentation of scrambled faces was indicated by an information screen.

2.1.3 Timing and Presentation

In total, 1080 different and self-made black and white stimuli were used (see next Chapter 2.4.1: Stimuli). In the MEG experiment 750 (faces only) and in the fMRI experiment 330 (faces, animals and scrambled) stimuli were presented. The presentation time of each stimulus was 200ms regardless of condition and experiment. The presentation timings differed between the MEG and fMRI experiments. In the MEG experiment, the expectation, delay and question mark interval were exactly timed (0.8s, 1.5s, 2.7s), and only the ITI was jittered from 4 to7 seconds (average 5.5s). In the fMRI experiment, all time intervals were jittered except for the question mark interval. This means that the delay and the expectation phases were jittered between 1 and 3 seconds, resulting in an average of 1.5 seconds.

The presentation distance in the MEG was 53 cm and the resulting visual angle was 16.7°. The luminance, beamer setting (60Hz refresh rate, resolution 1024x768 pixels) and surrounding light setting were kept constant.

2.1.4 Stimuli

All face stimuli were self-made. We started with taking photos. 56 recruited people voluntarily participated as a face model in a photo session. Within the photo session, 245 pictures were taken, covering all combinations of set manipulations. The set manipulations were the illumination direction (differing on the frontal plane) and the portrait angel (differing on the horizontal plane). The portrait angles were 0° (frontal portrait), 30°, -30° (for right and left 1/4th portrait), 45°, -45° (for right and left 1/2 portrait), 60° and -60° (for right and left 3/4th portraits). The Illumination direction varied by 10°, covering a full rotation (Figure 2-3), which resulted in 36 conditions of illumination direction.

In the following, the protocol of the photo session is described. Volunteers were completely informed about the purpose and usage of the conducted photo material, and they allowed by their signature the photos and the resulting stimuli to be free for research use. After informed consent, the volunteer was seated in front of a homogenous black background and behind a self-made and fixed vertical ring construction, which enabled the variations in the illumination angle. Ring construction, camera and face were centered. The distances between the ring construction camera and the volunteer were kept constant (ring construction – Camera, 40 cm, +/- 1 cm; Ring construction – nose, 30 cm, +/- 5 cm). During the conduction of photos, the volunteers were asked to move as little as possible, to keep their eyes open and to try to mimic a neutral face. After completing the task, the volunteers received a 10€ compensation for their time.

All manipulations of the photographs were done in GIMP (GNU, v2.6). The first steps were to cut out the face from the background and in the following to gray scale, resize and center the image. Resizing and centering was done by hand to fit the image size of 860x1090 (width x height). To center the face in the image space, the middle of the triangle spanned by the eyes and the nose was used. The centering was validated by merging all black and white pictures of the target identities, which turned out to result in a gray value picture (Figure 2-4). Merging means, that for each voxel at a specific coordinate an average value was computed. The centering was declared valid when the eyes and nose appeared as sharp-edged features.

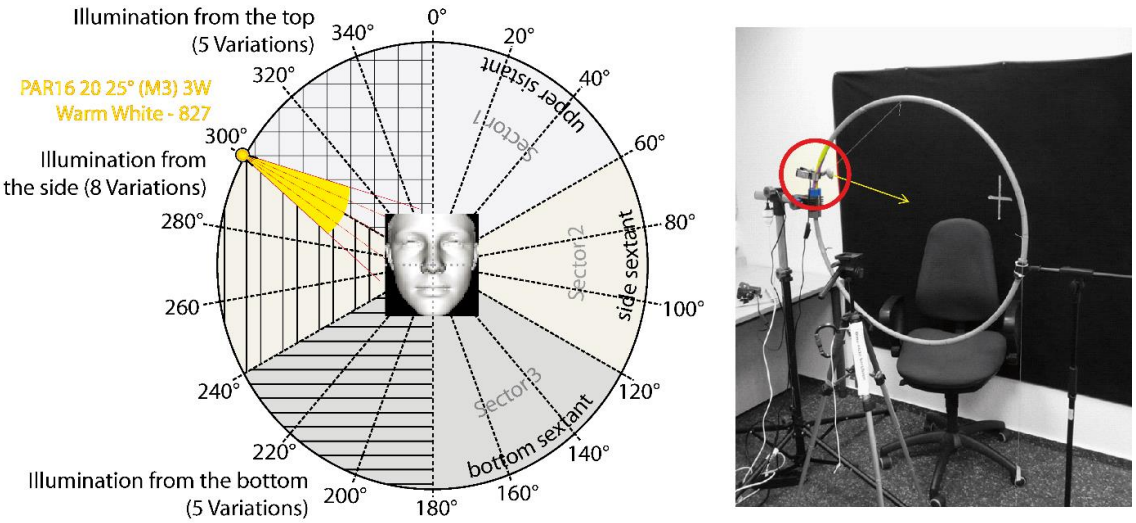

Figure 2-3: *Control of Illumination conditions*. The experiment used 18 illumination directions varying by 20°, covering top, side and bottom illumination (LEFT). During the photo session, the illumination was controlled with a single light source in a darkened room, and the person sat in front of a black background. While taking photos, the illuminations were changed by 10°, covering 36 illuminations across a full rotation.

The last step towards stimulus creation was to adjust the contrast and brightness to obtain black and white images, similar to stimuli that are called Mooney face stimuli (Mooney, 1957). However, our stimuli did not fulfil a specific criterion of a Mooney stimulus, which is that in a Mooney stimulus it is difficult to recognize a face. This is due to a missing high spatial filter. Yet it is difficult to decide whether two two-tone face stimuli belong to one identity, as pretests have revealed.

In sum, our stimuli are similar to Mooney face stimuli, as they also require a closure process due to the massive information reduction (colour, curvature, surface). Yet, our stimuli were clearly perceived as faces and could not be mistaken for meaningless shapes of black and white patches or other objects. Even if in each stimulus a face is perceived, reidentification of identity is hard, because features are differing across different illumination directions.

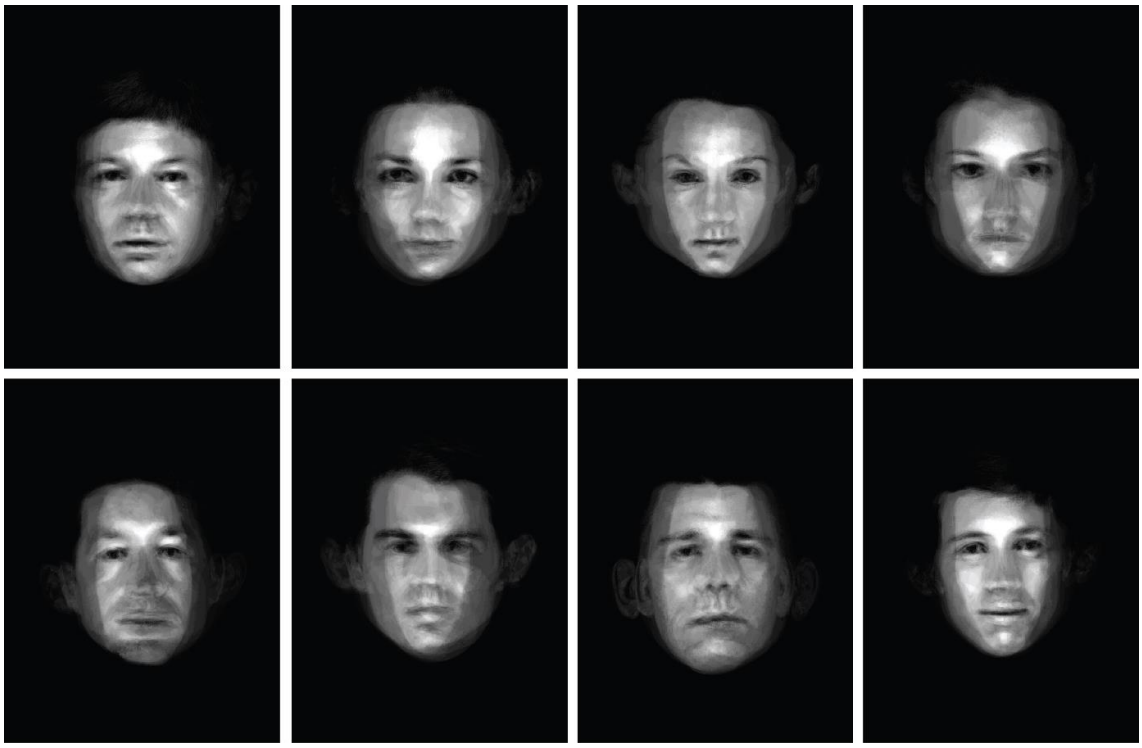

Figure 2-4: *Results of merging all two-tone stimuli of a target face identity.* All 36 two-tone stimuli of one target identity were merged resulting in a grey value picture. The grey values of a pixel indicate the probability of the pixel being white or black across the 36 stimuli. Here, eight representative images of female and male target face identities are shown. This procedure was applied to check the centring of the face across the 36 stimuli. The centring was improved(redone) in cases when features like eyes, nose and mouth were not that clearly visible as displayed here.

2.1.5 Implications and Assumptions Regarding the Experimental Settings

First, we briefly summarize the crucial details of the experimental design. Then we introduce the processing model (PM) illustrated in Figure 2-5. Regarding this PM, we formulate hypotheses, which are testable with our experimental setting and neurophysiological measures.

One crucial detail of the experimental design is the use of the two-tone face stimuli. Two-tone face stimuli were perfectly suited for our experiment, because the recognition of objects in two-tone stimuli relies on prior knowledge (PK) (Dolan et al., 1997). Two recognition models proposed for two-tone stimuli by Ahissar and Hochstein (Ahissar and Hochstein, 2004; Ahissar et al., 2009) and Cavanagh (Cavanagh, 1991) posit that PK is sent top-down to be compared to the sensory input and is able to 'complete' missing information/content. This is in line with the concept of PCT that top-down information flow refers to memory-related content (Clark, 2013). In our experimental setting, we used

the two-tone recognition model to investigate the PCT by associating PK and predictions. According to Bubic (Bubic, 2010), predictions in the sense of the PCT are related to expectations. Considering this, the participants were instructed to expect the target face identity (TFID) in each sample stimulus. This is underpinned by the 100% confidence that a stimulus of the TFID was presented at the sample stimulus position. Thus, in the sample pre-stimulus interval, the expectation interval, we can investigate predictive coding-related processes.

In our experimental setting, we manipulated the PK used for the perceptual closure by learning. That means that before the experiment started each TFID was unknown to the participants and that the participants acquired and gathered visual information about the TFID across the trials. Thus, the available PK for the perceptual closure process differed across (several) trials. Further, this gathered visual information was supposed to be utilized for forthcoming perceptual closure processes. This means that for the next presentations of the TFID in the sample and test stimuli a more detailed internal model of the TFID was supposed to be available to explain the presentation of the TFID. Next, the experimental setting included a detection task in the form of a WM task. This means that each test stimulus of the trial presented by chance either the TFID or a differing (stranger's) identity. The presentation of the test stimulus required the participants to reply whether the TFID was recognized in the test stimulus or not.

2.1.5.1 Processing Model Based on the Experimental Design

Based on the experimental setup, we have reason to conclude that the sample and test stimulus were matched to the internal model and not, as the structure of the WM trial setup might suggest, to the prior sample stimulus of each trial. We illustrated this 'stimulus match to internal model' in the PM in Figure 2-5-B using lines that point to a (green) thick line illustrated above in the sketch. This thick line shall represent the internal model across the trials, which increases in detail across the trials by accumulating evidence. This accumulation of evidence is illustrated by arrows pointing from the stimuli to the thick line above, and with each arrow the thick green line grows in diameter. Also, these arrows pointing at the thick line represent a successful match. Considering that the

sample stimuli enabled a constant and reliable visual information gain, the sample stimuli are always incorporated into the internal model. In turn, only test stimuli of the match-response type are integrated into the internal model.

Based on a missing trial-wise feedback and the presentation of a TFID at chance level at the test stimulus position, we assume that the test stimuli are crucial for the dynamics of the learning progress (Figure 2-5-C). These dynamics are theoretically based on two mechanisms: 1) identifying and rejecting false-positive and 2) identifying and included false-negative evidence. Regarding the first point, false-positive evidence is a non-target stimulus mistakenly identified as a target. This false-positive evidence can by identified by a target stimulus in a sample position containing the same or nearly the same condition of this non-target stimulus included in the internal model. Regarding the second point, a false-negative evidence would refer to a target stimulus not identified as a target but maintained in (visual short term) memory until the next target stimulus in a sample stimulus reveals this test stimulus in memory to refer to a target. In the first place this scenario seams possible when considering limitations of visual short-term memory (VSTM). Cowan (Cowan, 2010) proposes for working memory that about 3 to 7 items are stored in parallel, Sligte and colleagues (Sligte et al., 2008) found for that the VSTM capacity were much higher. The storage of the VSTM were found to contain 5 to 15 items. However, the work of Pinto and colleagues (Pinto et al., 2013) showed that VSTM is highly dependent on the similarity of the condition and location of the item. That means the more likely the items are the less participants were able to store different items in memory. Also, if only the first mechanism is more likely to occur, we respect both introduced mechanisms for the illustration of the dynamics of the PM.

Further, the experimental setting included a visual *cue*. The interval between the cue and the sample stimulus was referred to as 'expectation interval.' The expectation has been related to predictive coding related processes (Bubic, 2010), and on the behavioural level it has been demonstrated that expectation can shape perception (Clark, 2013; Lupyan, 2015). Further, on the neurophysiological level it had been shown that if expectations are modulated in the experimental design, then the pre-stimulus interval is well-suited to investigate predictions (Brodski-Guerniero et al., 2017; Kok et al., 2017; Mayer et al., 2016).

Thus, in the expectation interval we associated predictions with the re-activation of the internal model of the TFID. In other words, the internal model is being used to form a prediction of the upcoming stimulus. With respect to this, we illustrated this by a line starting at the point in time from the cue onset pointing to the green thick line and back again. Again, this ought to illustrate that the cue led to retrieve the internal model to form a prediction. As mentioned above, the internal model is increasing in detail about the TFID, thus, we conclude that the precision of the prediction in the expectation interval should increase.

If the prediction is described as a probability density function, the precision of the prediction is the inverse variance (Feldman and Friston, 2010). According to this and to our assumptions related to the PM, we also hypothesize about a change of the precision of the prediction by a decreasing variance of the probability density function when the internal model increases in detail (see bottom line in Figure 2-5-B). In line with this increase in details of the prediction and according to the PCT of Bastos and colleagues (Bastos et al., 2012), as mentioned in the introduction, we assume changes in low frequencies when analysing the changes across the sequential positions in the expectation interval.

2.1.5.2 Pilot Project

A pilot study was conducted to investigate the influence of the order of stimulus conditions in the sample stimuli across the trials in a series. We compared the presentation of the sample stimulus condition in a series being incremental or (pseudo)randomized. (Pseudo)randomized means that we checked that the randomization applied did not by chance represent an incremental sequence. Incremental means that we randomly set a starting point of illumination direction and an illumination movement direction, which could be clockwise or anti-clockwise. Given the start of the illumination direction and movement direction of illumination direction, an incremental sequence was built: Every next stimulus in the presentation adds (or subtracting) 20° to the previous illumination direction. In doing so to gain enough stimuli with a full circle turn we added stimuli not changing in illumination but changing in

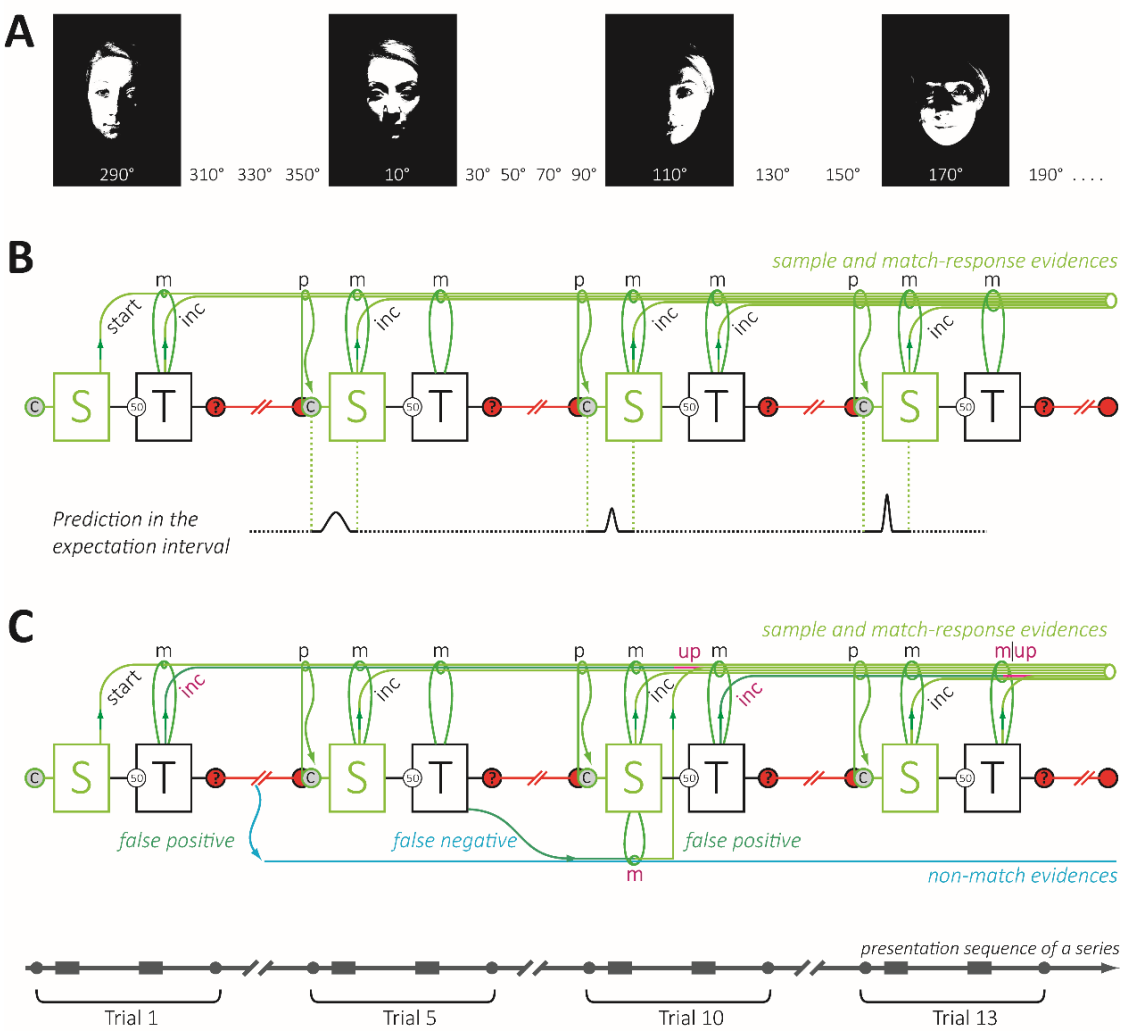

Figure 2-5: *Processing model based on the experimental design.* From left to right, a series is illustrated by four exemplary trials, the first, fifth, tenth and the thirteenth trial. **A**: The series of sample images represents four example stimuli that show the same TFID from left to right. The numbers indicate the illumination degree. The four sample stimuli correspond to each of the sample stimuli indicated by a capital S in the two schemata in B and C. **B**: The processing model illustrates which stimuli are used to accumulate evidence: These are all sample stimuli, and test stimuli with a match response. This is illustrated by the bundling of individual lines into a single green line. Thus, line thickness increases with every additional evidence from left to right. This green (thick) line can be associated with the internal model increasing in detail across evidences. Bottom line: We propose a decrease in variance for the predictive signal when the internal model about the target is refined by accumulating evidence. **C**: Dynamics of the processing model. This is a copy of the processing model shown in B with additionally indicated dynamics based on corrections of false-positive and false-negative evidences. For more details see text. Abbreviations: S = sample stimulus; T = test stimulus; c = cue; m = match operation; p = prediction; up = update; inc. = incorporation.

camera position on the horizontal plane. This means that additionally to frontal portraits also stimuli of faces of a side view (30° angle) were respected to obtain a sufficient number of 24 stimuli. Presentation timings and other parameters were as introduced above in the MEG experiment. It must be said that prior to this pilot study few

measurements had been conducted for investigating the visibility of the stimulus. Here we tested three different stimulus sizes. The results revealed the above-mentioned visual angle of 16.7° as the best size for the stimuli.

2.2 Participants

The volunteers were recruited at the Goethe University of Frankfurt am Main and the Technical University of Darmstadt. 55 participants passed the screening procedure. The screening criteria were grouped into technical, task and health demands. The technical demands summed up to standard fMRI and MEG exclusion criteria. The task demands investigated the capability of 3D perception, normal or corrected to normal vision and the ability of face recognition. To check the ability of face recognition, we asked the participants to do the online famous face task (https://www.faceblind.org/facetests/ff/ff_intro.php). In order to make sure that we measured a healthy group, we asked for a neurological and psychiatric diagnosis in the past and current drug intake for medical purposes (to identify drugs with neurological side effects like antihistamines, antibiotics and others). Before the measurements, the participants gave consent by signature and confirmed by signature that they did not meet the exclusion criteria (fMRI). The applied protocols were accepted by the ethic committee of the University hospital of Frankfurt.

From the 65 participants, ten participants participated in the pilot study. From the remaining 55 participants, four exclusively participated in the fMRI Experiment and 12 exclusively in the MEG experiment. At last, the data of 41 participants for MEG (mean age 24.87, min. age 21, max. age 31; 16 males) and 36 for fMRI (mean age 24.58, min. age 21, max. age 31; 14 males) measurements were respected for a final analysis. 10 participants had been excluded from final MEG analysis, mostly because no anatomical MRI data were present, one participant had to be excluded because of only few trials remaining after preprocessing. For fMRI data analysis, 5 participants were excluded because of sleeping in the scanner, processing difficulties due to scanner noise and excessive movements during the measurement.

2.3 Premeasurement Procedure – Instructions

Before measuring the brain response in the MEG or fMRI, the participants were twice informed about the paradigm, first in written form by an information sheet with graphical abstracts and second in a short interview. In the interview, the instructor made sure the participant understood the task. We decided to repeat (almost) word by word to every participant before every measurement: 1) 'One trial consist of two face stimuli presented in quick succession. The first always represents the target identity, the second only in 50% of the cases. Do not feel pushed by the 50%, we are interested in your true perception, there is no correct or incorrect response unless you failed to respond your subjective perception correctly'. 2) 'This is not a speed test. Take your time to respond correctly; however, stay with your responses in the time frame of the presentation of the question mark. Please try to answer by only once pressing the button. Do not correct your answer with a second response. If you feel you must correct your replies due to too fast a response, adapt your speed.' 3) 'Be aware that the trial begins with the colour change of the fixation circle and not with the first face stimulus. We do not show a picture twice, so please expect that new information about the target face will come up. So, try to learn the appearance of the target identity to get better in discriminating the target identity in the second face stimulus.

Additionally, the participants were familiarized with muscle activity, eye blinks and eye movements being artefacts for the MEG recording in the information sheet. These issues were not mentioned in the interview. However, verbally we only stressed that blinks increase the likelihood to miss stimuli, thus we asked to reduce blinks during the trial interval.

2.4 MEG Data Acquisition

Magnetoencephalographic signals (MEG signals) were recorded using a whole-head system (Omega 2005; VSM MedTech Ltd.) with 275 channels. MEG signals were collected at a sampling rate of 1200 Hz, filtered online with a fourth-order Butterworth bandpass filter (300 Hz low pass and 0.1 Hz high pass) and recorded in a synthetic third-order gradiometer configuration.

The head position relative to the gradiometer array of the MEG system was determined continuously during the recording session. The head position was determined by three coils: two placed with ear moulds left and right above the ear channel *(Canalis acusticus externus)* and the third placed at the base of the nose *(Nasion)*. The head position was monitored in reference to the initial head position of a recording block. To maintain a head position within a deviation of 5 mm across the blocks, the recordings of the first head position of a block were used for each following block to determine the difference for possible corrections. Corrections of the head position were done by the participants themselves, as we projected the actual and the reference head position to the screen in front of the participant.

Artefact detection in the MEG signal was supported by a separate electromyogram (EMG) of eye movements and heartbeats. The EMGs for eye movements were recorded via four skin electrodes: distal to the outer canthi of each eye (horizontal eye movements) and above and below the right eye (vertical eye movements and blinks). The EMG of the heartbeat was recorded by placing an electrode medial at each collarbone (*Clavicular ossaris*). The EMG reference and ground electrodes were placed right and left at the forehead. The impedance of each electrode was measured with an electrode impedance meter (Astro-Med, Inc Grass Instrument Division, W. Warwick RI USA) and was kept below 10 kΩ.

During the MEG recordings, the responses of the participants were collected by a four-button response box (current design), the visual stimuli were projected on a translucent screen via a projector with a sampling rate of 60 Hz, and eye fixations were additionally monitored by an eye tracker (eye link).

2.5 MRI data acquisition

MRI data acquisition was performed with a 3 Tesla head scanner of the type Allegra by SIEMENS with a four-channel transmitter coil. The haemodynamic responses and field inhomogeneities were collected by echo planar imaging sequences. Before field inhomogeneities measurements, a shim measurement was manually conducted and used to adjust the scanner settings for temperature and frequency shifts. For structural imaging, a T1 sequence was used. The settings of the EPI and T1 sequences are given in Table 2-1.

Scanner recordings and stimulus delivery synchronization were controlled by the software *Presentation* (Version 9.90, Neurobehavioral Systems) collecting the triggers from the scanner and controlling the stimuli delivery. The stimuli were projected on a translucent screen outside the bore. Inside the bore, a mirror system attached to the receiver coil enabled the participant to see the stimuli on the screen. The responses of the participants were conducted by a 4-button response device by *current design* and recorded by *Presentation*.

The MR acquisition protocol started with a circle localizer to adjust the position of the participant's head to the field of view. Then functional recordings were started in three sessions. One session lasted about 14 min (13.42 min) and included two *series,* which were separated by a *brake-series* which consists of four scrambled faces. In-between the sessions, inhomogeneity maps were recorded. After the third session, a structural recording was applied.

To find the exact coil position of the MEG recordings in the structural MR image, we placed an ear mould with the same size as in the MEG recording (for reasons, see MEG-source-localization) in the participant's ear and fixated a Vitamin-E-capsule at the position at which the coil was placed in the MEG recordings.

To locate a Vitamin-E-capsule at the same position as the MEG coils, little plastic sticks were glued on Vitamin-E-capsules which fitted in the tube inside the ear mould. To reuse constructions like this more than once, they were cleaned and disinfected after each use.

Table 2-1: *Parameter list of the MR sequences*

	BOLD.Resp.	Phase map	Magnitude map	T1(MPRAGE)
Echo time	30 ms	4.89 ms	7.35 ms	3.93 ms
Time of repitition	2500 ms	570 ms	570 ms	2200 ms
Voxel size	3x3x2.5 mm	3x3x2.5 mm	3x3x2.5 mm	1x1x1 mm
Foveal read	192 mm	192 mm	192 mm	256 mm
Slice thickness	2.5 mm	2.5 mm	2.5 mm	1 mm
Distance factore	30%	30%	30%	50%
Slice number	40	40	40	160
Phase encoding	64	96	96	192
Flip Angle	90°	60°	60°	9°
Series	descending	interleaved	interleaved	

2.6 Behavioural Analysis

Behavioural measures were hit rates (HRs) and response rates (RRs). The HR was classified as the correct response rate and correct is determined by the stimulus condition. RR was classified as the given responses independent of being correct in respect to the stimulus condition. HR and RR were and subjected to match and non-match responses. This resulted in four different response types (HR for match and non-match; RR for match and non-match). For all four response types, reaction times (RT) were measured. A fifth class of RT measures was *overall* responses, which were averaged RT for match and non-match responses of one sequential position.

Further, we computed the discriminability (d-prime) and the response bias (C-Criterion) as proposed by the signal detection theory (SDT) (Green, 1966; Macmillan and Creelman, 2005) by the following formulas: d-prime: $d' = z_{(\text{Hit rate})} - z_{(\text{False alarm})}$. response bias: $C = 0.5 * (z_{(\text{Hit rate})} + z_{(\text{False alarm})})$. The four response types, SDT measures and RT were subjected to each of the four conditions (sequential position one to four) for a one-factorial design with the factor *Sequence position*. Last, behavioural data were split into match and non-match responses for HR and RR, irrespective of sequential position.

To investigate the main effect of the factor *Sequence position,* a one-way repeated measure ANOVA and an effect size (ES) analysis were applied. For an ANOVA design Levine and Hullett (Levine and Hullett, 2002) suggested to report Eta^2 for a measure of

ES. Eta² was computed using the Toolbox 'Measures of Effect Size Toolbox' (Version 1.5, January 2015) written by Hentschke and Sttgen. In this toolbox, Eta² was realized by values of the ANOVA table and was computed by the formula: $Eta^2 = SS_{(effect)} / SS_{(total)}$.

RT are known not to be normally distributed. We tested for normal distribution, as it is preferred by Ghasemi (Ghasemi and Zahediasl, 2012) by the Shapiro-Wilk test and the histogram. Normality was tested also on transformed data (log-transform / inversion). However, no transformation revealed normality for RT across all experiments and measures. Therefore, a Friedman test was applied on RT data. The ES were measured by computing Eta² with the formula mentioned above.

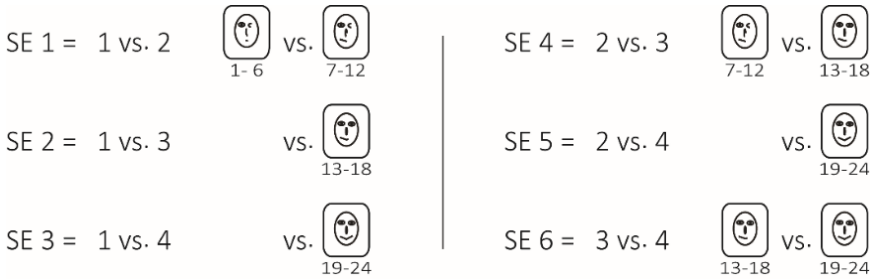

Figure 2-6: *The order of the six simple effects (SE)*

A post-hoc analysis was carried out by investigations of each simple effect. Given four conditions, six simple effects exist (the numbering is shown in Figure 2-6). Simple effects were investigated by means of a dependent paired *t*-test on HR and RR and by means of the Wilcoxon signed rank test on RT. For each of those tests, the ES measure Cohen's D was computed (Cohen, 1988). For HR and RR, the following formula was used: $d = (Mean_{(1)} - Mean_{(2)}) / SD_{(1,2)}$; where the pooled standard deviation is $SD_{(1,2)} = ((SD_{(1)}^2 + SD_{(2)}^2)/ 2)^{0.5}$. Cohen's D was not implemented in the effect size toolbox and was implemented by a self-written code. For RT, the ES measure Cohen's D was realized by the formula: $r = z/n^{0.5}$, where z is the Z-transformation of the data. In his appendix, Durlak (Durlak, 2009) provides formulas to transform ES. Formula eleven was used to transform r into Cohen's D. To correct for multiple comparison, the alpha level was corrected with the Bonferroni-Holm sequential method (Holm, 1979). Additionally, all ES results were

corrected for sample size by a factor that Nakagawa and Cuthill (Nakagawa and Cuthill, 2007) suggested and implemented in the ES toolbox.

Behaviour data analysis was realized by a self-written code in MATLAB (The MathWorks, Inc., Natick, Massachusetts, United States, version 2012b). The variance analysis and signal detection measures were realized by functions from the statistics toolbox offered by Mathworks for MATLAB.

For visualizations, means for response types and medians for RT were plotted. Visualization were performed with MATLAB for initial illustration, and adjacent refinement was done with the vector-based program Adobe illustrator (CS3).

2.7 MEG Data Analysis on Sensor Level

2.7.1 MEG Pre-processing

MEG-Data handling and analysis were performed with MATLAB (MATLAB 2012b; The MathWorks) and the open source MATLAB toolbox FieldTrip (Oostenveld et al., 2011) (Version 2013 11-11), which provides low- and high-level functions for time series analyses. First, the time scale was corrected for the projector delay (45ms) and a 50Hz (for DC) and a 60Hz (projector refresh rate) discrete Fourier transformation (DFT) filter was applied. Second, the trials were defined in the stimulus categories as sample trials or test trials. Sample trials were cut 0.8 s before and 0.5 s after the sample stimulus onset and sorted into the four sequential positions. In detailed that meant to define the 2^{nd} to 7^{th} trials to belong to the condition *first sequential position*, the 8^{th} to 13^{th} trials to belong to the condition *second sequential position,* the 14^{th} to 19^{th} trials to belong to the condition *third sequential position* and finally the 20^{th} to 25^{th} trial to belong to the condition *fourth sequential position*.

Trials containing sensor jump artefacts or muscle artefacts were rejected using automatic Fieldtrip artefact rejection routines. Most default values were kept as suggested by the tutorial, however, we were stricter in the *z*-value cut-off (*z*-value = 4) for muscle activity. Further, trials were discarded when they deviated more than 5 mm from the mean head

position. The mean head position was calculated based on all artefact-free trials of one trial category (sample or test stimulus).

Eye movement artefacts (vertical and horizontal) were identified and rejected based on components of an ICA (independent component analysis) as proposed by the Fieldtrip tutorial. Components referring to eye movement artefacts were identified by the correlation between the independent component and the EOG channel and by data inspection.

2.7.2 Permutation Test

A permutation test is used when a non-parametric method is required, which is the case with neurophysiological data. First, we need a measure that quantifies the effect of the 'treatment,' this can be, for example, a calculation of the *t*- or the F-value. The assumption of a permutation test is that the null hypothesis is true when the treatment did not have any effect. Thus, the sampling distribution for the test statistics (for a true null hypothesis) will be created out of samples from a shuffled distribution. This is realised by shuffling the dataset, computing a quantified measure (computing *t*- or F-value) and repeating this a lot of times for sampling the distribution. Usually one starts with doing this 1000 times. Next, the histogram is computed for these (1000) randomizations, which is the test statistic. Another random product would ideally be mapped around the mean of that test statistic, this means that we do not reject the null hypothesis. But when the measure is located at one of the ends of the distributions the alternative hypothesis is favoured. In other words, with a decision threshold (alpha level), usually 5%, we decide to reject (or not to reject) the null hypothesis under the assumption that the treatment is not one of the population mean with a 95% (1-alpha) confidence. For a two-sided test, this means the confidence level is centred and the quantified measure of the treatment group is observed to be below 2.5% (left) or above 97,5% (right) in the sampling distribution.

The uncertainty of the sample of the treatment being below the threshold is dependent on the number of permutations. For 1000 permutations the smallest possible p-value is 0.001, thus the uncertainty of a p-value of 0.05 is 1%. The uncertainty can be reduced by

increasing the permutation. For example, one can apply 100,000 permutations and therefore reduce the uncertainty of a p-value to ± 0.1%. A strategy to follow is to start with 1000 permutations and to continue with applying more randomizations only when p is small enough to be interesting, e.g., $p < 0.1$.

2.8 Event-Related Field Analysis

For event-related field analysis, the pre-processing step "trend removal" was skipped and a bandpass filter from 1 to 35Hz was applied. The data were time-locked to the sample stimulus and averaged across trials for each participant and each condition (sequential positions). The average across trials had been computed for the first (2st – 7th) and the third sequential position (14th – 19th) and a dependent samples *t*-test was applied. As Schweinberger and Neumann (2016) suggested in their simplified cognitive model of face perception that the early components in the range from 200 to 400 ms are sensitive to identity recognition, the latencies for the *t*-test were 0 to 500 ms on 1200 Hz sampled data. The N250 component is discussed to be prominent for familiarity (Tanaka et al., 2006; Leleu et al., 2010; Pierce et al., 2011) and has been reported over occipitotemporal channels, thus 105 MEG occipitotemporal sensors were selected. The permutation statistics was chosen with a cluster correction method (cluster alpha level, 0.05; 2 neighbours; alpha level 0.05).

2.9 Time Frequency and Spectral Analysis in Sensor Space

Time frequency and spectral transformation were both based on conventional Hanning tapers (Percival and Walden, 1993). The time frequency transformation was applied to all of the trials in an interval from 1 to 200 Hz in 1 Hz steps. Regarding the spectral transformation, the transformation was applied to the baseline interval -800 ms to -5 ms before the sample stimulus only. A time frequency - and spectral smoothing were applied by an adaptive window varying in height (frequency range), and for time frequency transformation the length varied with respect to each frequency. The height of the sliding

time window was computed by the function: 0.2 * f. The width (for time frequency only) of the sliding time window was computed as 7 cycles for each frequency.

In the first instance, the average power spectrum was computed across all conditions (sequential positions) and participants for the baseline in sample trials. With that, the spectral bands were determined on the TFR of parietal sensors, with a less pronounced alpha frequency peak ('MLC31', 'MLC41', 'MLC42', 'MLC52', 'MLC53', 'MLC54', 'MLC55', 'MLC61', 'MLC62', 'MLC63', 'MLP11', 'MLP12', 'MLP22', 'MLP23', 'MRC23', 'MRC31', 'MRC32', 'MRC41', 'MRC42', 'MRC53', 'MRC54', 'MRC55', 'MRC61', 'MRC62', 'MRC63', 'MRP11', 'MRP12', 'MRP22', 'MRP23', 'MRP34', 'MZC03', 'MZC04'). Temporal and occipital sensors picked up a large pronounced alpha peak, and no beta frequency peak was observable. Based on this, we determined 2 non-overlapping low frequency intervals: (1) 7 - 13 Hz (alpha frequency), and (2) 15 – 19 Hz (beta frequency).

In the second instance, time frequency representations (TFRs) were averaged for all conditions and participants to identify time differences in the determined frequency bands. The average TFR showed no specific difference in the response pattern in the baseline. Only in a selection of frontal sensors we measured a time difference in the 17 Hz beta frequency band peak beginning at -400 ms lasting to -90 ms before stimulus ('MLC11', 'MLF31', 'MLF32', 'MLF41', 'MLF42', 'MLF43', 'MLF51', 'MLF52', 'MLF53', 'MLF61', 'MLF62', 'MRC11', 'MRC12', 'MRF31', 'MRF32', 'MRF41', 'MRF42', 'MRF43', 'MRF51', 'MRF52', 'MRF53', 'MRF61', 'MRF62', 'MZF02', 'MZF03'). As support for this time window, we notice a very similar length and position of the baseline time window used by Aruu and colleagues (Aru et al., 2016) who also investigated the pre-stimulus activation and expectation.

In the third and last instance, we computed a dependent sample permutation *t*-test for TFRs of Task 5-500ms) and baseline (-500 to -5 ms) interval. To correct for multiple comparisons across time, frequency and sensors, we used a cluster-based correction method (Maris and Oostenveld, 2007). This means that clusters were defined as a population of adjacent samples (time, frequency and sensor) whose *t*-values exceeded a critical threshold. Cluster values were defined by the sum of all *t*-values of the sample of a given cluster. The critical threshold was set by alpha = 0.05. The randomization procedure has already been explained above (Chapter 2.7.2). In that case, the quantified measure is the cluster value and permutations were applied 1000 times.

2.10 Source Localization of the MEG Signal

2.10.1 Source Grid

For a multi-participant analysis in source space, we transformed each individual participant's source grid into the common source space, the MNI space (Collins et al., 1994). For this individual transformation, a structural scan from the MRI session and a standard T1 template from the SPM Toolbox (http://www.fil.ion.ucl.ac.uk/spm) was used. First, out of the T1 template a cortical mesh was created and warped into MNI space. Second, this warped mesh was transformed to fit the individuals T1 structural recording (Mattout et al., 2007). The resulting individual transformation matrix was then used to create the individual source grid. For that, an inverse version of the transformation matrix was taken to warp a regular 3D dipole grid based on the same standard T1 template with a spacing of 1 cm to obtain an individual dipole grid and a size of 6783 vertices. The individual dipole grid locations and a (realistic) single shell forward model (Nolte, 2003) were used to compute a lead field at these locations. This allowed us to perform source localization in a common space for each participant, enabling a multi-participant analysis.

2.10.2 Beamformer

A frequency domain beamformer was used to localize the sources of the A&BBA (Gross et al., 2001). The beamformer algorithm utilized was the 'dynamic imaging of coherent source algorithm' (DICS), implemented in the Toolbox Fieldtrip. However, we were interested in the local source power, thus, we used the real-valued filter coefficient of the DICS algorithm which only reflected the instantaneous magnetic field changes from the source to the sensors (Nunez and Srinivasan, 2006). The beamformer approach uses an adaptive spatial filter that enables power estimation in the frequency of interest at any grid location. The spatial filter requires the lead field (mentioned above) and the cross spectral density matrix (CSD) for each participant. The CSD matrices were computed for the expectation interval (-400ms to -90ms; pre-sample interval) and for the post-sample interval (25ms to 325ms) in the spectral alpha (7 to 13Hz) and beta (15 to 19Hz) frequency

bands. The CSD matrices were computed using the Hanning taper approach implemented in Fieldtrip. The spectral bands were predefined by the spectral analysis. The time intervals were predefined by the time frequency grand average (expectation interval) and the Task vs Baseline statistic in the time frequency domain (post-sample interval). To counterbalance the short intervals, we used the beamformer with a regularization of lambda of 5% and computed the beamformer sensor filters for all conditions (sequential position) at once (common filter). This common filter was used to project single trial data into source space for each condition separately to be able to apply statistics to individual trials. Projections using a common filter ensure that the differences that the statistics reveal are not due to differences in filter computations.

2.10.3 Source Statistic

Trials were averaged for each condition (sequential position) and participant. The equal amount of trials for each condition was drawn – constrained by the minimum trial number across the four conditions within participants. The resulting mean values for each grid point and condition across all participants were subjected to a 1x4 repeated measurements permutation ANOVA with the one factor *Sequence position*. The aim was to identify the effect of condition-dependent source power changes across the 41 participants. To consider the multiple comparison problem, a cluster-based correction method was used (Maris and Oostenveld, 2007) as described above (see Chapter 2.7.2 Permutation Test). The critical alpha threshold was 0.05, but the cluster value was computed as the maximal cluster size.

2.10.4 Post-hoc Statistic on Peak Voxel

To investigate the direction of the main effect of the factor *Sequence position*, a permutation dependent-samples *t*-test was applied on peak voxel values separately. That means six permutation *t*-tests (according to six simple effects) had been applied to each location. Correspondingly, effect sizes had been computed. For this, the *t*-values were used for an estimate by the following formula: Cohen's D ≈ t2 / sqrt(df-1).

2.11 Correlation Analysis

2.11.1 Correlation of Source Activity and Behaviour

We investigated the relationship between neural activity in the expectation interval and the behavioural measure discriminability as a function of the factor *Sequence position* by correlating the source power differences between the first and the third sequential positions and the corresponding behaviour d-prime differences in a given frequency band. The difference between the third and the first sequential position was motivated by the post-hoc result of the behaviour, which indicated the best discriminability in the third sequential position. The frequency source power differences were based on the A&BBA results which the ANOVA had revealed. First, we investigated the network activity by computing the mean across all voxels given by the significant ANOVA cluster for each frequency.

2.11.2 Correlation of Source Activity and ERF Components

We investigated the relationship between the main sources of neural activity in the expectation interval and the local field power (LFP) of the post-sample stimulus interval as a function of the factor *Sequence position* by correlating the source power differences in a given frequency band between the first and the third sequential positions and the related contrast of the LFP. The ABA was identified to show a significant effect; thus, this frequency was considered for the correlation only. The LFP was computed based on the standard deviation across sensors as it was proposed for global or local field power (Skrandies, 1990). The model of Schweinberger and Neumann (Schweinberger and Neumann, 2016) proposed two processes regarding identity recognition, beginning at 200ms (representations for recognizing individual faces, N250) and lasting until 400ms (Person identity node, N400). This broad time window of interest was separated into five time-windows according to the peaks of the ERF time course over occipitotemporal sensors. The time windows were cut based on the position of the global peaks identified at: (1) 220ms with +/-20ms; (2) 300ms +/-20ms; (3) 340ms with +/-20ms and (4) 390ms +/- 20ms. For these peaks, a time average was computed to correlate with the 6

predefined sources. All time windows were tested for left and right occipitotemporal sensor selections. This lead to 60 comparisons (Bonferoni correction, alpha level = 0.000834).

2.12 Decoding Analysis

2.12.1 Features and Classes

A support vector machine (SVM) (http://www.csie.ntu.edu.tw/~cjlin/libsvm/, LIBSVM toolbox for MATLAB) was used to assess the decodability in the form of pattern classification across the four sequential positions (Chang and Lin, 2011). This SVM was applied on the trials of each individual participant. The trial information was spectral source power values – the result of the beamformer analysis.

The beamformer projected sensor time course information into source space, averaging time and frequency of interest. The source space of each participant consisted of 6783 voxels representing the brain space. That means each trial contains 6783 voxels. For the pattern classification, these trials were reduced to the peak voxels representing a brain location revealed by the permutation ANOVA. For the ABA, six peak voxels were defined and used as features for the pattern classification.

Before the source power values of the trials were subjected to the 4 classes, the scale was transformed to fit zero to one by dividing each value by the maximum value of the data set, because power values are always positive. The trials were separated into four classes referring to the four sequential positions.

2.12.2 SVM Parameter Settings

The data set was separated into five equal subsets to apply a fivefold cross-validation. Thus, the data were separated into 80% training and 20% test sets. For each set, four subsets were pooled to train the classifier (80% of the data), and the remaining subsets was used to test the classifier (hold-out data). This procedure was repeated five times

such that each subset was tested with a training applied to the remaining others. For each subset, an inner cross-validation was applied to find the best parameter. The best parameter was searched by the libsvm function that searches for the best kernel and its regularization parameter C (cost parameter) and decision boundary parameter gamma. This approach is described in the tutorial offered by Kittipat Kampa (https://sites.google.com/site/kittipat/libsvm_matlab). The code for the inner cross-validation was adopted from his libsvm_demo_script 13. The concept of outer and inner cross-validation was proposed by Nowotny and colleagues (Nowotny, 2014) for best feature selection. Here we used the inner cross-validation to find the best parameters. The best feature selection was computed by a sequential classification approach that is described in the next Chapter.

The decodability is expressed in a mean accuracy. The mean accuracy was computed across five independently computed accuracies, which corresponded to the outer cross-validation. To estimate the significance of the mean accuracy, a randomization approach was applied. The train and test data sets of the inner cross-validation were permuted, and one proceeded with the permutation result as described above with a non-permuted dataset. That means one proceeded with a search for the best parameters for classification and tested on the permuted hold-out test dataset. This was applied 100 times to each inner cross-validation, so 500 times in total. Out of these 500 accuracy values, a mean of five accuracies values, one of each inner cross-validation, was computed and reduced the distribution again to 100 mean accuracies values. The distribution of these accuracies of a random set was used for the distribution of the null hypothesis. Thereafter, the procedure continues with a standard permutation method (see Chapter 2.7.2 Permutation Test) with an alpha level of 5%.

2.12.3 Sequential Classification Procedure

The best feature identification was achieved by a sequential classification approach. The aim of this approach was to identify a sequence of voxels that were most informative for the pattern classification. In the following, we will describe the procedure.

First, the pattern classification was applied to each voxel and participant separately. This means that the number of voxels determined the number of applied pattern classification for each participant. In other words, each pattern classification used one voxel only as a feature. Then, the median accuracy across the participants was computed for each feature, and the best feature was determined by the highest median accuracy across participants. Next, the pattern classification was applied on two-dimensional feature vector including always the best feature of the one-dimensional feature pattern classification and one of the remaining features. Continuing this led the last run consider all features for one pattern classification. Again, for each run the best feature was determined by the median accuracy across participants. Each proceeding pattern classification, which was applied on a n-dimensional feature vector, used a feature combination, always including the best feature of the previous pattern classification applied. This continued until all voxels as a feature were included for pattern classification.

For a better understanding, I will give the following real-life example: The beamformer revealed six peak voxels that changed significantly across the sequential positions. With a pattern classification approach introduced above one can answer the question if some of the peak voxels were more relevant as others, or if all peak voxels are equally relevant. Therefore, each voxel is determined as a feature for the single pattern classification. Thus, six pattern classifications were applied with a unique one-dimension feature for each participant. This results in that many accuracy values as participants times features exist: 41 participants times 6 features are equal to 246 accuracies values. That means for each feature 41 accuracy values of 41 participants exist. For each of these features the median accuracy was computed across participants. This revealed that the third feature reached the highest median accuracy. Next, this third feature was selected to build five two-dimensional features with each of the remaining features, resulting in these feature pairing: 3-1, 3-2, 3-4 and 3-5. This results to continue with five pattern classifications (for each participant) with one unique two-dimensional feature vector and again to compute the median accuracy across the participants. The best two-dimensional feature determined by the best median accuracy results to continue the same procedure with four feature triplets, a three-dimensional feature classification. This continues until the

last pattern classification is applied to a six-dimensional feature vector. After all, one determined a sequence of the best voxels and identifies which feature dimension had the by the highest median accuracy.

2.13 fMRI Data Analysis

2.13.1 fMRI Data Pre-Processing

MR image processing and analysis were performed using the MATLAB toolbox *Statistical Parametric Mapping (*SPM12b c2014, Welcome Trust Centre for Neuroimaging, University College http://www.fil.ion.ucl.ac.uk/spm). The first five volumes were deleted to remove the initial T1 magnetic transient. The echo planar images were subjected to a standard pre-processing procedure including distortion, motion and slice scan time correction. B0 distortion was corrected by recorded phase and magnitude maps that were recorded in-between the sessions. The first and second sessions were corrected with the same maps recorded in-between, the third with phase and magnitude maps recorded between the second and third sessions. The bias-corrected images were motion-corrected by a realignment procedure, obtaining 6 linear regressors describing the correction parameters applied at each volume. Realigned images were corrected for differences in acquisition time of each slice by using the mid slice (slice 20) as reference within one volume. In parallel, the anatomical T1 images were segmented with a light bias regularization of 0.001 into six different tissues that were 1) grey matter, 2) white matter, 3) CSF, 4) bone, 5) soft tissue and 6) air/background. These maps were used to segment the corrected echo planar images to improve a followed-up whole brain co-registration of echo planar and T1 images. Co-registered images were spatially normalized into standard space to the EPI MNI template in SPM and finally were smoothed with a Gaussian filter in each coordinate direction with a kernel of 6 mm.

2.13.2 First and Second Level Analysis

For each participant, an F-contrast was performed for the factor *Sequence position* in the cue phase (first-level statistics) and parametrically modulated as the average pattern of discriminability of the behavioural analysis revealed. This was a stepwise increase from the first to the third and a decrease to the fourth sequential position (like: $1 < 2 < 3 > 2$). Each further event of the event-related design was defined as a regressor, which were the durations of (1) sample stimuli, (2) test image, (3) question mark, (4) ITI, (5) animal stimuli, (6) scramble stimuli, (7) information screens. The (8) button press was set as an event with no duration specified. Theses contrast images of each participant were employed for the second-level analysis. We conducted a whole brain analysis using a group t-contrast. Eklund and colleagues (Eklund et al., 2016) pointed out that a multiple comparison correction applied cluster-wise increase the false positive rate. Thus, we proceed with a voxel-wise FWE correction implemented in SPM. The FWE correction implemented in SPM estimated the actual number of independent tests by using random filed theory and corrects the threshold accordingly. Here, an FWE correction was applied with a statistical threshold for all voxels at $p < 0.05$, with a minimum voxel cluster of 10 contiguous voxels, to maintain minimal type I and II errors.

3 Results

3.1 Behaviour Results

To investigate the behavioural effect of the factor *Sequence position,* hit rates (HR), response rates (RR), reaction times (RT) and signal detection theory (SDT) measures (discriminability and response bias) have been analysed. The main effect of the factor *Sequence position* was investigated by means of a repeated measure ANOVA. Because the ANOVA does not reveal any directionality, post-hoc a permutation *t*-test was applied on HR, RR and SDT measures. For RT, the factor *Sequence position* was analysed by means of a Friedman test and for post-hoc a Wilcoxon signed rank test was applied to determine directionality. To compare the results for the different behavioural measures and the three studies, the effect sizes of the main effect and simple effects were compared.

3.1.1 Pilot Study

The pilot study revealed effects of the factor *Sequence position* for the incremental sequence and randomized sequence conditions (in the following, 'IS and RS condition'), but in different types of response measures. First, the significant effects for the IS condition and second the significant effects for the RS condition were summarized.

For the IS condition, the ANOVA revealed a main effect of the factor *Sequence position* in (1) HR for match responses (F=8.11, p=0.001, Eta^2=0.18), in (2) RR for match responses (F=9.50, p=0.0008, Eta^2=0.19) and (3) non-match responses (F=9.50, p=0.0006, Eta^2=0.19) (Figure 3-1 and Table 3-1). The post-hoc analysis of each main effect revealed two significant simple effects, which were consistently the same for each of the significant main effects. These two simple effects were the second and the third simple effects. Both simple effects indicated an increase in match responses for HR (1vs3: t=-3.47, p=0.0348, CoD=1.19; | 1vs4: t=-4.19, p=0.0140, CoD=0.97) and and RR (1vs3: t=-4.44, p=0.0098, CoD=1.34; | 1vs4: t=-3.96, p=0.0165, CoD=0.99). In contrast, these two simple effects indicated a decrease in the non-match responses of the RR (1vs3: t=-4.44, p=0.0098, CoD=1.34; | 1vs4: t=-3.96, p=0.0165, CoD=0.96). The mean of the HR and

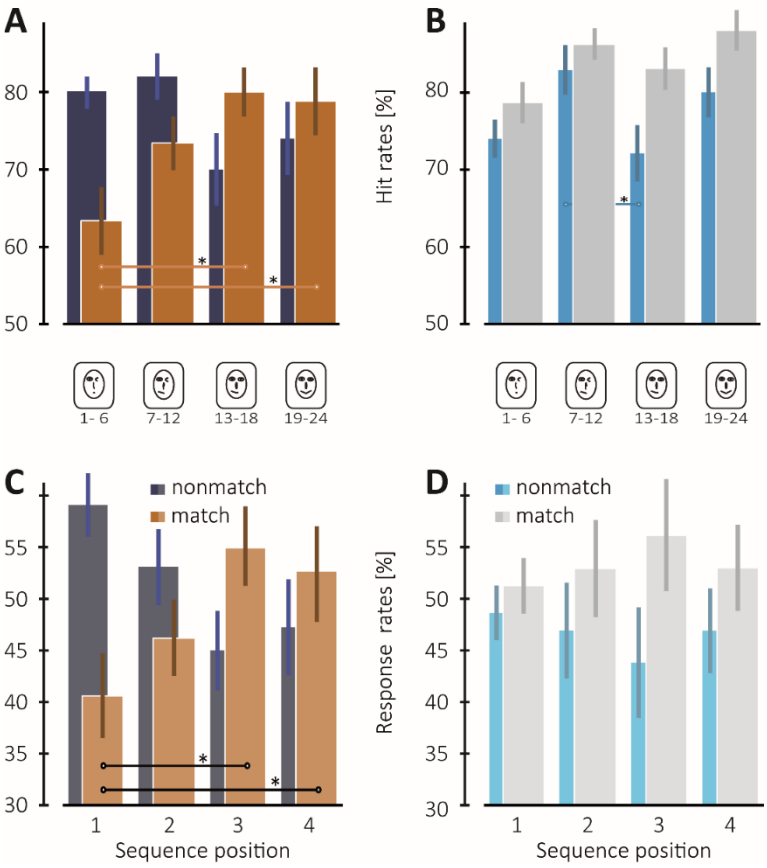

Figure 3-1: *Behaviour measures of the pilot study: Hit and response rates for incremental (IS) and randomized sequence (RS) conditions*. **A**: The IS condition revealed that the participants got better in target identification across the sequential positions by the increase in the mean hit rate for match response but not of the non-match responses. **B**: For the RS condition, the participants showed a high performance by hit rates already for the first sequential position and performance drop in the middle. **C**: For the IS condition response rates for match and non-match responses followed an opposing trend across the four sequential positions: The match responses increased while the non-match decreased. **D**: For the RS condition, no significant changes were observed regarding the match and non-match responses. The error-lines represent standard error. Horizontal lines and an asterisk indicate a significant effect of simple effects ($p<0.05$, corrected for multiple comparison). A horizontal line connecting two bars and together with an asterisk indicate a significant post-hoc dependent sample *t*-test of a simple effect. (Red asterisks = $p<0.001$; Black asterisks = $p<0.05$). The icons between the upper (A & B) and the lower (C & D) panel indicate from left to right from the first to the fourth sequential position. The number below the icons referred to the six trials the sequential position consisted of. One example, the first icon referred to the first sequential position and consisted of the first six trials of a series.

RR led to the interpretation of a stepwise increase (match) or decrease (non-match) until the third sequential position, but only the second and third simple effects verified a significant increase (or decrease) in comparison to the first sequential position. Regardless of the sequential position, there is no effect between the HR of match and non-match responses ($HR_{(match)}$=73.96%, $HR_{(non\text{-}match)}$=76.55%; t=-0.43, p=0.6771

CoD=0.25) and RR of match and non-match responses ($RR_{(match)}$=48.82%, $RR_{(non-match)}$=51.18%; t= 0.37, p=0.7190, CoD=0.2454).

Analysing the RT, the Friedman test revealed no significant effect of the factor *Sequence position* in any of the response types of interest (Figure 3-2 and Table 3-2). However, the RT for HR for match and non-match responses showed a tendency towards longer latencies for non-match responses compared to match responses ($RT_{(match)}$=0.833s, $RT_{(non-match)}$=0.972s, Z=-1.78, p=0.074, CoD=1.31).

For the RS condition, the ANOVA revealed a main effect of the factor *Sequence position* in HR for non-match response only (F=4.44, p=0.0464, Eta^2=0.10; see Table 3.2). The post-hoc analysis of HR for non-match responses revealed one significant simple effect. This simple effect revealed a decrease in HR between the second and the third sequential positions (2vs3: t=3.97, p=0.0195, CoD=0.72).

Table 3-1: *Overview of the test results of the pilot study for the different response types.* Repeated measure ANOVA for the factor *Sequence position* for four different response types and for the incremental and randomized sequence conditions. The ANOVA results are related to Figure 3-1. Only between group results are shown. P-values were Bonferroni-Holm corrected.

	SS	df	MS	F	P-Value	Eta^2
Incremental sequence condition						
Hit rate, match responses	0.17	3	0.05	8.10	0.0010	0.1886
Hit rate, non-match responses	0.09	3	0.03	2.87	0.0545	0.1195
Match response rate	0.12	3	0.04	9.49	0.0007	0.1947
Nonmatch response rate	0.12	3	0.04	9.49	0.0005	0.1947
Randomized sequence condition						
Hit rate, match responses	0.05	3	0.01	2.13	0.3577	0.1037
Hit rate, non-match responses	0.08	3	0.02	4.44	0.0464	0.1017
Match response rate	0.01	3	0.00	1.06	0.7614	0.0493
Nonmatch response rate	0.01	3	0.01	1.06	0.3807	0.0493

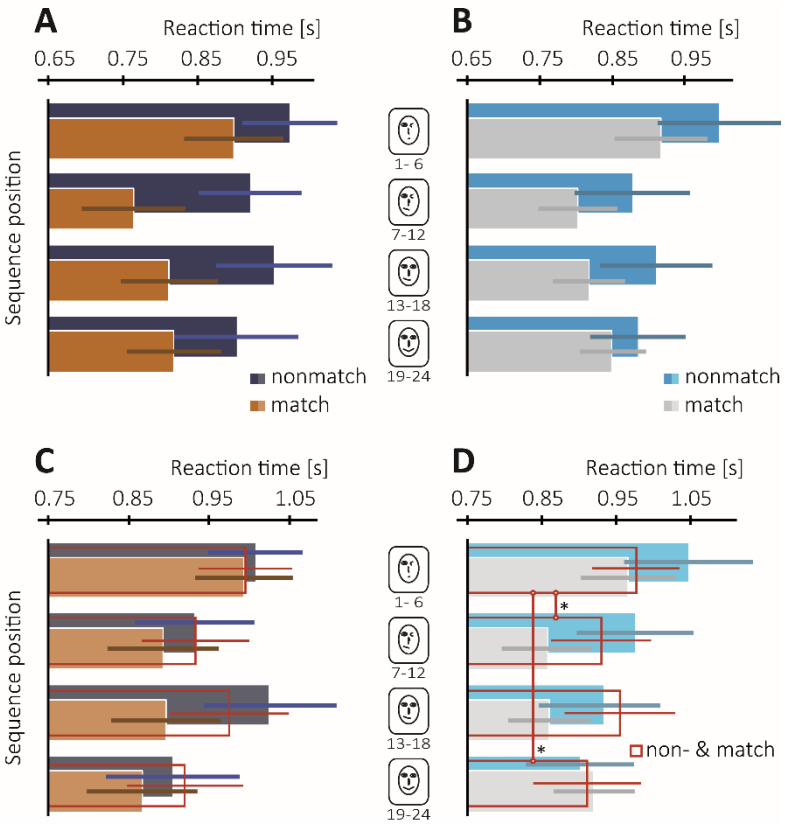

Figure 3-2: *Reaction time (RT) measures of the pilot study for incremental (IS) and randomized sequence (RS) conditions*. Overall, long RT were measured and only a significant decrease of RT for the overall responses was observed. **A:** RT for the hit rates regarding the IS condition revealed no significant differences. **B:** RT for the hit rates regarding the RS condition revealed no significant differences. **C:** RT for the response rate regarding the IS condition revealed no significant differences. **D:** RT for the response rates regarding the randomized sequence condition. The mean difference across the sequential positions was significant for the overall responses (match and non-match responses; indicated by the red squares) when comparing the first versus the second and fourth sequential position. The error-lines represent the standard error. Icons represent the sequential positions and are described in more detail in Figure 3-1. A vertical line connecting two bars together with an asterisk indicate a significant post-hoc dependent sample *t*-test of a simple effect with $p < 0.05$.

Regardless of the sequential position, there is no effect showing a difference between match and non-match responses regarding HR ($HR_{(match)}$=84.02%, $HR_{(non\text{-}match)}$=77.42%, t=1.75, p=0.1133 CoD=0.6684) and RR ($RR_{(match)}$=53.33%, $RR_{(non\text{-}match)}$=46.67%, t=1.70, p=0.1229, CoD=1.08).

Analysing the RT, the Friedman test revealed no significant main effect of the factor *Sequence position* for RT in any response types of interest. But post-hoc a significant decrease from the first to the fourth sequential positions for the *overall* responses was observed. *Overall* responses were defined as all responses regardless of HR or RR of match or non-match responses. The post-hoc analysis of RT for *overall* responses

revealed shorter latencies from the first to the second (Z=2.49, p=0.0125, CoD=2.47) and from the first to the fourth sequential positions (Z=2.60, p=0.0467, CoD=2.76). Nevertheless, regardless of the sequential position, there was no significant difference between RT for match and non-match responses regarding HR ($RT_{(match)}$=0.841 s, $RT_{(non-match)}$=0.926 s, Z=1.68, p=0.0926, CoD=1.20) and RR ($RT_{(match)}$=0.884 s, $RT_{(non-match)}$=0.953 s, Z=1.68, p=0.0926, CoD=1.20).

In sum, the IS and RS conditions tested in the pilot study revealed different main effects for the factor *Sequence position* across the response types of interest. For the IS condition, a main effect was observed for HR and RR of match responses, and for the RS condition a main effect was observed for the HR for non-match responses. The simple effects of HR and RR for match and non-match responses reveal a different response pattern across the sequential positions for the RS and the IS conditions: An increase was observed in HR and RR for match responses for the IS condition which is not present in the RS condition. The missing main effect of the factor *Sequence position* in RT accounted for both.

Table 3-2: *Overview of the test results of the pilot study for the different reaction times.* Friedman test results for the factor *Sequence position* for five different reaction times and for the incremental and randomized sequence conditions. The results are related to effects shown in Figure 3-2. Only between group results are shown. P-values are Bonferroni-Holm corrected.

	SS	df	MS	Chi²	P-Value	Eta²
Incremental sequence condition						
Hit rate, match responses	5.20	3	1.73	3.12	0.3735	0.104
Hit rate, non-match responses	2.00	3	0.67	1.20	0.7530	0.040
Match response rate	0.60	3	0.20	0.36	0.9484	0.012
Nonmatch response rate	5.60	3	1.87	3.36	0.3394	0.112
Overall response	3.60	3	1.20	2.16	0.5399	0.072
Randomized sequence condition						
Hit rate, match responses	4.20	3	1.40	2.52	0.4717	0.084
Hit rate, non-match responses	11.6	3	3.87	6.96	0.2927	0.232
Match response rate	7.8	3	2.60	4.68	0.3936	0.156
Nonmatch response rate	11	3	3.67	6.60	0.2574	0.220
Overall response	15.2	3	5.07	9.12	0.1387	0.304

3.1.2 Response Behaviour in the MEG Experiment

For the MEG experiment, we continued with the incremental sample sequence and the double amount of trials (compared to the pilot study) enabled MEG response analysis. For the behaviour analysis of the MEG experiment, we introduced two additional measures proposed by signal detection theory (SDT) which were discriminability measured by d-prime and response bias measured by criterion C. This was also made possible by the larger number of trials, which increased the probability of false alarms for every sequential positions. Responses of 41 participants were respected.

The ANOVA revealed four significant and one tendency of a main effect of the factor *Sequence position*. These significant main effects were observed in: (1) HR for match responses ($F=15.43$, $p=0.00001$, $Eta^2=0.095$), (2) RR for match responses ($F=11.17$, $p=0.00001$, $Eta^2=0.070$), (3) RR for non-match responses ($F=911.12$, $p=0.0006$, $Eta^2=0.070$) and (4) response bias ($F=4.83$, $p=0.0098$, $Eta^2=0.033$). The tendency was observed in the SDT measure discriminability ($F=4.83$, $p=0.0582$, Eta^2 0.027).

The post-hoc analysis of HR for match responses revealed three significant simple effects, which indicated a stepwise increase until the third sequential position. The first simple effect indicated an increase (1vs2: $t=-4.57$, $p=0.0002$, $CoD=0.605$), so did the second (1vs3: $t=-6.00$, $p=0.00001$, $CoD=0.852$) and the third simple effects (1vs4: $T=-5.65$, $p=0.00001$, $CoD=0.813$).

The post-hoc analysis of response rate for match and non-match responses revealed five significant simple effects each. The stepwise increase of response rates for match, and decrease for non-match, was validated by all simple effects except the fourth (2vs3) simple effect, which probably indicated a plateau effect in-between the increase (or decrease) from the first to the last sequential positions. Regarding the pattern of the RR, both match and non-match responses reached a chance level at the last sequential position. The significant main effect of response bias was accompanied by a significant decrease from the first to the last sequential positions ($t=3.30$, $p=0.0123$, $CoD=0.497$). This registered decrease of response bias was a decrease within a conservative response bias.

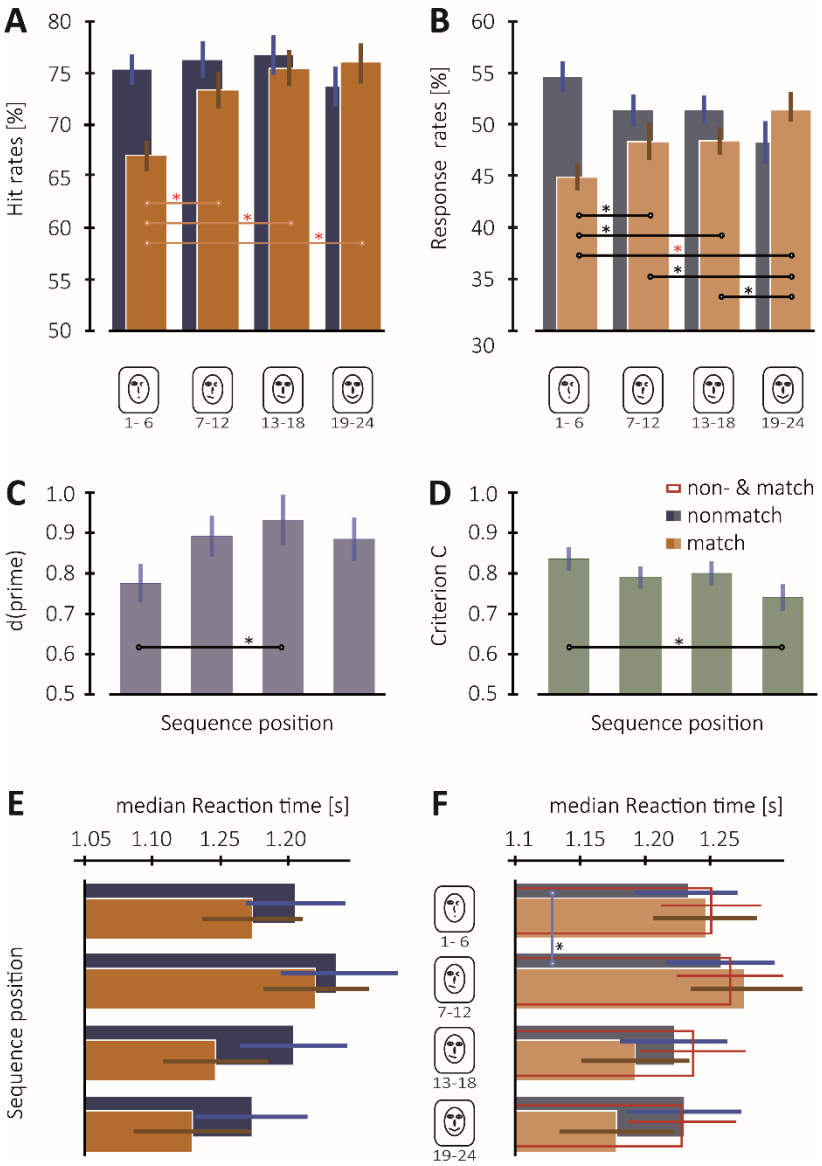

Figure 3-3: *Behaviour measures of the MEG study: hit- and response rate,* discriminability *and response bias and reaction times*. The behaviour measures revealed a positive progress of target identification across the first three sequential positions. **A:** Hit rates of match responses significantly increased from the first sequential position onward. No significant changes of hit rates of non-match responses were observed across the sequential positions. **B:** The response rates of match and non-match responses followed an opposing trend across the sequential positions: The match responses significantly increased while the non-match significantly decreased reaching chance level. **C:** A post-hoc analysis revealed that the discriminability increased significantly from the first to the third sequential positions. Participants detected the target face better upon a better signal to noise ratio. **D:** Criterion C values between 0.7 and 0.9 indicated no change in response bias. However, the significant drop from the first to the last sequential position indicates a minor shift in a less conservative response bias. **E:** Long reaction times for match and non-match hit rates indicate a difficult task and no significant changes were observed. **F:** A post-hoc analysis revealed that the RT increased for the non-match response rate from the first to the second sequential positions. A horizontal line connecting two bars and together with an asterisk indicate a significant post-hoc dependent sample *t*-test of a simple effect. A vertical line connecting two bars together with an asterisk indicated a significant post-hoc Wilcoxon signed rank test (Red asterisks = p<0.001; Black asterisks = p<0.05). The error-line at each bar represent the standard error. The icons between the panels are described in Figure 3-1.

This means that participants responded in a less conservative manner across the sequential positions and did not develop a more liberal response pattern as a decrease could suggest (C =0.793, SD=0.194).

Regardless of sequential position, no HR or RR effects for match vs. non-match responses were observed ($HR_{(match)}$=0.73%, $HR_{(non\text{-}match)}$=0.75%, t=-1.04, p=0.3037, CoD=0.2455 | $RR_{(match)}$=0.48%, $RR_{(non\text{-}match)}$=0.51%, T=-1.30, p=0.2016, CoD=0.4067.

Analysing the RT, the Friedman test revealed no significant effect of the factor *Sequence position* in any of the response types of interest. The post-hoc analysis revealed the first simple effect to be significant for RT for the non-match responses (1vs2: T=-2.55, p=0.0109, CoD=0.867). Regardless of the sequential position, no RT effects for match vs. non-match responses were observed for HR (Z=-0.99, p=0.3232, CoD=0.312) and RR (Z=-1.05, p=0.2918, CoD=0.33).

Table 3-3: *Overview of the test results of the MEG study for the different response types and reaction times.* Repeated measure ANOVA for four different response types and the signal detection theory measures discriminability and response bias. Friedman test for the factor Sequence position for five different reaction times. The results are related to effects shown in Figure 3-3. Only between group results are shown. P-values are Bonferroni-Holm corrected.

Response types	SS	df	MS	F	P-Value	Eta²
Hit rate, match responses	0.21	3	0.06	15.43	0.0000	0.0950
Hit rate, non-match responses	0.02	3	0.00	1.66	0.1788	0.0098
Match response rate	0.09	3	0.03	11.17	0.0000	0.0697
Nonmatch response rate	0.09	3	0.03	11.12	0.0000	0.0690
Sensitivity	0.54	3	0.18	3.11	0.0581	0.0267
Response bias	0.21	3	0.07	4.83	0.0098	0.0332
Reaction times	SS	df	MS	Chi²	P-Value	Eta²
Hit rate, match responses	4.76	3	1.59	2.85	0.4147	0.0017
Hit rate, non-match responses	6.56	3	2.19	3.94	0.5368	0.0011
Match response rate	7.05	3	2.35	4.23	0.7132	0.0010
Nonmatch response rate	13.29	3	4.43	7.97	0.2326	0.0017
Overall response	13.01	3	4.34	7.83	0.1989	0.0011

3.1.3 Response Behaviour in the fMRI Experiment

For the fMRI experiment, the paradigm was altered to meet the criteria of fMRI measurements, which was jittering the timings. Further, another stimulus category (animal) was included to disentangle match operations from visual memory and visual model building but also to disentangle the time dependencies across the sequential positions. That means in every series the animal stimuli did appear at a different position within in a sequential position. In a post-measures questionnaire, all participants reported that the animal stimuli did not intrude the identification and learning of the target face. For the fMRI experiment, 6 series were measured, which was half of the number of series of the MEG experiment. For all behaviour measures, 36 participants were respected.

The ANOVA revealed for all response types but the response bias significant main effects of the factor *Sequence position* (Table 3.4). Considering the effect size, the strongest effect was observed in the HR for match responses (F=21.40, p=6.7*10^-11, Eta²= 0.167), followed by discriminability (F11.26, p=3*10^-6, Eta²=0.133).

The post-hoc analysis of HR for match responses revealed three significant simple effects. These significant simple effects were the first three simple effects, which indicated via the mean HR and the effect sizes an increase from the first to the second sequential positions (1vs2: t=-5.38, p=1.3*10^-5, CoD=0.913) but not further. The subsequent two simple effects (1vs3: F=-5.77, p=0.00015, CoD=1.014; 1vs4: F=-5.88, p=1.1*10^-6, CoD=1.088) were significant and hardly differed in effect size. This could indicate a stabilizing saturation effect of HR across sequential positions. The post-hoc analysis of HR for non-match responses revealed only an increase from the first to the third sequential positions by a significant second simple effect (1vs3: F=-3.10, p=0.0277, CoD=0.430).

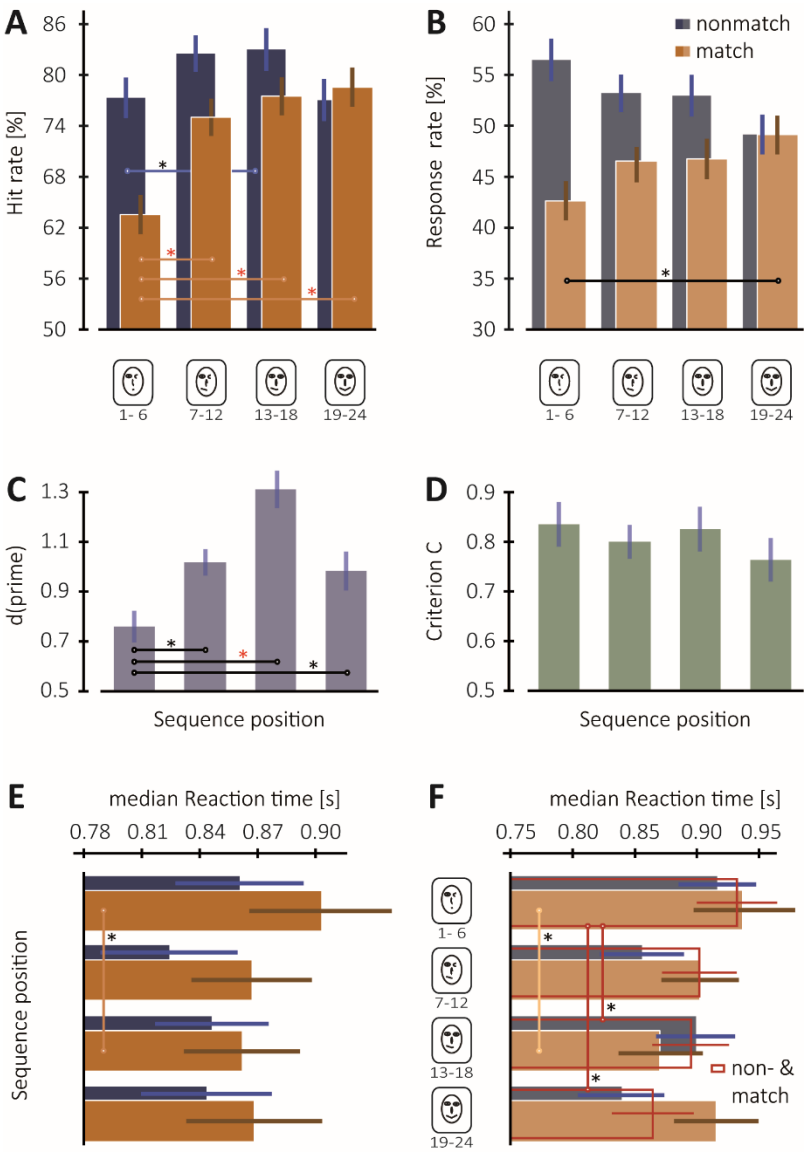

Figure 3-4: *Behaviour measures of the fMRI study: Hit and response rate, discriminability and response bias, and reaction times.* The behaviour measures revealed a positive progress of target identification across the first three sequential positions. **A:** Hit rates of match responses significantly increased from the first sequential position with a saturation effect beginning at the second sequential position. Hit rates of non-match responses increased significantly from the first to the third sequential positions only. **B:** The response rates for match and non-match responses followed an opposing trend across the sequential position: The match responses significantly increased while the non-match responses significantly decreased reaching chance level. **C:** Discriminability significantly increased always compared to the first sequential position. Participants detected the target face better upon a better signal to noise ratio. **D:** Criterion C values between 0.7 and 0.9 across the sequential position indicated no change in the response bias. Participants remained conservative when responding with 'Yes'. **E:** Long reaction times of hit rates of match and non-match responses indicate a difficult task. Only a post-hoc analysis revealed a significant decrease in reaction times of hit rates of match responses. **F:** Reaction times of response rates significantly decreased from the first to third sequential position for the match responses and when considering overall responses (match and non-match responses together) also from the first and the fourth sequential position. A horizontal line connecting two bars and together with an asterisk indicate a significant post-hoc dependent sample *t*-test of a simple effect. A vertical line connecting two bars together with an asterisk indicated a significant post-hoc Wilcoxon signed rank test (Red asterisks = $p<0.001$; Black asterisks = $p<0.05$). The error-line at each bar represent the standard error. The icons between the panels are described in Figure 3-1.

The post-hoc analysis of RR for match and non-match responses revealed the third simple effect to be significant. The RR for the match responses increased from the first to the last sequential positions (1vs4: F=-3.5, p=0.0078, CoD=0.571), and simultaneously the RR for non-match responses decreased (1vs4: F=3.62, p=0.0055, CoD=0.542). The curse of the mean RR across the sequential positions indicated an increase (match responses) and decrease (non-match responses) to chance level until the fourth sequential position.

The post-hoc analysis of the discriminability revealed three significant simple effects. These were the first (1vs2: F= -4.48, p=0.0069, CoD=0.678), the second (1vs3: F=-5.95, p=2.4*10^-6, CoD=0.923) and third simple effect (1vs4: F=-3.61, p=0.0061, CoD=0.585). All revealed an increase across the sequential position. The post-hoc analysis of the response bias indicated no difference in criterion C across the sequential positions. This means that the participants stay on the same level of conservative responses.

Table 3-4: *Overview of the test results of the fMRI study for the different response types and reaction times.* Repeated measure ANOVA for four different response types and the signal detection theory measures discriminability and response bias. The results are related to effects shown in Figure 3-3. Only between group results are shown. P-values are Bonferroni-Holm corrected.

Response types	SS	df	MS	F	P-Value	Eta²
Hit rate, match responses	0.52	3	0.17	21.40	0.0000	0.1669
Hit rate, non-match responses	0.10	3	0.03	4.548	0.0049	0.0332
Match response rate	0.08	3	0.03	5.392	0.0034	0.0421
Nonmatch response rate	0.08	3	0.03	5.437	0.0049	0.0382
Sensitivity	2.15	3	0.72	11.26	0.0000	0.1326
Response bias	0.08	3	0.03	1.20	0.3161	0.0161

Reaction times	SS	df	MS	Chi²	P-Value	Eta²
Hit rate, match responses	15.28	3	5.09	9.16	0.0815	0.0849
Hit rate, non-match responses	8.00	3	2.67	4.80	0.3741	0.0444
Match response rate	20.44	3	6.81	12.26	0.0261	0.1136
Nonmatch response rate	4.17	3	1.39	2.50	0.4753	0.0231
Overall response	28.72	3	9.57	17.23	0.0032	0.1596

Analysing the RT, the Friedman test revealed two main effects the factor *Sequence position* for RT. One main effect was observed for RT regarding RR for match responses (Chi^2=12.26, p=0.0261, Eta^2=0.114) and for RT regarding the *overall* responses (Chi^2=17.23, p=0.0032, Eta^2=0.160). The post-hoc analysis revealed for both main effects a decrease in RT for the second simple effect and for the *overall* responses additionally for the third simple effect.

3.1.4 Summary of Behaviour Analysis by Effect Sizes

The pilot study demonstrated that the incremental sequence of sample stimuli revealed main effects of the factor *Sequence position* of HR for match and not for non-match responses, so did the MEG study. The fMRI study additionally showed a main effect of the factor *Sequence position* of HR for non-match responses. However, the comparison of effect sizes across the studies revealed that there was the same pattern of effect sizes across the response types for every study: First, the effect sizes measured for HR for match responses were always about 0.1 bigger than for non-match responses. Here, for the MEG experiment the weakest effect size for non-match responses altogether were observed (Figure 3-5). Second, the effect sizes measured for RR for match and non-match responses showed for every study that the differences were minor between match and non-match. However, across the studies we measured overall high effect sizes for the pilot study. Prominently for the fMRI study were the high effect sizes for HR for the match responses and discriminability. Whereas for the MEG study high effect sizes for the HR for match responses but also for RR for either match and nonmatch responses was considerable.

The SDT measures discriminability and response bias were only present for the MEG and fMRI studies (Figure 3-5-A). Only for the fMRI study high effect sizes were observed for discriminability, all others were small. However, for the MEG experiment the small effect sizes for response bias refer to a significant effect and the small effect sizes for discriminability to tendency. The comparison of effect sizes regarding the RT across the three studies indicated that the MEG experiment only revealed (very) small effect sizes. These weren't even visually not detectable in the visualization (Figure 3-5-B). Further,

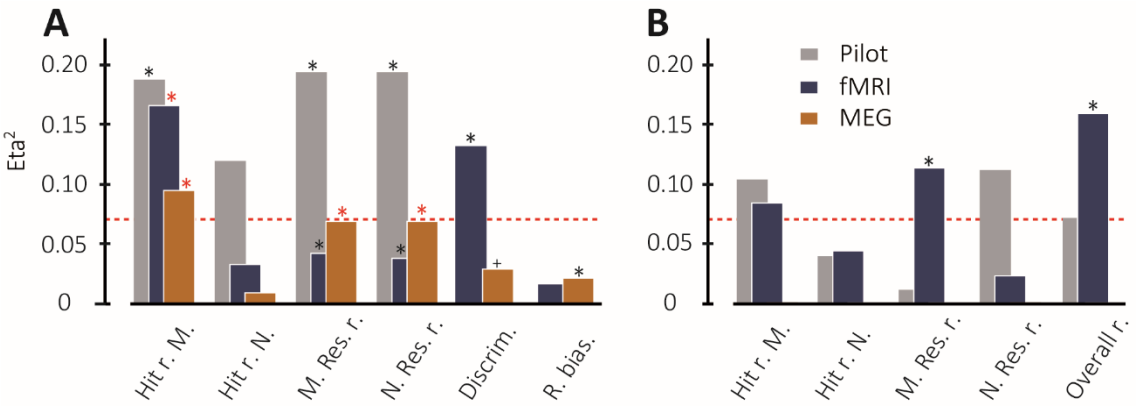

Figure 3-5: *Comparison of the effect size (ES) regarding the main effect for the factor Sequence position across the three studies.* **A**: ES of the different response types. For hit rates of match responses all three studies show a high ES and a significant main effect. This is not the case for hit rates for non-match responses. For match responses, the Pilot study revealed highest ES but regarding this all studies showed a significant main effect. For Discriminability only the fMRI study revealed a high ES and a significant main effect. Here the MEG study revealed a tendency with a small ES only. For response bias the ES are small for both studies but significant for the MEG study. **B**: ES related to main effects of reaction times were only possible to be comparable between the Pilot and the fMRI studies because the effect sizes regarding the MEG study did not exceed 0.01. For the RT only two main effects were observed in the fMRI study. These were a main effect for RT of match response rate and RT of overall response rate. Both ES refer to high ES. The red dashed line in the background indicates the threshold of an ES called medium (Eta-square 0.06). Asterisks indicate the corresponding main effect to be significant (red asterisks: $p<0.001$; black asterisks $p<0.05$). Abbreviations: Hit rates of match (Hit r. M) and non-match (Hit r. N) responses; response rates for match (M. Res.r.) and non-match (M. Res.r.), discriminability (Discrim.) and response bias (R. bias).

we observed two main effects of the factor *Sequence position* for the RT for the fMRI study. For these two significant main effects, we observed large effect sizes.

The effect sizes with regards to the simple effects are illustrated in Figure 3-6 and picture a remarkably overall result: The first three simple effects revealed in almost all response types the higher effect sizes, and within these the largest was observed in the second or third simple effects. That clarifies that most processes happen in contrast to the first sequential position. This also holds for the discriminability and differs from the response bias. Regarding the response bias, the MEG study revealed a maximum medium effect size only for the third simple effect and all others remained below.

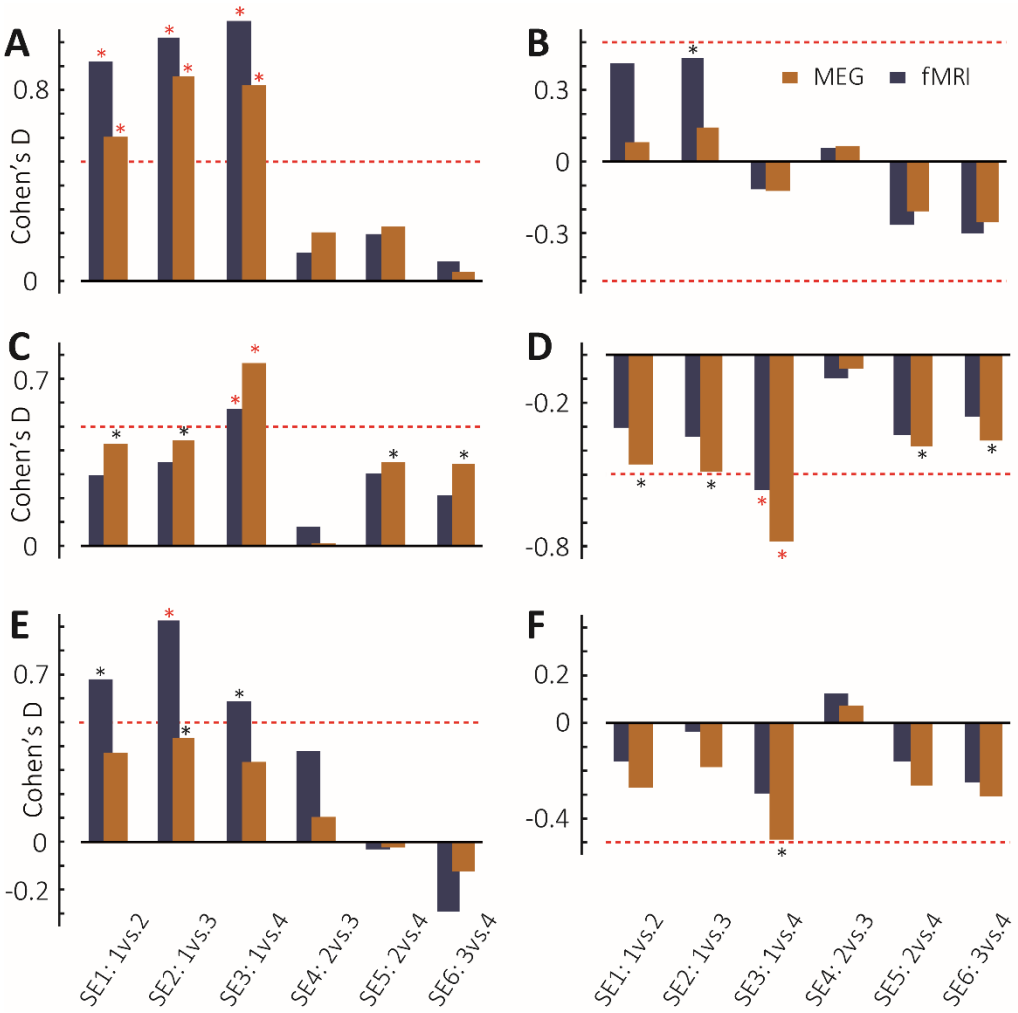

Figure 3-6: *Comparison of effect sizes (ES) for the MEG and fMRI study as a function of simple effects for all response types and the signal detection theory measures.* Given this overview, the MEG and fMRI studies revealed a similar pattern with minor differences. **A:** ES for hit rates of match responses: In both experiments, high ES were observed for the first three simple effects. **B:** ES for hit rates of non-match responses: Only ES below medium were observed. **C:** ES for match response rates: A medium ES was observed for the third simple effect for both studies only. **D:** ES for non-match response rates: A medium ES was observed for the third simple effect for both studies only. **E:** ES for discriminability: The ES regarding the fMRI was always higher and reached high ES for the second simple effect. **F:** ES for response bias: A medium ES for the third simple effect was observed for the MEG study. The red dashed line in the back ground indicates the threshold of an ES determined medium as proposed by Cohen (1966) (Coh. D < 0.8). Asterisks indicate the corresponding significant simple effect. Red asterisks: p<0.001; black asterisks: p<0.05).

3.2 MEG Sensor Data

At the MEG sensor level, we investigated two additional effects to validate the paradigm. First, the learning task was compared to other learning studies using face stimuli in sequences. For this comparison, we employed an event-related field (ERF) analysis and the wide field of ERF literature reporting differences in the N250 component when measuring familiarity with EEG or MEG (which would then correspond to the M250). In particular, we tested the hypothesis that the visual learning process should be measurable in the ERF response regarding the sample stimulus and this with the contrast for which the best discriminability was observed. Second, the perceptual closure task was compared to previous studies using two tone images by means of an activation versus baseline analysis of time frequency responses (TFR) (Brodski and Paasch et al., 2015; Grutzner et al., 2010) .

3.2.1 Event-related Fields

As can be seen in Figure 3-7, a strong peak in the ERF responses over occipitotemporal sensors was observed at 90 ms (+/-20 ms), referring to the prominent M100, followed by a second at 140 ms (+/-20 ms) expanding to temporal sensors which we refer to as the prominent M170. Few global peaks can be discriminated best in the Figure 3-8 at: 220 ms, 300 ms, 340 ms and 390 ms, mostly with a width of 30 to 40 ms.

A permutation *t*-test revealed a difference in ERF between the first and the third sequential positions at 157 – 272 ms (p=0.034) for left occipitotemporal sensors. For these sensors and period, a lower amplitude was recorded for the third sequential position than for the first sequential position. For right occipitotemporal sensors, the reverse pattern was observed. The time course indicated a peak at 220 ms over more occipital sensors and a peak 20 ms later (at 240 ms) over frontotemporal sensors. The M250 is ill-defined in time and is usually detected in a broader time window between 200 and 300 ms. However, the M250 is determined by a subsequent global peak after the M100. In the present time course, the M250 component could be the earlier measured and less pronounced peak at 220ms or the later, broader peak at 290ms. A compelling

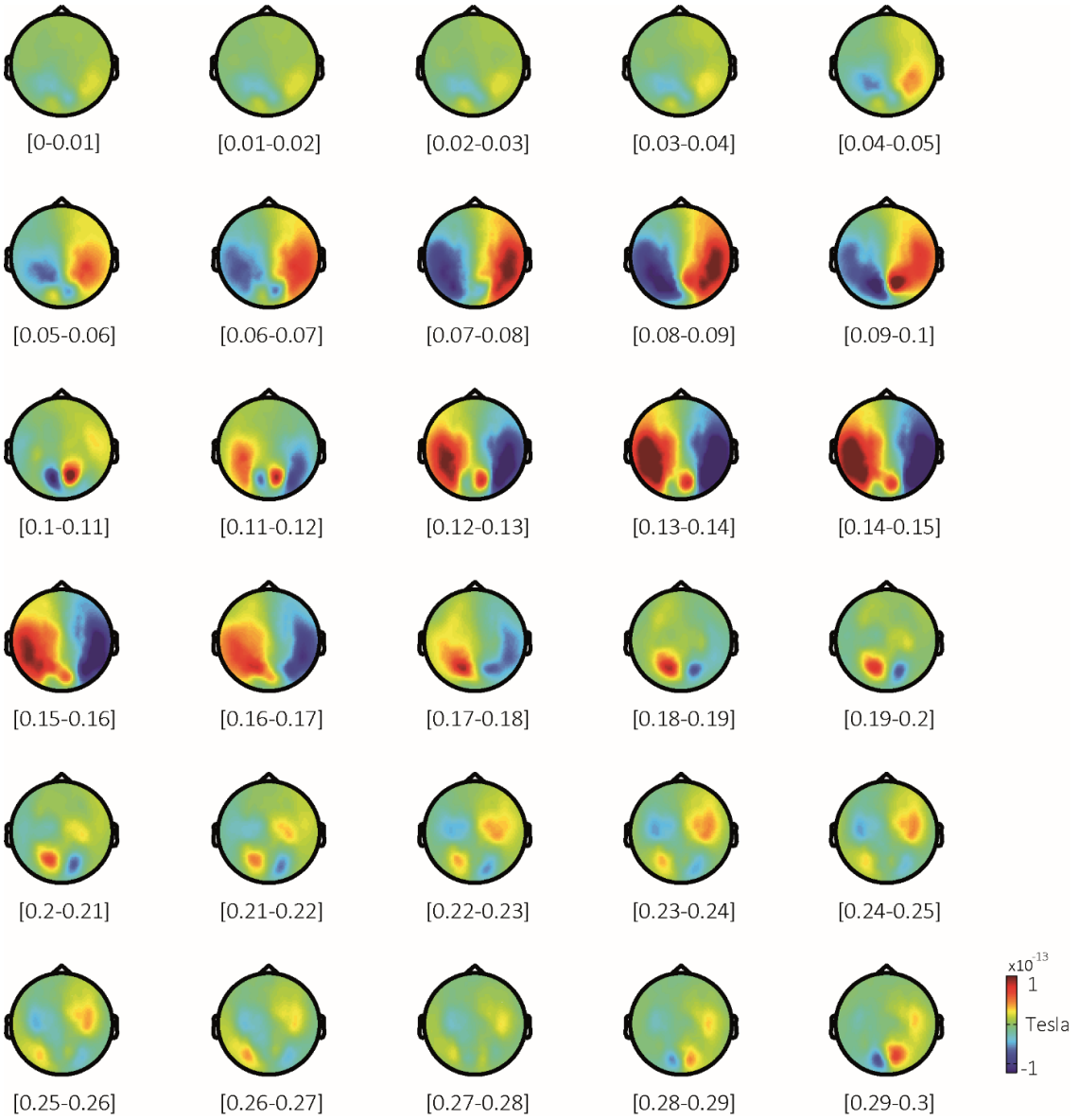

Figure 3-7: *Series of topographical representations of event-related fields (ERF) from 0 to 300 ms for the first sequential position*. Each topography represents an average of non-overlapping consecutive 10ms of ERF signal time-locked to stimulus. Left and right temporal sensors recorded two strong peaks of magnetic field strength, one at 80 to 90 ms and another one at 140 to 150ms. The sign reverses for each side from the one to the other peak. Occipital sensors recorded the two peaks of magnetic field strength at 100 to 110 ms and 170 to 180 ms. Frontotemporal sensors recorded a peak at 230 to 240 ms. The numbers below each topography indicate the starting point and the end of the time in seconds for the represented time average.

reason to assume that M250 might correspond to the earlier peak at 220ms is that the components M100 and M170 are also detected earlier and the peak at 290 ms could refer to one of the adjacent stages proposed by Schweinberger (2016). However, the

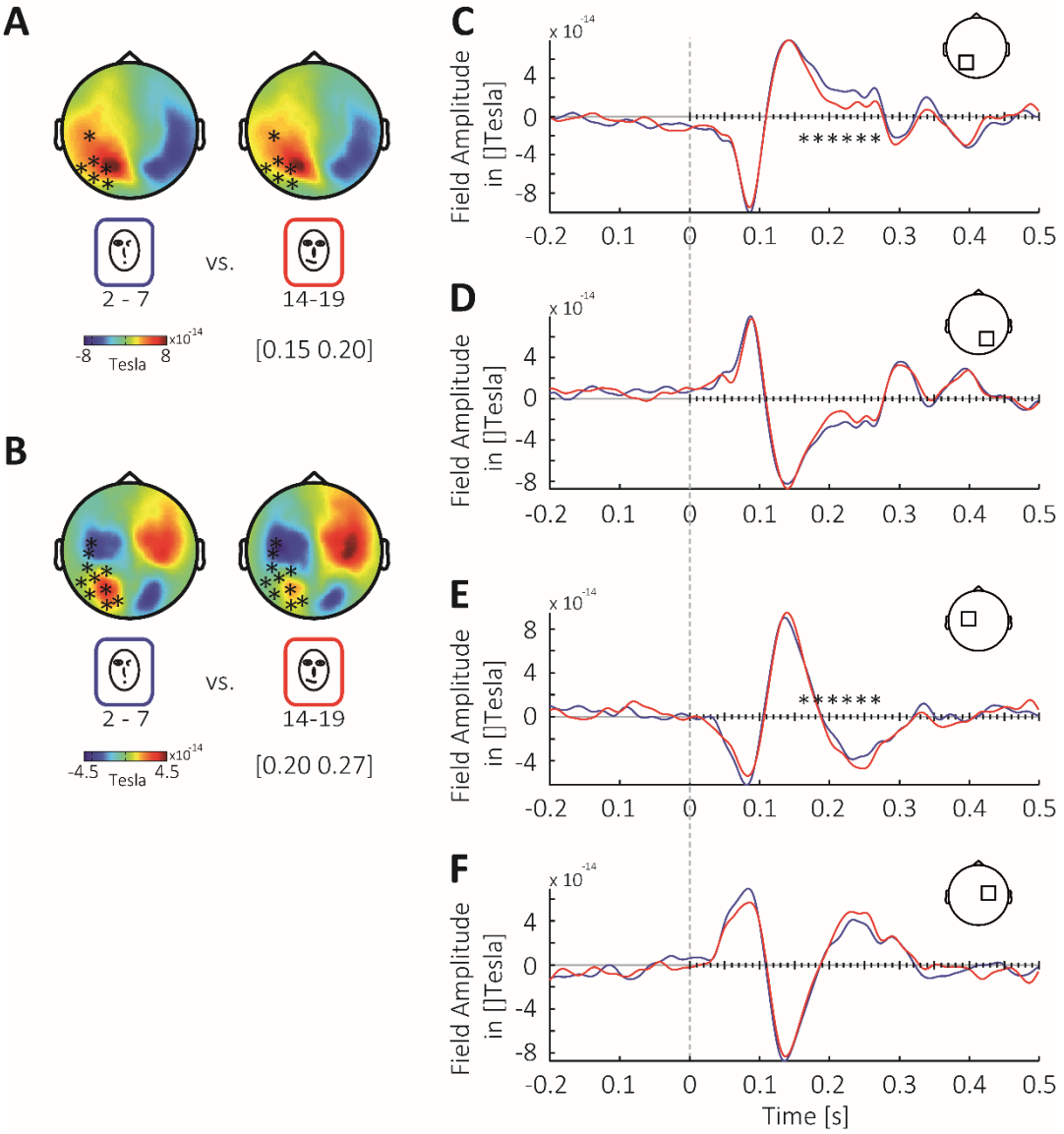

Figure 3-8: *Topography and time-locked signal of significant difference between the first and the third sequential positions*. The permutation *t*-test across all sensors from 1 to 500 ms revealed a significant difference between the first and the third sequential positions in occipitotemporal sensors expanding to frontotemporal sensors from 150 to 270ms. **A:** The left and right topographies show group averages for the first (left) and the third (right) sequential positions. These sequential positions are indicated by icons below the topographies. These two topographies show the earlier effect which revealed peak activation in the occipital sensors with a significant increase on the left side. **B:** The two topographies show the later effect and revealed spatially four global peaks. The peak in frontotemporal sensors and occipitotemporal sensors showed a significant difference between the time course of the first and third sequential positions. **C:** The ERF time course of the left sensor selection (indicated by the icon top right): The ERF-signal was significantly lower for left occipitotemporal sensors of the third than of the first sequential positions with peaks at 220ms and 265ms. Further peaks without a significant difference were at 300ms, 340ms and 390ms. **D:** Here the corresponding right sensors to C are shown. **E:** The ERF time course of left frontotemporal sensors revealed one global peak at 230ms and a significant decrease from the first to the third sequential positions. **F:** Here the corresponding right sensors to F are shown.

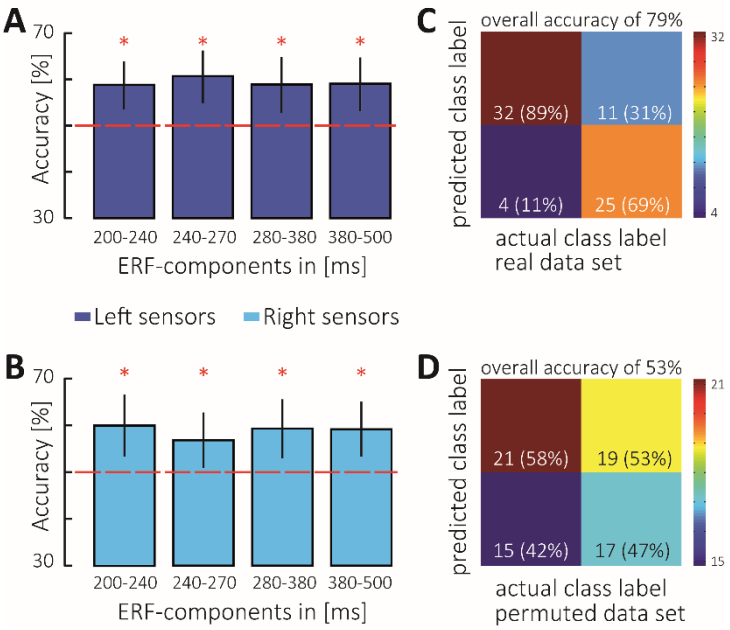

Figure 3-9: *Accuracies of* SVM *classification analysis on ERF-data*. A SVM pattern classification was performed on time- and sensor average ERF for each participant separately. **A:** The participant average accuracies across 41 participants for the left ERF components are displayed. All reached significant results (binomial test), however, the M250 component showed a higher average accuracy than the others. **B:** The average accuracies across 41 participants for the right ERF components are displayed. All reached significant results (binomial test), but here the M250 component showed a slightly lower accuracy than the others. **C:** The confusion matrices of a single participant's result (240 to 270 ms) visualized that trials of the first sequential position are better determined by a decision boundary than trials of the third sequential position. **D:** The confusion matrices of the corresponding (to C) permuted data set revealed accuracies around chance level (50%) as expected. The error-lines at each bar represent the standard deviation.

components could be refined in parsing the time window of interest in an M200 and an M250 component.

A classifier (SVM) analysis was applied to the two different time windows which the *t*-test revealed and additionally two more later components which were determined by the ERF time course. This resulted in five time-windows. The classification performance is illustrated by the median accuracy across the participants for each component for the left and right sensor selection in Figure 3-9-A|B. The significance of a component across the participants was determined by a binomial test. For all components, half or more of the participants revealed significant accuracies above chance level (component 200-240: 22 of 41 participants; component 240-270: 27 of 41; component 280-380: 21 of 41; component 380-500: 22 of 41 participants). The best accuracies were observed for the component 240-270 on the left occipitotemporal sensors (median accuracy=65.28%, SD=6,39). The lowest accuracies were observed for the same component but the right

occipitotemporal sensors selection (median accuracy=56.81%, SD=5.96). On the right occipitotemporal sensors selection, the second-best accuracy was observed for the component 200-240 (median accuracy = 60%, SD = 6.64).

Figure 3-9-C shows the result of a pattern classification for one participant by means of a confusion matrix (participant 31, component 170-200). The average confusion matrix (fivefold cross validation) indicates that the first class, which was the first sequential position, could be correctly predicted by 89% (32 correct and 4 false trials), whereas the second class, which was the third sequential position, could be predicted by 86% (25 correct and 11 false trials). This resulted in an overall performance of 79%.

The significance of a classification performance was determined by locating the accuracy of a classification in a generated null-distribution of accuracies. This distribution was created by applying 100 classifications on permuted data sets. The accuracies of a permuted data set were expected to reach chance level only. The confusion matrix of these accuracies confirmed this (Figure 3-9-D).

3.2.2 Time Frequency Representations

Having established a clear behavioural and neurophysiological effect of familiarity acquisition across the sequential positions, we proceed to motivate the time frequency window for the source analysis in the pre-sample stimulus period which we refer to as

the expectation interval. The grand average of spectral responses across subjects for the expectation interval revealed a peak at 10 Hz which was identified as the distinctive alpha frequency peak (Figure 3-10-A). Limiting this grand average to central-frontal sensors a peak at 17 Hz can be observed which was identified as the distinctive beta frequency peak. Accordingly, we defined the associated frequency band from 7 Hz to 13 Hz (alpha frequency band) and from 15 Hz to 19 Hz (beta frequency band).

Further, in the time frequency representation (Figure 3-10-B) a peak was observed for the beta frequency at around 245 ms for the central-frontal sensor selection. In respect to this peak we defined a time window from -400 ms to -90 ms for the subsequent beamformer analysis.

It was of interest to compare the time frequency representation (TFR) at sensor level of this study with the previous studies of our laboratories (Brodski and Paasch et al., 2015; Grutzner et al., 2010). Therefore, the activation versus baseline contrast was computed. In this contrast, a pronounced GBA was observed in one big significant cluster (p=0.002; Figure 3-11). In more detail, a high GBA (from 70 to > 120 Hz; +-10 Hz) was observed from 50 to 275 ms and a low GBA (from 40 Hz to 70 Hz; +-10 Hz) in a later subsequent time interval until 350 ms.

Previous studies of our laboratories used two-tone stimuli and applied a high spatial filter which made the stimuli more schematic and, therefore, it became more difficult to detect a face. In this present study we skipped the high spatial filter to ensure identity recognition. Comparing the TFR we observe no major differences in the post-stimulus GBA related to post-stimulus processes.

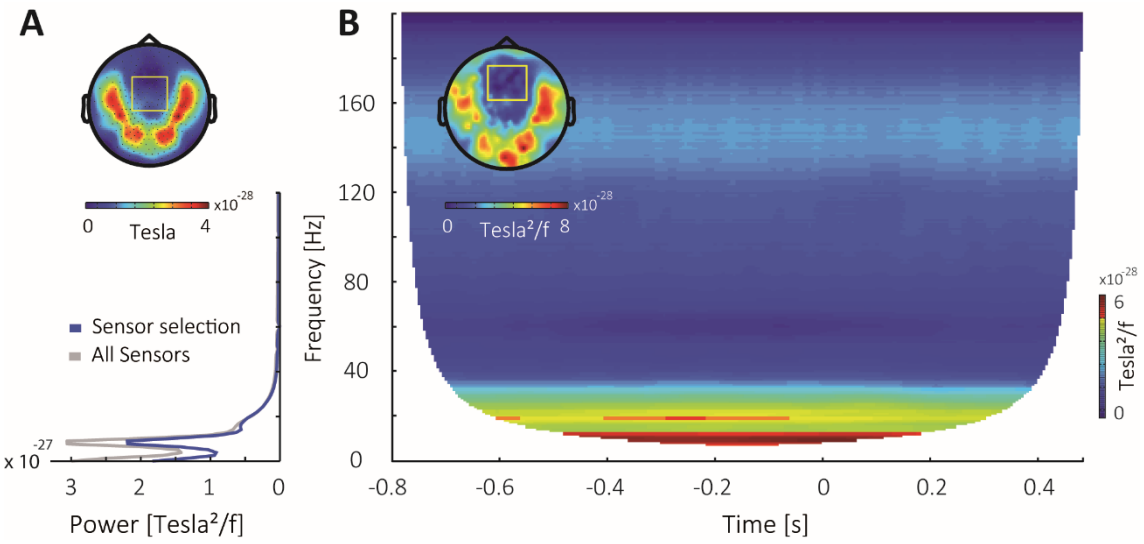

Figure 3-10: *Raw power spectra and time frequency representation of the sensor signal*. **A:** Two power spectra are plotted as a function of frequency (here on y-axis). When averaging the power spectra of all sensors, a pronounced peak in the fieldstrength at 10 Hz and a smooth decrease with frequency were observed (grey line). This peak refered to the center frequency of the alpha frequency band. The related topography indicates large a pronounced fieldstrength in occipital, occipitotemporal and temporal sensors. When selecting central sensors (as indicated by a yellow square in the topographical plot), a second peak was observed at 17 Hz: This peak referred to the center frequency of the beta frequency band. **B:** Time frequency representation grand average of all participants and sequnetial positions of sample trials. At the time point zero, the sample stimulus was presented. The pre-sample stimulus interval (-800 ms to 0 ms) we call the expectation interval. A sharp edge in the colour scale was set from 5 to 5.1 $x10^{-28}$ Tesla to visualize the time interval of pronounced beta (17Hz) from -400 ms to -90 ms pre-sample stimulus.

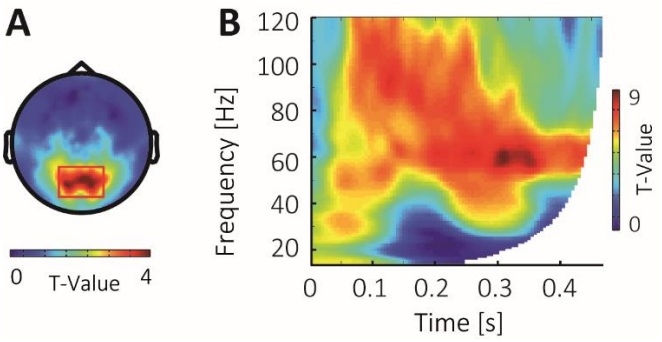

Figure 3-11: *Activation versus baseline statistics of the time frequency representation.* **A:** The topography of the permutation-dependent *t*-test result for activation (0.05ms-500ms) vs. baseline (-500ms to -0.05ms) revealed a significantly enhanced activity in occipital sensors by one big cluster. **B:** The time frequency spectra of the occipital sensors as indicated by the cluster activation in A (MLP51, MRO11, MRP51, MRP52, MZO01). A pronounced high Gamma frequency band activity (GBA) was observed from about 40 Hz to 120Hz.

3.3 MEG Source Localization

A beamformer source analysis of MEG responses was performed to assess the responses in source space that corresponded to the expectation interval. For this purpose, a time frequency analysis at the sensor level was applied which revealed two non-overlapping low frequency bands, which were the alpha frequency band from 7 Hz to 13 Hz and the beta frequency band from 15 Hz to 19 Hz. These two frequency bands were investigated in a time window beginning -400 ms pre-stimulus and lasting 310 ms. The starting point at -400 ms was motivated by two facts. First Mayer and colleagues (Mayer et al., 2016) reported a relationship with the alpha frequency band activity and expectations and analysed a pre-stimulus time interval beginning at -400 ms. Second, the time frequency grand average indicated an increase in the predefined beta frequency band at around -400 ms. Furthermore, to analyse the alpha frequency band with three cycles a minimum of 300 ms time is required. Taken these facts together results to define the time range from -400 to -90 ms.

3.3.1 Source Analysis

For the alpha frequency band activity (ABA), a cluster-based permutation ANOVA revealed a main effect of the factor *Sequence position* in the expectation interval (p=0.00019, cluster corrected; uncorrected for testing two frequencies). The significant cluster observed includes 170 voxels. Peaks were defined by global and local maxima of F-values. Six cerebral peak voxels were found, which are illustrated in the Figure 3-12. The first peak voxel was in the superior part of to the lateral occipital cortex (LOC, MNI: -40, -70, 20).

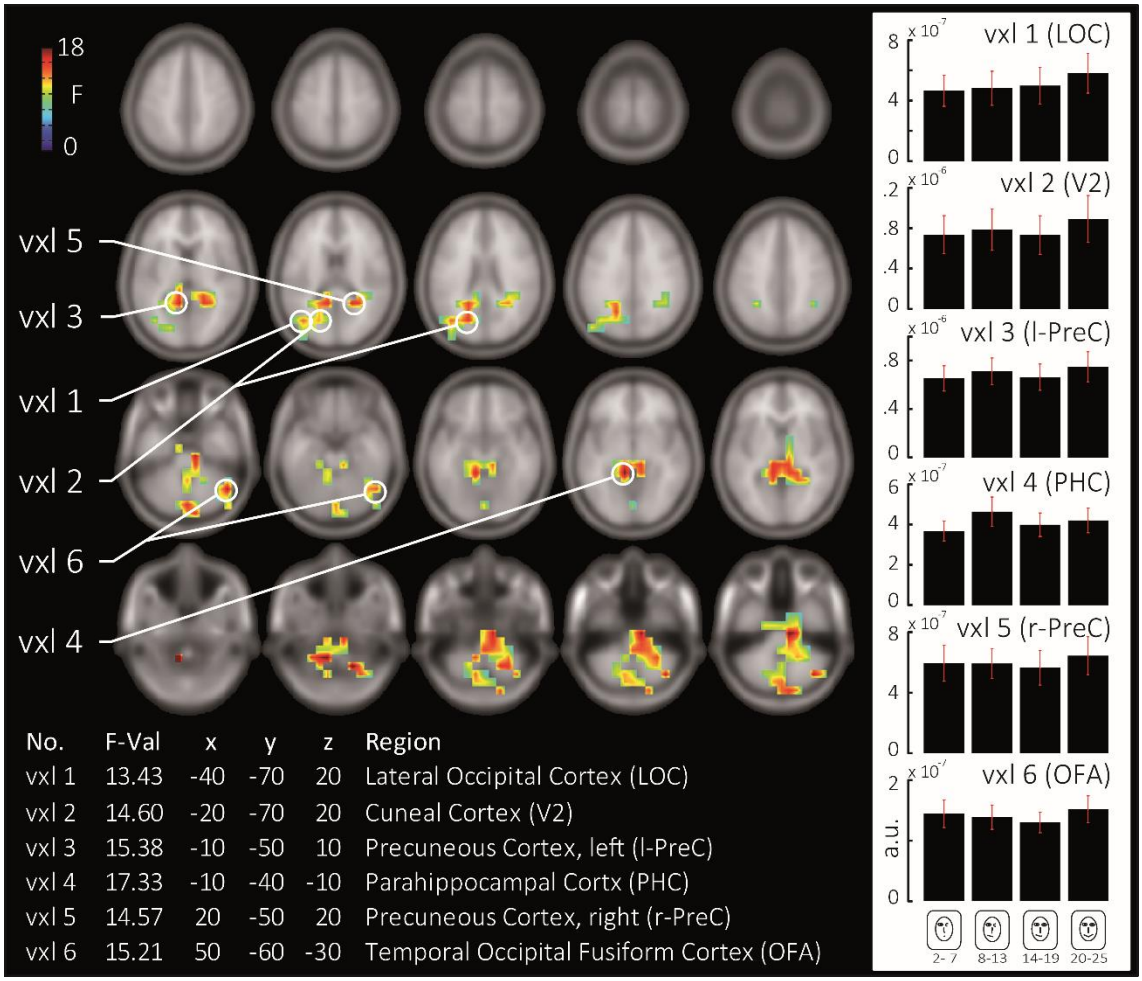

No.	F-Val	x	y	z	Region
vxl 1	13.43	-40	-70	20	Lateral Occipital Cortex (LOC)
vxl 2	14.60	-20	-70	20	Cuneal Cortex (V2)
vxl 3	15.38	-10	-50	10	Precuneous Cortex, left (l-PreC)
vxl 4	17.33	-10	-40	-10	Parahippocampal Cortx (PHC)
vxl 5	14.57	20	-50	20	Precuneous Cortex, right (r-PreC)
vxl 6	15.21	50	-60	-30	Temporal Occipital Fusiform Cortex (OFA)

Figure 3-12: *Source statistics on alpha frequency band power for the factor Sequence position in the expectation interval*. A beamformer source localization was applied to a centre frequency of 10 Hz (+-3 Hz) in the expectation interval (-400 ms to -90 ms pre-sample stimulus). A permutation ANOVA revealed one significant cluster (n=41, p=0.0002, cluster corrected, threshold p<0.05) with 6 cerebral peak voxels. These peak voxels are labelled 'vxl 1' to 'vxl 6'. Their anatomical description is given in the table below the slices. Anatomical labels were based on the *Harvard-Oxford Cortical Structural Atlas*. The bar graphs right to the slices refer to the average power of each sequential position of each peak voxel (a. u. = arbitrary units). The error-lines at each bar represent the standard error. The icons represent the four sequential positions.

The second peak voxel was in the cuneal cortex (cuneus, MNI: -20, -70, 20) and expanded into the supracalcarine cortex. The Juelich Histological Atlas (JHA) refers to this location as V2. The third peak voxel was in the left precuneus (l-PreC, MNI: -10, -50, 10) and expanded into the posterior part of the cingulate gyrus. The fourth peak voxel was in the posterior part of the parahippocampal gyrus (MNI: -10, -40, -10) which expands into the lingual gyrus. As for the functional diversity along the parahippocampal gyrus, we redefine this peak voxel in the parahippocampal gyrus in respect to the work of Raslau and colleagues (Raslau et al., 2015) with the parahippocampal cortex (PHC). The fifth peak voxel was in the right precuneus (r-PreC, MNI: 20, -50, 20).

Last, the sixth peak voxel was in the cerebellum (MNI: 50, 60, 30) but expanded into the temporal occipital fusiform gyrus (MNI: 50, 60, 20). This region was associated to the occipital face area (OFA) in comparison when considering the OFA coordinates in the work of Pitcher and colleagues (Pitcher et al., 2011). Other significant voxels were observed in the cerebellum and in the thalamus. MEG responses from the thalamus are located deep in the brain, and an analysis of the activation in the thalamus requires special modelling during localization (Attal et al., 2007). Thus, we omit the analysis of the voxels located in the thalamus. Activations in the cerebellum are related with associative motor learning, and the cognitive participation of the cerebellum is questioned. As we investigate the microcircuit theory of predictive coding by Bastos and colleagues (Bastos et al., 2012), which is based on cortical layers, we focus on cerebral peak voxels only.

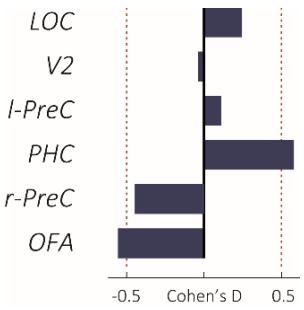

Figure 3-13: *The effect size of the discriminability contrast with each beamformer peak voxel values of ABA.* Effect sizes were computed for the simple effect first versus third sequential positions. Highest effect sizes were observed for the parahippocampal cortex and the occipital face area (OFA) but with a different sign of the effect.

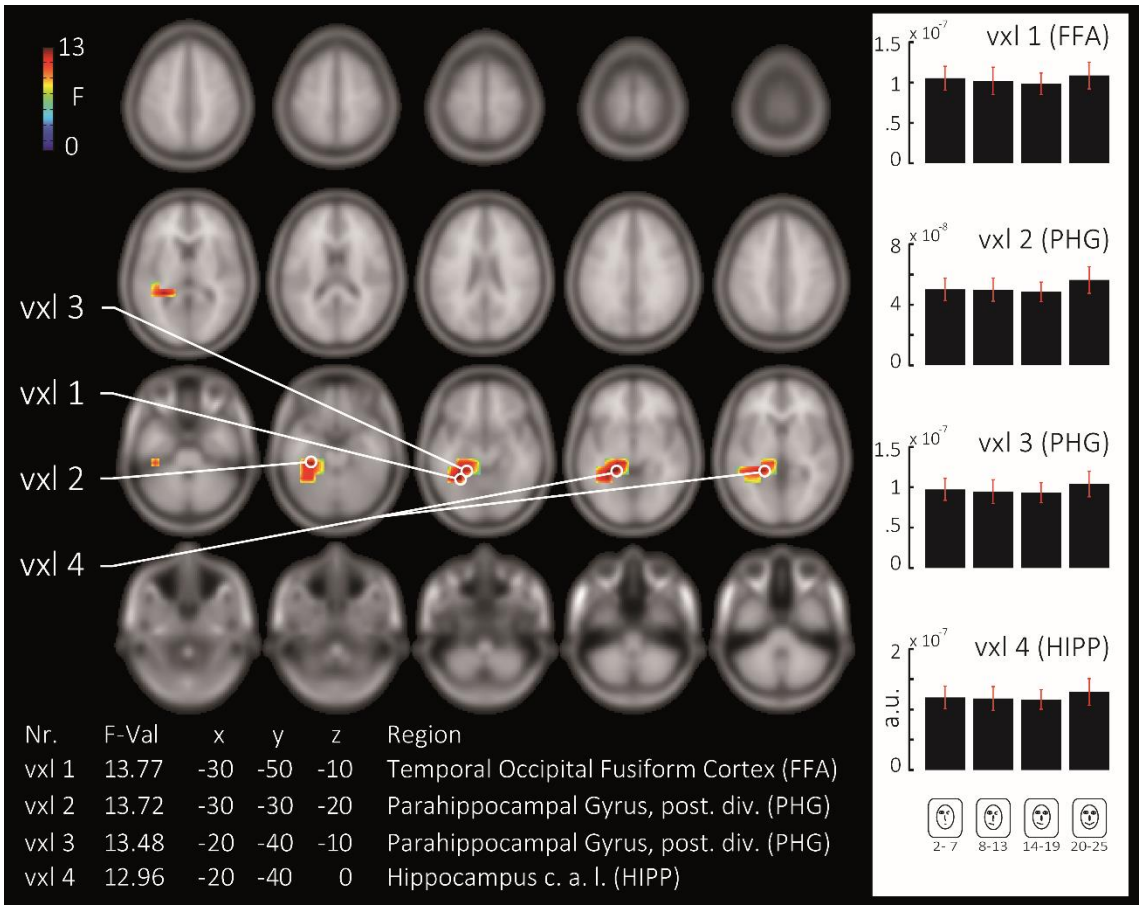

Figure 3-14: *Source statistics on beta frequency band power for the factor Sequence position in the expectation interval*. A beamformer source localization was applied to a centre frequency of 17 Hz (+-2Hz) in the expectation interval (-400ms to -90ms pre-sample stimulus). A permutation ANOVA revealed one cluster (n=41; p=0.0458, cluster corrected, threshold p<0.05) with 5 peak voxels. These peak voxels are labelled 'vxl1' to 'vxl5'. Their anatomical description is given in the table below the slices. Anatomical labels were based on the *Harvard-Oxford Cortical Structural Atlas*. Voxel 5, the hippocampus, was labelled by the *Juelich Histological Atlas*. The bar graphs right to the slices refer to the average trial power of each sequential position of each voxel (a. u. = arbitrary units). The error-line at each bar represent the standard error. The icons represent the four sequential positions.

For all peak voxels of the ABA, a post-hoc permutation *z*-test on mean source power revealed no simple effect to be significant. Furthermore, we estimated the effect sizes based on the *t*-values (Figure 3-13) for the second simple effect (first versus third sequential positions), as motivated by the behavioural analysis and discriminability. The OFA, the r-PreC and the PHC reached medium ES and showed different signs. For the remaining four voxels, weak ES were observed.

For the beta frequency band activity (BBA), a cluster-based permutation ANOVA revealed a tendency towards a main effect of the factor *Sequence position* in the expectation interval (cluster-based permutation ANOVA, p=0.04589, cluster corrected, but

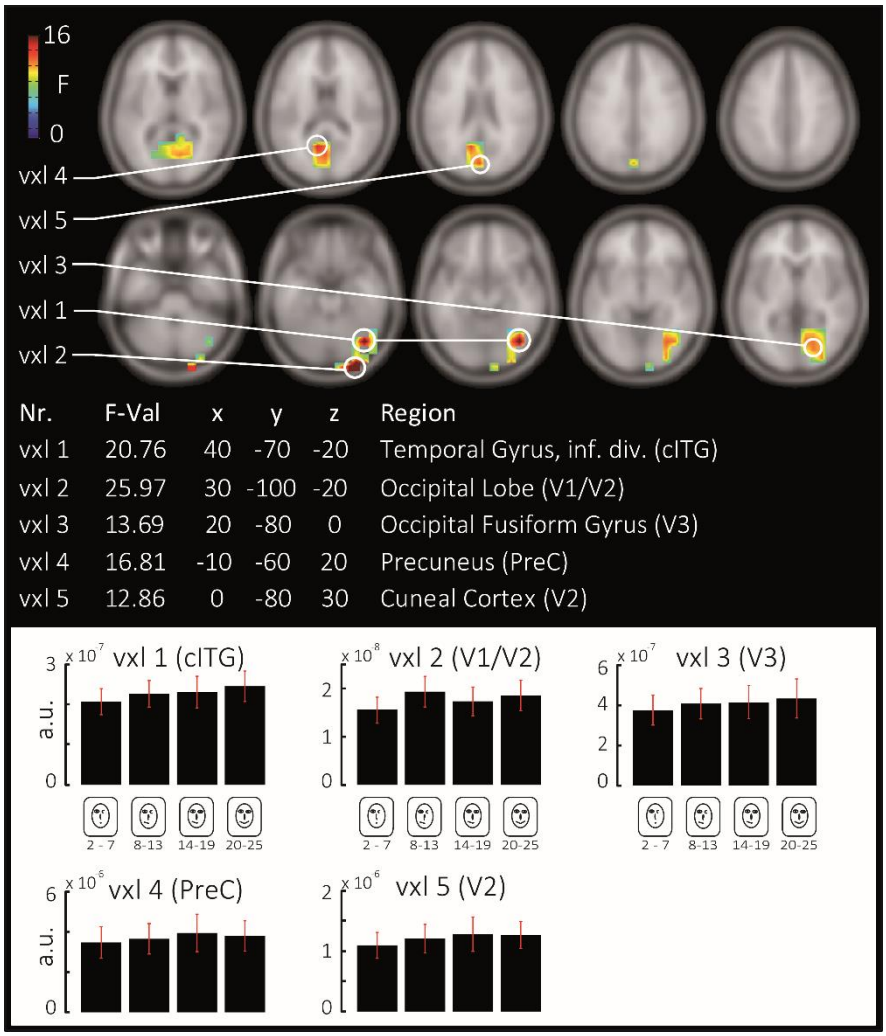

Figure 3-15: *Source statistics of alpha frequency band activity for the factor Sequence position in the post-stimulus interval.* A beamformer source localization was applied to a centre frequency of 10 Hz (+-3 Hz) in the time interval post-stimulus (25ms to 325ms). A permutation ANOVA revealed one significant cluster (n=41, p=0.024, cluster corrected, threshold p<0.05) with 5 cerebral peak voxels. These peak voxels are labelled 'vxl1' to 'vxl5'. The anatomical description of the peak voxels is given in the table below the slices. Anatomical labels were based on the Harvard-Oxford Cortical Structural Atlas. The bar graphs at the bottom refer to the average trial power of each sequential position of each voxel (a. u. = arbitrary units). The error-line at each bar represent the standard error. The icons represent the four sequential positions.

uncorrected for testing two frequency bands, see Figure 3-14). The small cluster included 31 voxels on the left side of the brain. Four cerebral peak voxels were found, which are illustrated in the Figure 3-14. The first peak voxel was located in the inferior temporal occipital fusiform cortex (MNI: -30, -50, -10). According to Kanwisher (Kanwisher et al., 1997), this peak voxel can be referred to as FFA. The second and the third peak voxels were located posterior in the parahippocampal gyrus. The difference between these two voxels (voxel 2 and 3) was that the second expanded into the temporal fusiform cortex.

The fourth peak voxel was located in the hippocampus. The hippocampus also contains pyramidal cells which could be generators of a current dipole source detectable by the constraints of the used beamformer (Attal et al., 2007). Therefore, we considered the hippocampus in the network of BBA. For all peak voxels in the BBA, a post-hoc permutation *t*-test on mean source power for each peak voxel revealed no significant simple effect.

According to the source localisation analysis of the expectation interval, we also analysed ABA in the post-stimulus interval. A cluster-based permutation ANOVA revealed a main effect of the factor *Sequence position* (p=0.0244). The significant cluster included 49 voxels. Peaks were defined by global and local maxima of F-values. Five cerebral peak voxels were found, which are illustrated in the Figure 3-15. The first peak voxel was located inferior in the temporal gyrus (MNI: 40, -70, 20). A comparison of this coordinate to the localization of FFA by Kanwisher (Kanwisher et al., 1997) revealed higher distances then to the localisation of the cITG localized by Grützner and colleagues (Grutzner et al., 2010). Thus, we label this voxel cITG. The second peak voxel was in the occipital lobe (MNI: 30, -100, -20) and expanded regularly on the cortical surface. The JHA labels this location as the primary and secondary visual area V1 and V2. The third peak voxel was in the occipital fusiform gyrus (MNI: 20, -80, 0), and the fourth peak voxel was in the left PreC (MNI: -10, -60, -20). The fifth peak voxel was in the cuneal cortex (MNI: 0, -80, 30). The JHA suggests this voxel to be located in the secondary visual area V2.

3.3.2 Decoding Analysis

The weak main effect of BBA, which is correct for multiple comparisons only a trend, led to the continuation of training of a support vector machine (SVM) on alpha frequency source power values only. The SVM was trained to separate a (sub)set of trials into four classes, which referred to the four sequential positions.

This pattern classification of the SVM was measured by accuracy. Thus, the SVM computed accuracy value for each participant. An example pattern classification result is illustrated in form of a confusion matrix in Figure 3-16-B. This confusion matrix indicated that the first three sequential positions were differentiated by relatively high accuracies

(first sequential position, mean accuracy=61%; second sequential position, mean accuracy=57%; and third sequential position, mean accuracy=52%), and only the fourth sequential position was often mistakenly predicted as the third (mean accuracy=43%), second (mean accuracy=35%) or first (mean accuracy=22%) sequential position. This decreased the overall performance to 42% (17% above chance level).

The sequential classification approach (SCA) began with the best median overall accuracy across the participants for each peak voxel separately. The best median accuracy for this one-feature dimension pattern classification was observed for the peak voxel which was located in the PHC (median accuracy=31.6667%, mean accuracy=31.4409%, SD=3.8849, p=0.00001, binomial test; see Figure 3-16-A for values of other peak voxels). For this voxel, 26 participants achieved accuracies over 30%, of which 24 showed significant differences ($p<0.05$, permutation test). The SCA continued with a two-dimensional feature, which means that the next run of pattern classifications uses two features which is a pair of two peak voxels from which one voxel of this voxel pair was always the peak voxel located in the PHC. The best median accuracy for this was reached for the voxel pair located in the PHC and OFA (median accuracy=31.4286%, SD=3.3882, p=0.00001; 29 participants reached overall accuracies above 30% and 26 reached significant differences). The best median accuracy for the pattern classification which used a three-dimensional feature was the triplet voxel that considered the right PreC (median accuracy=31.25%, SD=3.65; p=0.00001). The best median accuracy with a four-dimensional feature was the quartet of voxels that considered the peak voxel located in the cuneal cortex; (median accuracy=31.07%, SD=3.42; p=0.00001). The best median accuracy with a five-dimensional feature was the quintet of voxels that considered the peak voxel located in the LOC (median accuracy=31.50%, SD=3.52; p=0.00001). The last run of the SVM was the pattern classification with six features corresponding to all six peak voxels. That means the last peak voxel in the sequence is the left PreC (median accuracy=31.43%, SD=3.44; p=0.00001; see Figure 3-16-C). The average accuracy across the feature dimensions for the best median accuracies reached 31% (SD=0.21). The course of the best median accuracies across the feature dimension revealed that there was no feature dimension that was more informative than any other.

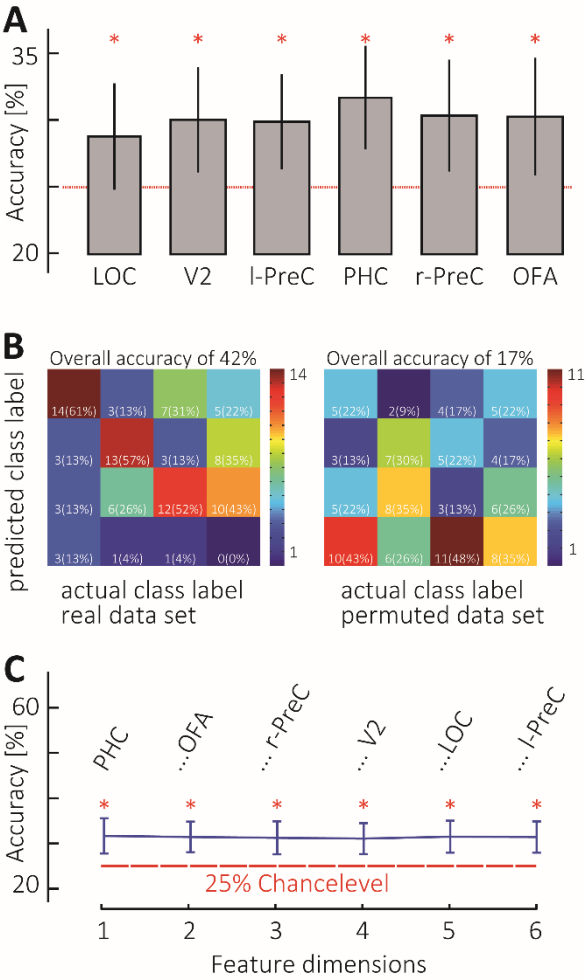

Figure 3-16: *Accuracies of* the pattern *classification on peak voxels of the alpha frequency band activity*. **A:** The average accuracy (n=41) for each peak voxel indicated that the trials were best separated into four classes by ABA values of the voxel in the parahippocampal cortex. The error-lines at each bar represent the standard deviation. **B:** The confusion matrix of a representative participant shows that trials of the first to the third sequential positions are better separated by a decision boundary than trials from the fourth sequential position. The confusion matrix of permuted data sets revealed that here the sequential positions were not well separated (B right). **C:** The best median accuracies were plotted as a function of feature dimension. With increasing feature dimensions, no changes in median accuracy were observed. Red asterisks indicate significant accuracies revealed by a binomial test.

3.3.3 Correlation Analysis

Next, we investigated the relationship between behaviour and frequency band activity (Figure 3-17). The correlation between the significant cluster of A&BBA and the two SDT measures discriminability and response bias were obtained to examine which of the behavioural measures had a relationship to which frequency band activity. The behaviour analysis motivated us to use the second simple effect (first versus third sequential

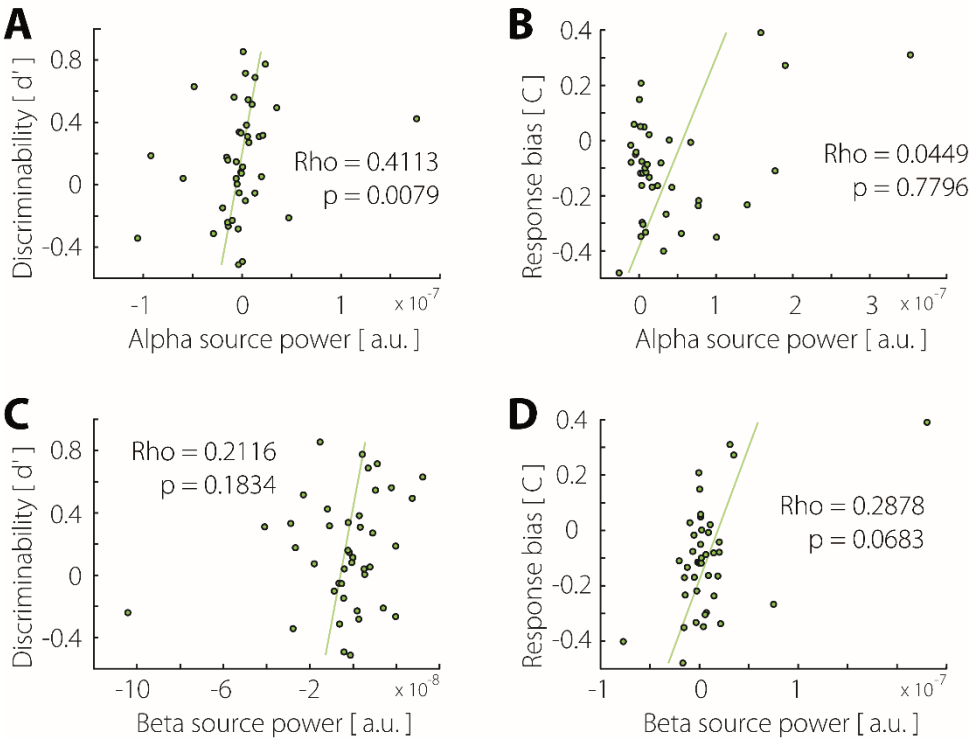

Figure 3-17: *Relationship between neuronal frequency band activity and behavioural measures like discriminability and response bias*. The correlation revealed a significant relationship between alpha frequency band activity and discriminability ($p<0.0125$). No other significant relationship was observed. The scatterplots display the relationship between the mean trial power difference of all voxels of the cluster revealed by the beamformer source statistics (Figure 3-12 and 3-14) and discriminability (A) or response bias (B) difference. These contrasts refer to the second and third simple effects motivated by the behaviour analysis which was for the discriminability the contrast between the first and third sequential positions (A, C) and for the response bias the contrast between the first and fourth sequential positions (B, D). In each scatter plot, the Spearman rank correlation value rho and the uncorrected p-values are displayed (the alpha level is therefore $p<0.0125$). A. u.=arbitrary units.

position) to correlate discriminability with frequency band activity and to use the third simple effect (first versus fourth sequential position) to correlate response bias with frequency band activity. The correlation results revealed that changes in the ABA have a strong relationship with discriminability (Rho=0.4113, p=0.0079, uncorrected), but not with response bias (Rho=-0.0449, p=0.7796). That means a higher ABA was associated with a higher discriminability. Further, the correlation analysis revealed for the BBA no significant relationship to any of the SDT measures (discriminability, Rho=0.2116; p=0.1834; response bias, Rho=0.2878, p=0.0683; uncorrected values). Correcting for the four comparisons, the relationship between ABA and remains significant ($p<0.0125$).

Post-hoc we verified the selection of the simple effects and SDT measures by exchanging the simple effects selected for discriminability and response bias for the ABA correlation

analysis. No significant result could be observed (ABA X discriminability $_{(1. vs. 4)}$: Rho=0.29, p=0.068; ABA X response bias$_{(1. vs. 3.)}$: rho=0.08, p=0.632).

Also, the relationship between the ERF amplitude and the ABA was of interest (Figure 3-18). The correlation between each peak voxel of the ABA and the ERF component was computed as a function of the contrast considering the second simple effect to examine which brain peak voxel had a relationship with which ERF component. The only voxel that showed a significant relationship with two ERF components was the OFA. The correlation revealed that ABA in the OFA had a strong relationship with changes in the amplitude of the M2 component and the M4 component. When the ABA in the OFA increased the ERF component, M2 was more negative (Rho=0.5128, p=0.00072) and the M4 was more positive (Rho=-0.5331, p=0.00041).

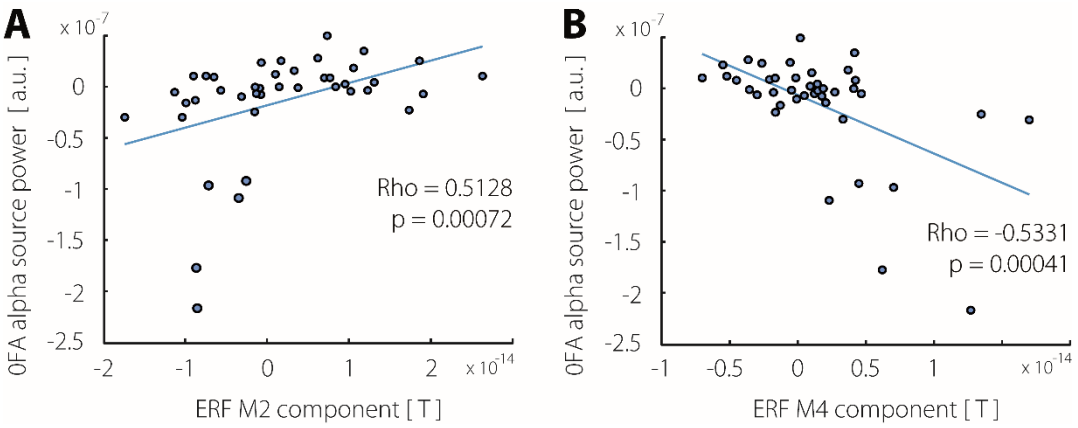

Figure 3-18: *Relationship between alpha frequency band activity in OFA and the ERF components*. The scatterplots display the relationship of the mean trial power difference of the OFA voxel in the alpha frequency band activity and the related ERF-component difference. The difference refers to the contrast between third and first sequential positions. **A**: When the alpha frequency power difference increased, one observed a higher positive difference in the ERF component M2. **B**: When the alpha frequency power difference increased, one observed a higher negative difference for the ERF component M4. This is due to a higher ERF signal for the third sequential position than for the first sequential position.

3.3.4.1 Haemodynamic Responses

The localization revealed 9 peaks located mostly in the posterior brain (Figure 3-19). The largest cluster was observed with a peak in the occipital pole (vxl 4, k_E=445) expanding anterior to the left precuneus and intracalcarine cortex. The second largest cluster was observed in the left occipital fusiform gyrus (vxl 2, k_E=90) expanding to the left temporal occipital fusiform cortex, this corresponds to left OFA activity. The third largest cluster was located with a peak voxel in the right superior division of the lateral occipital cortex expanding to the right precuneus cortex (vxl 8, k_E=59). Also, in the left lateral occipital cortex two clusters were observed by a peak voxel (vxl 7, k_E=18; vxl 9, k_E=27), with one expanding to the superior parietal lobe.

In the right posterior brain, two additional clusters were found, one cluster with a peak voxel in the precuneus cortex (vxl 6, k_E=20) and the second one in the temporal occipital fusiform cortex (vxl 1, k_E=15). Further, two more clusters were observed, one in the right posterior division of the middle temporal gyrus (vxl 3, k_E=17) expanding to the superior temporal gyrus, the other one located in the left inferior frontal gyrus (vxl 5, k_E=16) expanding to the middle frontal gyrus.

3.3.4.2 Haemodynamic and Magnetoencephalographic Responses

For both measures, BOLD responses and MEG responses, we investigated the expectation interval and observed a main effect of the factor *Sequence position*. Further, for the beamformer source localization of ABA a positive relationship with discriminability was observed. For the BOLD response, a parametrical modulation by the pattern of behavioural discriminability was applied. Both measures, BOLD and MEG responses, revealed a predominantly posterior brain activity (Figure 3-19). Shared functional brain regions which showed increased activity were the right temporal occipital fusiform cortex (OFA), the precuneus (PreC), the lateral occipital cortex (LOC) and the cuneus/V2.

However, the coordinates of the peak voxel hardly overlapped, thus, surrounding voxels were respected. When considering the surrounding voxels, the LOC and cuneus/V2 were only neighbouring each other. But considering the rough localization of the MEG with a

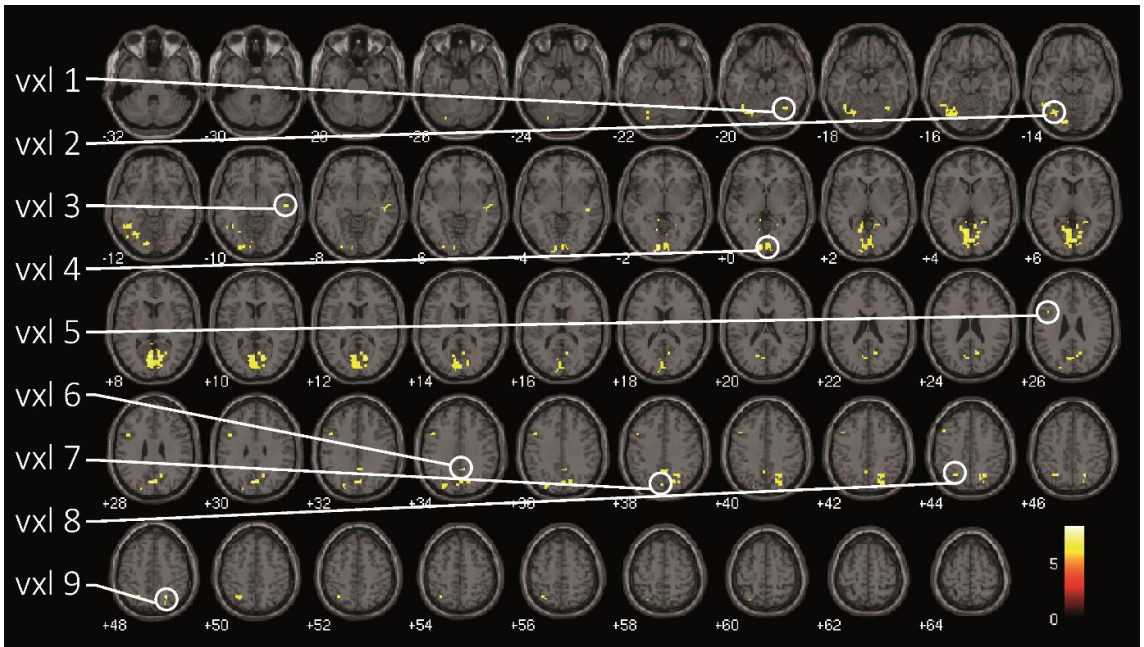

Nr.	x	y	z	Region
vxl 1	33	−58	−19	Temporal Occipital Fusiform Cortex (rOFA)
vxl 2	−30	−67	−13	Occipital Fusiform Gyrus (lOFA)
vxl 3	54	−19	−10	Middle Temporal Gyrus, post. div.
vxl 4	−9	−91	−1	Occipital Pole, expansion in: Intracalcarine Cortex, Lingual Gyrus
vxl 5	−42	11	26	Inferior Frontal Gyrus, pars opercularis
vxl 6	9	−52	35	Precuneus Cortex
vxl 7	−24	−82	38	Lateral Occipital Cortex, sup. div. (lLOC)
vxl 8	24	−61	44	Lateral Occipital Cortex, sup. div. (rLOC
vxl 9	−30	−61	47	Lateral Occipital Cortex, sup. div. (lLOC)

Figure 3-19: *BOLD response for the factor Sequence position in the expectation interval*. Nine peak voxels were selected from the corresponding clusters for the factor *Sequence position*. The peak voxels were labelled based on the *Harvard-Oxford Cortical Structural Atlas*. The biggest cluster was the cluster with 445 voxels (3x3x3 mm) and the voxel 4 refers to. This peak voxel also expands into the precuneus on the left side (for better understanding, see the Table 3-6).

precision of 1 cm³ and the precise localization of the BOLD response with a voxel 3 mm³ a neighbouring of voxels could be carefully interpreted as overlapping region. The overall observation is that within the posterior brain activation of both measures, the ABA is more anterior and the BOLD response more posterior located.

The first brain area considered is the precuneus. The BOLD response localized the right precuneus by one global peak (56%; MNI: 9, -52, 35) and by one local peak (26%; MNI: 18, -70, 41) which referred to activity in the superior division of the precuneus. Further, the large cluster (k_E=445) with the peak in the occipital pole expanded across the lingual

gyrus to the inferior division of precuneus. The beamformer localized ABA in the right precuneus (global peak; MNI: 20, -50, 20) which expanded into the inferior division (20% MNI: 20, -50, 10) of the precuneus. Considering the expansion of the clusters, these regions do not overlap by their peak voxels and surrounding voxels.

Further, the beamformer localized ABA in the left precuneus. The left precuneus was localized by BOLD response with two local peaks (84% precuneus; MNI: -3, -55, 38; 12% precuneus; MNI: -6, 73, 29). The beamformer localized ABA in the left precuneus by one global peak (11%; MNI: -10, -50, 10) which expanded into inferior division again (20%. MNI: -10, -50, 0; MNI:), ending up in the lingual gyrus. Again, these regions do not overlap by their peak values but here by their surrounding voxels.

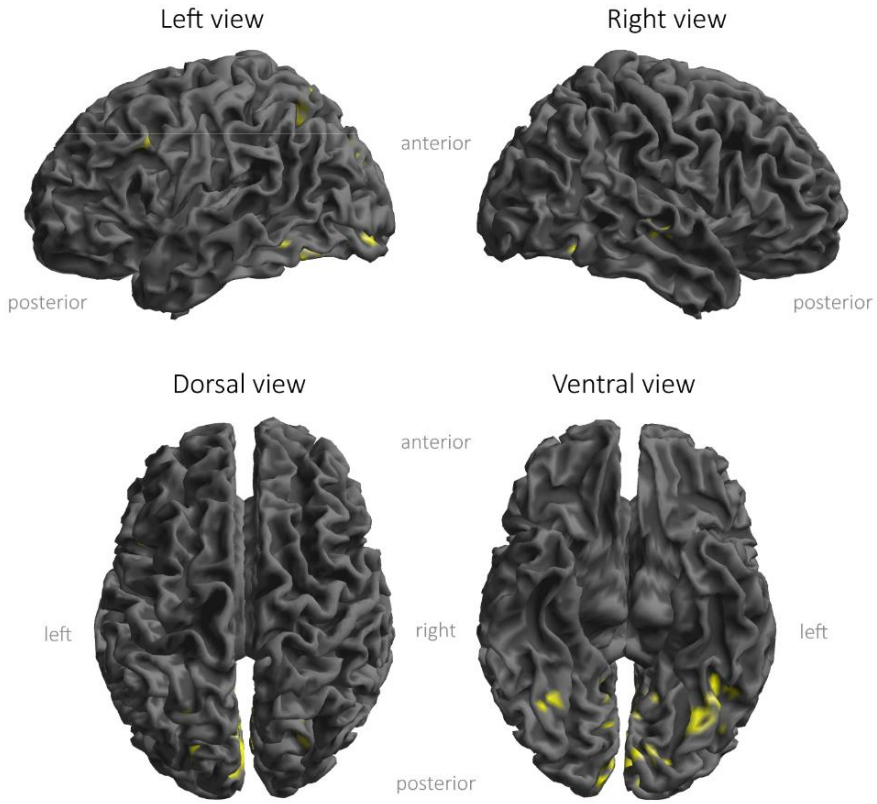

Figure 3-20: Rendered *BOLD response for the factor Sequence position in the expectation interval*. The sources shown in Figure 3-19 are rendered on a standard T1 anatomy.

The beamformer localized ABA in the right OFA (MNI: 50, -60, -20) and so the BOLD response (MNI: 33, -59, -20). The localization in the right OFA by the BOLD response revealed one global peak (Table 3-6) with 15 voxels. Respecting these neighbouring voxels revealed a direct overlap. The projection onto the brain surface of both measures illustrates the overlap in the ventral view (Figure 3-21).

The beamformer localized ABA in the inferior division of the lateral occipital cortex (LOC; MNI: -40, -70, 20) and the BOLD response located several global peaks in the superior division of the LOC (46 %, MNI: 24, -61, 44 | 59 %, MNI: -24, -82, 38 | 45 %, MNI: -30, -61, 47). These voxels of the BOLD response were at the edge of the expansion of the ABA observed in the LOC, thus, they hardly overlap, and (only) neighbour each other. A similar neighbouring could be observed for the Cuneal/V2 brain region. The peak voxel observed for the ABA for the Cuneal/V2 (MNI: -20, -70, 20) was found surrounded by voxels of the large cluster with the peak voxel in in the occipital pole (MNI; −9, −91, −1).

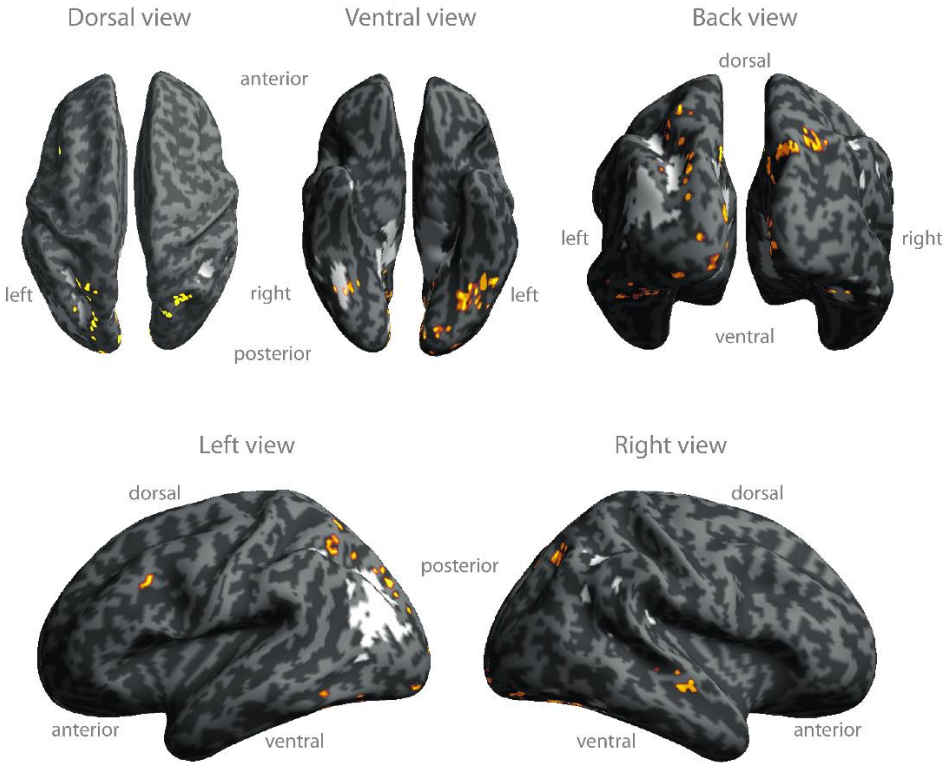

Figure 3-21: *Comparison of BOLD and MEG responses*. BOLD (yellow) and alpha frequency band activity (white) of the factor *Sequence position* displayed on an inflated brain. The activity shows all significant voxels of each measure in a two colour code white and yellow. For the OFA a clear overlapping activity was found (ventral view). For further explanation see text.

Table 3-6: MRI coordinates of global and local peaks of the BOLD response for the factor Sequence position.

cluster level			peak-level				MNI [mm]			Harvard-Oxford Cortical Structural Atlas	
$p_{(FEW)}$	$q_{(FDR)}$	k_E	$p_{(FEW)}$	$q_{(FDR)}$	T	Z	x	y	z		
0.0000	0.0000	15	0.0020	0.9240	7.19	5.44	33	−58	−19	R	48% Temporal Occipital Fusiform Cortex, 8% Occipital Fusiform Gyrus
0.0000	0.0000	90	0.0020	0.9240	7.21	5.45	−30	−67	−13	L	53% Occipital Fusiform Gyrus, 8% Temporal Occipital Fusiform Cortex
			0.0020	0.9240	7.18	5.43	−39	−64	−19	L	35% Temporal Occipital Fusiform Cortex, 33% Occipital Fusiform Gyrus
			0.0030	0.9240	7.09	5.39	−24	−70	−19	L	15% Occipital Fusiform Gyrus, 4% Lingual Gyrus
0.0000	0.0000	17	0.0030	0.9240	7.11	5.40	54	−19	−10	R	47% Middle Temporal Gyrus, post. div., 11% Superior Temporal Gyrus, post. div.
			0.0030	0.9240	7.00	5.35	48	−25	−4	R	32% Superior Temporal Gyrus, post. div., 27% Middle Temporal Gyrus, post. div.
0.0000	0.0000	445	0.0000	0.6400	8.36	5.96	−9	−91	−1	L	37% Occipital Pole, 23% Intracalcarine Cortex, 6% Lingual Gyrus
			0.0000	0.6400	8.22	5.90	0	−73	29		61% Precuneous Cortex, 27% Cuneal Cortex, 5% Supracalcarine Cortex
			0.0000	0.6400	7.96	5.79	−6	−64	8	L	36% Intracalcarine Cortex, 26% Lingual Gyrus, 12% Precuneous Cortex
0.0000	0.0000	16	0.0110	0.9240	6.56	5.13	−42	11	26	L	36% Inferior Frontal Gyrus, pars opercularis, 16% Precentral Gyrus,
			0.0140	0.9240	6.49	5.09	−42	14	41	L	57% Middle Frontal Gyrus, 1% Inferior Frontal Gyrus, pars opercularis
0.0000	0.0000	20	0.0000	0.6400	7.95	5.79	9	−52	35	R	56% Precuneous Cortex, 23% Cingulate Gyrus, posterior division
			0.0060	0.9240	6.77	5.24	−3	−55	38	L	84% Precuneous Cortex, 13% Cingulate Gyrus, post. div.
0.0000	0.0000	18	0.0060	0.9240	6.79	5.25	−24	−82	38	L	59% Lateral Occipital Cortex, superior division,
			0.0300	0.9290	6.20	4.94	−18	−88	26	L	34% Lateral Occipital Cortex, sup. div., 24% Occipital Pole, 2% Cuneal Cortex
0.0000	0.0000	59	0.0000	0.6400	8.05	5.83	24	−61	44	R	46% Lateral Occipital Cortex, superior division, 4% Superior Parietal Lobule
			0.0030	0.9240	7.02	5.36	18	−70	41	R	26% Precuneous Cortex, 24% Lateral Occipital Cortex, sup. div., 3% Cuneal Cortex
			0.0060	0.9240	6.80	5.25	27	−76	41	R	66% Lateral Occipital Cortex, sup. div.
0.0000	0.0000	27	0.0010	0.9240	7.54	5.60	−30	−61	47	L	45% Lateral Occipital Cortex, superior division, 17% Superior Parietal Lobule
			0.0060	0.9240	6.81	5.26	−30	−64	56	L	58% Lateral Occipital Cortex, sup. div., 6% Superior Parietal Lobule

Table shows 3 local maxima more than 8mm apart: Height threshold: T = 6.02, p = 0.00001 (0.050) (FDR corrected); Extent threshold: k = 10 voxels, p = 0.000 (0. Degresees of freedom = [1, 30 .0].

4 Discussion

4.1 Summary

Predictive coding theory (PCT) is a popular theory which in the first place provides an intuitive explanation for most behavioural and neurophysiological results on the conceptual level, or in Marr's terms, an explanation at the top level called *'abstract computational theory'* (Marr, 1982). The PCT is almost three decades under investigation: Books have been published (Bar, 2011; Clark, 2013; Hohwy, 2013), and many studies refer to PCT. In the last decade, new hypotheses about predictive coding have arisen and have recently been under investigation. Especially, there is an ongoing debate regarding the implementation level of PCT. It is suggested that low frequencies (< 30 Hz) are linked to predictions sent top-down the cortical hierarchy and high frequencies (> 30 Hz) are linked to the information sent up the cortical hierarchy. The information sent up the hierarch is thought to reflect the discrepancy between the sensory signal and the prediction (Arnal and Giraud, 2012; Bastos et al., 2012; van Kerkoerle et al., 2014) (Figure 1-2). The latter, called prediction error (PE), has extensively been investigated by revising established mismatch paradigms suited to investigate PE. These studies confirmed high frequencies mediating PE (Arnal et al., 2011; Bauer et al., 2014; Brodski and Paasch et al., 2015). Still in debate is the question as to which of the classical low frequency bands, i.e. alpha or beta frequency band, marks the predictive top-down information flow (Brodski-Guerniero et al., 2017).

Our study served two aims; first, to introduce a new, simple paradigm suited to investigate predictive signals in the brain, and second, to investigate the neural correlates of the precision of prediction via measuring the relationship of low frequency source activity and behavioural discriminability.

At the behavioural level, we could verify a familiarity acquisition by an increase in hit rates and discriminability, as it was proposed by our processing model of the experimental setting (Figure 2-5). Next, we investigated low frequencies at the MEG sensor level and observed an enhanced alpha frequency band activity (ABA) across the expectation interval and observed an increase in beta frequency band activity (BBA) with a peak at -

245 ms. A&BBA in the expectation interval were source-localized, and an analysis of variance (F-test) with the factor *Sequence position* was applied on source power values. As hypothesized, a significant effect in the low frequencies was found. A large cluster for the alpha frequency band was found in the more posterior brain, and a smaller cluster for the beta frequency band was found in the midbrain. Correcting for multiple comparison only the cluster found for the alpha frequency remained significant. However, for both frequencies, peak voxels were found in brain areas associated with memory. The ABA revealed peak voxels in the left and right precuneus (PreC) and the posterior parahippocampal cortex (PHC). The BBA revealed peak voxels in the hippocampus and in the posterior parahippocampal gyrus (PHG). Furthermore, both clusters revealed activity in face-related brain regions. For the ABA, a peak voxel was in the posterior division of the temporal fusiform cortex and associated with the occipital face area (OFA). For the BBA, a peak voxel was in the inferior division of the temporal fusiform cortex and associated with the fusiform face area (FFA). At last, for the ABA we found peak voxel related to vision, like a peak voxel in the early visual area V2 and in the lateral occipital cortex (LOC).

However, in a follow-up analysis, only for the ABA we found a relationship with the behavioural discriminability measure d-prime. Thus, we only considered the ABA for further analysis. The brain areas determined by the cerebral peak voxels of the ABA were visualized into a *'face-identity-predictive network' (FIP-network).* Thus, the FIP network consisted of five functional brain areas: the PHC, left and right PreC taken together as one node, the OFA, the lateral occipital cortex (LOC) and the secondary visual areas (V2; Figure 4-2). Further follow-up analyses were applied to investigate whether each brain area was of equal relevance. For this reason, a sequential pattern classification approach was applied, and it revealed no source to be of higher relevance within the FIP network (Figure 3-16-C). However, regarding decoding analysis, the PHC could be cautiously interpreted as the brain area of higher relevance (31.6% correct classifications; Figure 3-16-A). Taken together the decoding analysis, the effect sizes and the F-Values, the sequence of sources supports the idea that the brain areas LOC and V2 are probably of less relevance. Grützner and colleagues (Grutzner et al., 2010) found by a Mooney face detection task activity in the LOC and associated it to perceptual closure processes. Since

we analysed baseline activity, we propose that LOC activity might signal some preparatory activity to facilitate upcoming perceptual closure processes. V2 activity was related to early vision which refers to edge and surface detection organized retinotopically. In our Network, activity in V2 could refer to model visualisation in terms of retinotopic representation.

Further, we verified the OFA to be of higher relevance, as indicated above, by an incidental finding. When investigating the familiarity acquisition by neurophysiological measures, we made use of the prominent ERF M250 component associated with familiarity (Kaufmann et al., 2009; Saavedra et al., 2010; Sagiv and Bentin, 2001; Tanaka and Pierce, 2009; Tanaka et al., 2006; Gosling and Eimer, 2011; Weibert and Andrews, 2015). In doing so, we revealed a significant change in the M200 and M250 components. Again, post-hoc a decoding analysis was applied to investigate whether the components were of equal relevance. The pattern classification performances revealed a slightly higher relevance of the M250 component. However, all selected components reached significant classification accuracies (Figure 3-9-A|B). Thus, we correlated each ERF component with the power change in each peak voxel and found a significant relationship of alpha frequency source power changes in OFA and changes in the ERF M200 and M400 components (Figure 3-18). In the first instance, this was surprising, but new models of face recognition (Schweinberger and Neumann, 2016) provide an explanation why these two components show a relationship with each other. In more detail, this is discussed in Chapter 4.3.1. However, to our knowledge it has not been shown before that modulations of pre-stimulus ABA in source space are related to changes in the context-specific ERF components on sensor level.

Last, OFA localization was verified by the BOLD response. Also, activity in the LOC and the PreC were found by the BOLD response analysis in the expectation interval, although without overlap and hardly neighbouring to the ABA cluster revealed by the MEG response analysis. Further, the fMRI experiment revealed additional sources not found in the MEG experiment, which mainly formed a big cluster within the visual ventral stream from V1 across the lingual gyrus but also comprised voxels expanding into the precuneus (see peak voxel 4 in Figure 3-19). The mapping of the FIP-network by the fMRI and MEG

will be discussed in more depth in Chapter 4.3.2. In the next Chapter 4.2, we continue with a detailed discussion of the behavioural results.

4.2 The Comparison of Behavioural Measures across Studies revealed consistent Learning Effects

Three studies were conducted with the same learning task: a pilot study (n = 10), a MEG study (n = 41) and a fMRI study (n = 36). The pilot study was conducted to investigate the difference in response behaviour when changing the sequence of stimuli conditions at sample position and with that to fine-tune the experimental setting for measures of brain responses. After that, a MEG study was conducted with the most suitable condition and setting. The paradigm then was altered to fulfil the criteria of an event-related fMRI-design, and haemodynamic brain responses were collected. Consistently, for all three studies a learning effect was verified by increasing hit rates for match responses and for the last two studies with an increase in discriminability across sequential positions. In the following, we discuss the decisions of the pilot study to measure magnetoencephalographic and hemodynamic responses and continue to compare the behavioural results of the MEG and fMRI studies.

4.2.1 The Incremental Sequence Condition best induced Visual Learning

The pilot study was conducted to investigate the differences in the learning progress while manipulating the sequence of stimuli at the sample position. Two different sequences were tested: One was a randomized (RS condition) and the other an incremental (IS condition) sequence of illumination changes at the sample position. We assume that the IS condition in face stimuli in the sample position more slowly reveals facial features, because the stimuli presented one after the other are less varying, and, thus, the unveiling of new features by new illumination situations is delayed. We assume that one consequence of this is that learning is delayed.

Speed and accuracy are two critical components to describe behaviour and brain responses (Heitz, 2014). Therefore, we assumed that we will observe a positive learning progress by an increase in hit rates (HR) and by a decrease in reaction time (RT) across sequential positions for the match responses. Further, we also assumed that the response rate (RR) for match responses will increase across sequential positions (in turn, the RR for non-match must decrease. The response rate refers to the given responses and was also considered, because the instruction to the participants was to responses as truthfully as possible based on their perception. Thus, an increase in RR becomes a viable measure of learning, but it also makes it necessary to investigate a response bias. The last aspect was only possible to investigate with the MEG and fMRI studies, because they had a higher false alarm rate due to a greater number of trials.

Overall, three observations from the pilot study were crucial: First, for the IS condition a positive learning curve could be verified by a significant main effect of the factor *Sequence position* for HR and RR for the match response condition. Post-hoc analyses revealed an increase in HR and RR by a significant second and third simple effect. Second, this increase is due to a low performance at the beginning for HR of match responses compared HR of non-match responses in the IS condition. It is also a low performance of HR when comparing it to the HR of match and non-match responses of the RS condition. Third, no main effects of the factor *Sequence position* for RT were observed. However, post-hoc analyses revealed a decrease in RT for the RS condition for the condition *overall* response. Overall responses are the responses not separated in match and non-match responses. In the following, we discuss these three points in more depth.

A positive learning curve was verified by a significant increase in HR and RR for the match condition in the tested IS condition. This was not observed for non-match responses in the IS condition and not for any of the response types of interest in the RS condition. The HR and RR for non-match responses referred to correctly identified non-target faces. We prevented people from not learning non-target face identities by using four different face identities as non-target faces, but we still used three stimuli of each, which left a little chance for learning non-target identities. Because the HR were high from the beginning, we tentatively interpret that non-target faces were not learned. Instead, we think that the high HR for match responses from the beginning onward could be explained by an

exclusion strategy. This means that the participants were able to identify face stimuli as non-target better than the target. We propose this was possible from the beginning on, because few pictures of the target face identity (TFID) were probably sufficient to extract traits of the TFID to identify non-target faces in face stimuli than to identify the TFID. These traits could refer to secondary (or global) identity features or also to holistic-configural identity features (Farah et al., 1998; Gauthier and Tarr, 2002; Tanaka and Farah, 1993). These are, for example, gender, shape of the head or haircut, but also the relative distances between eyes, nose and mouth. We suggest that this information about the TFID was sufficient to identify non-target faces from the beginning on by exclusion criteria.

However, also the high HR of match responses of the RS condition indicate that the identification of the TFID could also be high from the beginning on. This observation confirmed our assumption that the IS condition slowly revealed visual information of the TFID (see Chapter 2.1.5.1 Processing Model Based on the Experimental Design) and in contrast to that, the RS condition quickly reveals visual information by more varying illumination directions at the beginning. Participants already gain sufficient visual information, given the first six random samples, and, thus, were able to extract more facial features from the beginning on than in the IS condition. Consequently, it was possible for the participants to correctly identify the TFID in a test image with a higher chance in the RS condition then in the IS condition.

The hypothesized RT decrease for HR and RR for match responses across the sequential positions during the learning procedure was not met. Here, we argue that the missing RT effect was most likely due to the instruction we gave to the participants. In awareness of the speed-accuracy trade-off (Heitz, 2014; Knight and Kantowitz, 1974, 1976), we instructed participants to focus on accuracy rather than on speed to ensure responses that correspond to their true perception. Further, the instruction also included that in case of double responses only the first (which we determine the intuitive) answer would be considered. This could be interpreted as a penalty for quick responses. As a consequence of the above facts, the pilot study showed that the incremental condition is best suited to proceed with further measurements in which additional neurophysiological data are collected in parallel.

4.2.2 The Hit Rates and the Discriminability Best Describe the Visual Learning

In the MEG study, only the IS condition was used, and as a result, twice the number of series with the IS condition could be presented. Also, this increase of trials of the IS condition was necessary to make the MEG response analysis possible and increased statistical power for behavioural analysis. The behavioural results of the MEG study were very similar to the results of the pilot study and the results increased in statistical power. As hypothesized, a positive learning curve was observed with a significant main effect of the factor *Sequence position* for the HR of match responses exclusively. Contrary to our initial hypothesis, also the missing RT effect held for the MEG experiment. Furthermore, the increase in trials and participants narrowed the distances between the mean HR of match responses and therefore reduced the effect size (ES). This was probably due to the decrease in the inter-participant variance by the double amount of trials. Thereupon, the false alarm rate increased, which enabled us to compute the measures discriminability and response bias proposed by the signal detection theory (SDT) (Green, 1966; Macmillan and Creelman, 2005).

The SDT is based upon the simple idea that a perceptual signal comes with noise and the detection of the signal relies upon a decision boundary called criterion C, interpreted as a measure of response bias. For a model of SDT respecting the two measures response bias and discriminability, see Figure 4.1. The discriminability proposed by the SDT refers to the internal discriminability to external stimuli. Theoretically, discriminability refers to the distance between the internal noise and signal probability distribution, which is captured by trial-to-trial changes as information accrues to the observer (Atkinson, 1963).

The assumption of the dual-process signal detection model introduced by Yonelinas and colleagues (Yonelinas, 1994) was that recollection is a threshold process and familiarity a signal detection process. Fifteen years later Yonelinas and colleagues (Yonelinas et al., 2010) showed that this assumption is well supported by reviewing empirical evidences. For more clarification of the connection of the familiarity acquisition and the SDT measures, we illustrated the shift of the signal and noise distribution in the Figure 4-1 by two signal distributions. This shift of the signal distribution should indicate the sharper separation of signal and noise distribution.

With regards to this, our learning task is very similar to the experimental procedure of measuring familiarisation acquisition (Zimmermann and Eimer, 2013). Accordingly, we proposed that the discriminability increases across the sequential positions and indeed, for discriminability we observed a significant increase in the second simple effect (see Figure 3-6-E).

Considering the course of effect size of the HR (and RR), the strongest effect was also observed for the second simple effect. Further, the response bias revealed a significant decrease for the third simple effect. In the following, we review these evidences and point out arguments based on the experimental setting why it was the second simple effect which became the effect of interest.

Regarding the sample stimuli of a series, new visual information will always be presented until the end of the presentation of a series. This was realized by the incremental change of illumination on a 360° frontal plain. During a full rotation on that plain, the maximum illumination difference was reached by the half of the presentation sequence, and towards the end it came closer to the illumination situation it had started with. This means that the last sequential position presents new stimuli of the TFID, but not necessarily new facial features were revealed at the end. Evidence for this interpretation was that the maximum of discriminability is reached at the third sequential position. However, following this, the discriminability wold be expected to remain stable and not to decrease.

For a better understanding, we recapitulate how we think the internal model was built. In the light of the two-tone image perception, the internal model incorporates prior knowledge (Dolan et al., 1997; Mooney, 1957). That means we rely on face knowledge to complete the missing information. Accordingly, the internal model building starts with the very first stimulus presentation and, as the PCT proposes, it will be constantly being refined by prediction errors (PE) of further presentations (Apps and Tsakiris, 2013; Friston, 2003, 2005; Schultz and Dickinson, 2000). In consequence, it is the PE that transports the new information into the internal model by an initiated update process (Apps and Tsakiris, 2013), whereas already known information would be used for verification.

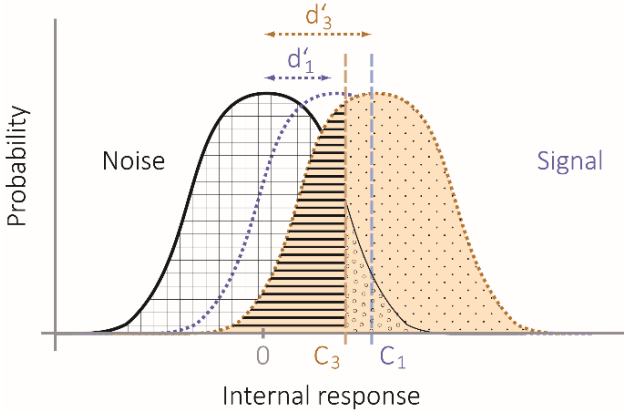

Figure 4-1: *Schema of the signal and response bias shift from the first to the third sequential positions*. The increase of the discriminability (d') across the sequential positions indicates for both the MEG and the fMRI study an increase in the Signal from the noise distribution. The maximum was reached at the third sequential position in both studies. For more clarity, the second and the fourth intervals were skipped, but as the results indicate, both would fit in between the d'1 and d'3 for both experiments. The small shift of the measure of response bias (C) is also indicated. The response bias refers to the threshold of a participant (observer) to respond with 'yes' (to the right) or 'no' (to the left).

To understand the update processes of the internal model driven by each further presentation of a two-tone stimulus, we review the recognition process of a two-tone stimulus described by the recognition model by Cavanagh (Cavanagh, 1991). Cavanagh proposes that first a contour analysis is applied and that hereafter a match of the contours and mnemonic templates is applied. This match is being done to separate the contours into object, cast and attached shadow borders, because mainly the object boarder led to select a template of the right object. According to Cavanagh the template provides 3D knowledge about the face and based upon that, a prototype is built. This prototype is used to disambiguate the residual contours by an estimate of the illumination direction and determines cast and attached shadows (Cavanagh, 1991).

Respecting this, the following assumption can be made: First that the initial prototype selected with the first stimuli of the TFID will be used for the further two-tone stimuli of the TFID to be learned. Second, in respect to Cavanagh recognition model, the illumination estimates in each subsequent two-tone stimulus will be used for prototype refinement by the of new extracted facial features revealed by new illumination directions. Third, according to our processing model of our experimental setting (Figure 2-5) we proposed when a prototype (= internal model) exists and is used for predictions,

the features just learned will immediately be incorporated in the prediction. This is supported by the finding of ABA in the cITG in the post-stimulus time window. The cITG was reported to be activated when shapes are extracted from shading cues (Georgieva et al., 2008). ABA in the cITG led to the interpretation that the knowledge of shape predicts shading cues.

The increase of discriminability at the second simple effect and the decrease of the response bias at the third simple effect could indicate an increase in uncertainty at the end of the sequential position. This interpretation is supported by the discrepancy between the features predicted upon the refined prototype and features extracted of a stimulus out of the last sequential position. This discrepancy could presumably arise, because the model building is an estimate and includes prior knowledge. However, an alternative suggestion is that the earlier stimuli the model building started with are linked to an innate uncertainty which the last stimuli of a series with similar illumination condition trigger. Given these facts, it is plausible that the second simple effect is the simple effect with the maximum difference in HR, RR, and distinctness.

4.2.3 Timing Differences are the Most Probable Cause of the RT Effects Measured in the fMRI Study

The pattern of the response types of the fMRI study met the previously discussed points of the pilot and MEG studies: The increase in HR and RR of match responses and an increase in discriminability indicated a positive learning progress referring to familiarization acquisition. The discriminability increase measured by the fMRI study confirmed the refinement of the internal model across the sequential positions by the same pattern: An increase was observed from the first to the third sequential positions. The missing response bias effect in the fMRI study diminished the hazard of the discriminability impeded by response bias. Further, the fMRI study confirmed the highest contrast for discriminability of the MEG study with the second simple effect, which was relevant for neurophysiological investigations. Hereby, we conclude the three studies showed converging evidence.

Remarkably, for the fMRI study a significant RT decrease was observed. The decrease was observed for RT for HR and RR for the match responses. All this observation refers to for the second simple effect. Thus, this observation is in line with our initial hypothesis that the learning should be measured with an increase in HR and a decrease in RT. According to our assumptions, we did not observe any significant effect regarding the non-match condition. However, we analysed the RT for the sequential position, regardless of the response type, and also observed a significant decrease in the second simple effect. The non-match responses also contribute to this effect, and, thus, we cannot completely rule out that an increase in the RT is solely due to the learning and that a certain improvement in the task per se drives the RT decrease as well in form of a contributing factor.

However, we argued earlier that the missing RT effect in the pilot study (and MEG study) was due to task instructions, but the task instruction did not change between these two studies. The question arises as to why do we measure significant RT decreases with the fMRI paradigm but not in the pilot and MEG paradigms. The factor which can be objectively examined are the alteration of the timing parameters in the experimental setting. Whereas the timing parameters in the pilot and MEG studies did not vary in the delay and cue latency, both were jittered in the fMRI. The jittered delay between sample and test stimulus led to a *Stimulus onset asynchrony* (SOA) of the test stimulus. We propose the best explanation why RT effects were observed arise with the SOA.

Support for this is that the use of a high SOA in fMRI studies is been done to separate the haemodynamic response function (HRF) to the corresponding events, thus, the conditions are able to separate for statistical analysis (see SPM guidelines). According to that, this means the stable delay between sample and test stimulus led to entangled sample and test post-stimulus processes in the MEG (and Pilot) study which is disentangled in the fMRI study. Therefore, applying SOA the proportion of RT decrease due to learning across the sequential positions becomes measurable in the fMRI experiment. Consequently, for the MEG (and Pilot) study the delay led to carry-over post-stimulus processes of the sample stimulus into post-stimulus interval of the test stimulus. However, the carry-over of processes does not alone explain the missing RT effect in the MEG (and Pilot) studies. In the assumption of the carry-over effect, another consequence is that the transferred process must counteract the RT-related learning effect, otherwise

RT effects would have been measured in all studies. In the following, we provide an explanation why sample post-stimulus processes most probably become longer.

We assume that across the sequential positions the PE become more which might be the contributing factor why sample post-stimulus processes increase. Again, we explain this with reference to the processing model. The early internal model is raw and contains less details, the consequence of this is that the early matching processes can be associated with rather raw update processes then detailed evaluation processes of the internal model. However, the later becomes the case with increasing details of the internal model. Thus, the PE become more detailed, but also become another quality due to an intermediate internal model which contains more and more sufficient information. This information is sufficient enough to separate the visual information input into new visual information and known information and further to separate the new information in conflicting (when features of a false positive are integrated) or coherent new visual information. Thus, these PE contain a different quality as that they led to reject information of the intermediate internal model to become a mature internal model. This concept of PR driving model refinement and referring this mechanism to familiarity acquisition was first described by Apps and Tsakiris (Apps and Tsakiris, 2013). Consequently, the probabilities of PE and related processes increased across the sequential positions, and, therefore the sample post-stimulus processes increased. This can be one explanation why RT effect were not measured in the MEG and Pilot experiment.

In summary, the measured RT effect in the fMRI experiment did meet all our hypotheses. We observed a positive learning effect by an increase in HR and a decrease in RT. The fMRI study revealed explanations for the missing RT effects in the MEG study by the presence of a SOA. We proposed that sample post-stimulus processes increased across the sequential positions due to PE related processes. Further, we proposed that these processes carry-over into the test stimulus interval and here counteracts the RT increase due to learning.

4.3 Neural Measures Reveal a Face-Identity Predictive Network

4.3.1 The Familiarity-sensitive ERF 250 Confirmed Sample Stimuli Participate in Learning

The positive learning progress was measured by an increase in HR and discriminability. These measures rely on the target detection in the test stimulus. Nevertheless, we proposed the learning was a consequence of both, sample and test stimuli of each trial. Thus, the next step was to confirm this by verifying a learning effect related to the sample position. For this, we use findings of electrophysiological studies that showed an enhanced brain activity when viewing familiar faces at a latency of about 250ms (Kaufmann et al., 2009; Saavedra et al., 2010; Sagiv and Bentin, 2001; Tanaka and Pierce, 2009; Tanaka et al., 2006; Gosling and Eimer, 2011; Weibert and Andrews, 2015). These studies are usually EEG studies. However, the MEG has the same time resolution and sensitivity, and the components are analogously described by an M for magnetic instead of N or P, indicating a negative or positive deflection. Thus, we propose that the contrast of maximum discriminability in the behavioural measure is accompanied by an enhanced component around 250 ms.

The time window which is related to the component around 250 ms varies across the studies from 200 ms to 400 ms. With a good fit, we measured a significant difference in the ERF time course from 150 to 270 ms by a *t*-test for the proposed contrast. We further selected the maximum amplitude within the significant time window and trained a support vector machine to discriminate between trials belonging to the first or third sequential positions. This analysis revealed a higher relevance of the time window from 240 to 270 ms, i.e. the time window that we referred to as the M250 component. This time window confirms previous reports of components around 250 ms related to familiarity. For example, a study by Kaufmann and colleagues (Kaufmann et al., 2009) found a higher negativity between 240 and 280 ms, which they refer to as the familiarity-related N250 component; this is in line with our results. In their task, the participants repeatedly detected the same face identities and different strangers in four different blocks. The familiarity effect was associated to the block effect for learned face identities. Another study by Zimmermann and Eimer (Zimmermann and Eimer, 2013) investigated familiarity acquisition by using of a pair of rendered face stimuli changing in identity

and/or viewpoint. They observed a N250 component related to familiarity in the time window of 210 to 260 ms for face repetition with the same view from the beginning on, but also in later trials for view-change trials indicating the face recognition had now become more view-independent. The N250 component of Zimmerman and Eimer (Zimmermann and Eimer, 2013) is wider and fits in with the unsegmented time window of ours. However, the segmentation of our significant time window, in accordance with the ERF amplitudes, is verified by a further correlation analysis (Figure 3-18).

After source localization of the ABA in the expectation time window, we investigated the relationships between each source activity determined by peak voxels and the defined ERF components. Hereby, we found a positive relationship between the occipital face area (OFA) and the M200 component. If the differences of alpha frequency band activity in the OFA in the expectation time window increased, the difference in the M200 amplitude also increased. It is suggested that the OFA in the face processing network between the primary visual areas and FFA is a crucial operator for face parts (for a review see Pitcher et al., 2011). The ABA of the OFA in the expectation time window could indicate the expectation of the changeable aspects in facial parts within the internal model due to changes of illumination conditions revealing new aspects of facial features. The relationship of the OFA and the M200 component indicated that the M200 needs to be considered separately from the M250 component: as an earlier component relevant for extracting facial parts. Further, the component around 200ms is also a face sensitive component referring to structural encoding, e.g., texture, reflectance and second order spatial relations preceding the individual face recognition-sensitive M250 component (Schweinberger and Neumann, 2016). Schweinberger and Neumann reviewed findings of the P200 component and concluded that the P200 is sensitive to facial prototypicality. Their interpretation was supported by a study by Schultz and colleagues (Schulz et al., 2012). The authors observed that morphed photographs decrease the P200 amplitude when the faces appeared more caricature-like and increased when the morph led to an anti-caricature percept of the face.

In respect to this, the increased amplitude in the ERF time course of the M200 component for the familiarity contrast could be interpreted to correspond to the perception of the two-tone stimuli becomes less caricature-like and more realistic. This means that in the

beginning the black and white stimuli are more perceived as a kind of caricature, and by gaining more knowledge (for example, volumetric and feature knowledge) and including prior knowledge of faces (faces contain texture and colour) the perception of the two-tone stimulus becomes a more of a “photorealistic” type of perception. This could be for one explained by the prototype refinement that we have already described in Chapter 4.2.2 The Hit Rates and the Discriminability Best Describe the Visual Learning. In this Chapter, we have already introduced the two-tone recognition model by Cavanagh (Cavanagh, 1991) which suggests, among other steps, that prototype selection is crucial for two-tone images of faces. We have suggested that the prototype selected for the target face recognition in a two-tone stimulus must be the same and further gets refined by new features detected in later stimuli of the TFID. A refined prototype should then lead to a more photorealistic perception. The enhanced M200 could refer to this.

We also respected later ERF components that were outside the significant time window the variance analysis revealed. Hereby, a relationship between the ABA and the OFA in the expectation time interval regarding the N400 component (right sensor selection, 440ms +/- 50ms) was observed. We first conclude that the N400 component is not exclusively linked to familiarity, because the *t*-test revealed no significance for this component. However, the N400 is often reported to come together with the N250 component in face learning paradigms (Boehm and Paller, 2006; Joyce and Kutas, 2005; Kaufmann et al., 2009; Trenner et al., 2004; Wiese and Schweinberger, 2015). Schweinberger and colleagues (Schweinberger and Neumann, 2016) described in their face processing model that the N400 component refers to the *person identity node* that covers semantic processes. These semantic processes are linked to high conceptual level processing which in turn correspond to several kinds of semantic or associative information (Coronel and Federmeier, 2016; Dietl et al., 2005; Wiese and Schweinberger, 2015). Wiese and colleagues (Wiese and Schweinberger, 2015) combined a semantic priming and faces learning paradigm and observed significant differences in the N400 component when semantic knowledge was involved in face detection. In line with this interpretation, the absence of a N400 component in patients with prosopagnosia strengthens the interpretation that the N400 component is associated with semantic memory processes for faces (Eimer, 2000). Last but not least, Olivares (Olivares et al.,

2015) resumed in his review that the modulation of the negativity around 400 ms is related to the retrieval 1) of content from face representations and 2) of its associated (verbal) semantic information. With regard to this, the observed M400 component might be an evidence for a strategy the participance used which is which is to associate attributes to the TFID like a name and character trait.

However, the link between ABA in the OFA and the M400 is surprising. We propose an explanation can be found by differentiating when the OFA serves a prediction or detects face parts. The difference is whether the OFA sends information top-down (prediction) or bottom-up (sensory integration). In experiments related to feedforward models of face perception (bottom-up sensory integration), the OFA activity was reported to be sensitive to facial parts (Pitcher et al., 2011). The function of the OFA in a face-identity-predictive (FIP) network is to exert top-down influence. This means that in the absence of a stimulus (and, therefore, with a weaker input of early visual areas) the OFA receives and integrates information receiving from hierarchically higher brain areas and must interpret other information than visual information. The relationship between the OFA and the M400 might be an evidence for the fact that the OFA integrates other information than solely face parts in the expectation interval.

The studies mentioned above report for the ERF components either activity on right sensor selection or both, left and right. Below, we discuss why the effects reported in our study were registered on the left sensor selection (e.g., the M2 and M250 components). Further, these arguments account for the left brain activation seen in the fMRI experiment. Left posterior brain activation had been linked to face learning (Bi et al., 2014; Leube et al., 2003). An interesting study by Tacikowski and colleagues (Tacikowski et al., 2011) showed that familiar names evoke a stronger signal in the left rather than in the right inferior temporal sensors. A patient study by Lambert and colleagues (Lambert et al., 2006) who examined face recognition and naming with patients concluded a greater face recognition impairment in patients with right temporal lesions and a greater naming impairment in patients with left temporal lesions. Thus, we propose that our registered left brain activation is due to learning and related strategies as, for example, naming.

An alternative explanation for a learning strategy of the participants could be that they attended to parts of the face, which was also found to enhance left temporal activity (Lobmaier et al., 2008; Martinez et al., 1997). Lobmaier and colleagues (Lobmaier et al., 2008) conclude, based on their results, that two distinct neural pathways exist for either featural (left brain activation) and configural information (right brain activation) integration.

With respect to our experimental setting, the following aspects across the sequential positions were verified by the ERF results: 1) revealing different facial features by illumination differences, 2) familiarity by repetition of target faces, and 3) forming associations to facilitate learning. We link this to the following ERF components: 1) Prototype refinement and facial feature extraction is referred to the M2 component, 2) familiarity acquisition is referred to the M250 component, and 3) familiarization associations are referred to the M400 component. At the end, the ERF result met our previous hypotheses, thereby we gain a neural index to show the familiarity acquisition is referred to the sample stimuli, but further we gained two more components due to the nature of the experimental setting. In sum, regarding the two introduced face processing model (Olivares et al., 2015; Schweinberger and Neumann, 2016), our findings fully support the current model of face recognition represented by ERF components.

4.3.2 The Expectation Interval Revealed Beta and Alpha Frequency Band Activity

Herewith, now we now turn to our main question of interest to identify a predictive network by familiarity-related changes in low frequencies in the expectation interval. The concept of expectation in the framework of predictive coding is suited to investigate predictions, as it is defined by “the representation of what is predicted to occur in the future” and separats from ‘anticipation and prospection’ (Bubic, 2010). It is noteworthy that it was suggested that expectation plays a major role when bottom-up sensory input is ambiguous (Pinto et al., 2015), and on the psychophysical level it has been shown that the experimental modulation of expectations improves response behaviour (Clark, 2013; Lupyan, 2015; Pinto et al., 2015). Moreover, there is some evidence of power changes in the A&BBA in the pre-stimulus time window when expectation was modulated and

predictions were investigated (Bauer et al., 2014; Mayer et al., 2016; Brodski-Guerniero et al., 2017; Kok et al., 2017). For example, the recently published study by Brodski and colleagues (Brodski-Guerniero et al., 2017) describes a face-predictive network in which power changes of A&BBA were recorded. In this study, the expectation was modulated by different blocks, e.g., house block, in which a house was expected, and face block, in which a face was expected, but stimuli of either category were presented. The face prediction network, which was found by the contrast face versus house blocks, comprised A&BBA in V1, PPA, aIT and FFA. Also, the OFA was part of this face-predictive network, but no link was determined within the face-predictive network by information-theoretical measures. In line with this, we found a change in ABA and BBA in the expectation interval. In the case of this study, it turned out that only ABA relates to our prediction network. First, the ANOVA revealed only a tendency towards a change in the BBA, and second, only the cluster of the ABA, but not the BBA, in source space has a positive relationship to the behavioural increase in discriminability (d-prime). Even if plausible brain regions in the BBA were located, we could not reliably relate BBA and the related brain areas to predictions in the expectation interval. One of these plausible brain regions is the hippocampus, which has (especially in the framework of PCT) recently been discussed to be involved in uncertainty (Harrison et al., 2006) and contextual predictive mechanisms (Mizumori, 2013). The second brain region is the FFA which is strongly associated to face recognition (Kanwisher et al., 1997; Kanwisher and Yovel, 2006) .

4.3.3 Verifications and implications of the MEG Sources by the fMRI Study

Based on the peak values of ABA in the expectation interval (Figure 3-12), we introduced a face-identity-predictive (FIP) network including (Figure 4-2). The FIP network comprises brain areas related to (1) early vision, like the cuneus that we referred to the secondary visual area V2, (2) early face recognition like the occipital face area (OFA) (Pitcher et al., 2011) and (3) brain areas that have been related to perceptual closure processes like the lateral occipital cortex (LOC) (Grill-Spector et al., 2001; Grutzner et al., 2010). Further, the FIP network comprises brain areas related to memory functions like the (4) precuneus (PreC) in the left and right hemispheres and (5) the parahippocampal gyrus (PHC).

The follow-up decoding analysis via a sequential classification approach (SCA) revealed a sequence of six sources which were, according to the SCA procedure, ordered by relevance: PHC, OFA, right PreC, V2, LOC and left PreC. Looking at the effect size (ES) a similar pattern was observed: A medium ES was registered for the first three voxels and a small one or less for the others. Even if all sources were respected, this tentatively suggests that the PHC, the OFA and the precuneus, that is to say the first three sources of the sequence, were probably the more relevant sources.

Further, three sources (OFA, LOC and PreC) were more or less verified by the fMRI study. While conducting the fMRI study, we expected to gain further insights into the mapping of the expectation interval in the assumption of a positive relationship of ABA and BOLD response. Considering the relationship between the electro-physiological frequencies band activity and BOLD responses, the literature refers to two main findings. First, higher frequencies are better correlated than lower frequencies (Niessing et al., 2005; Scheeringa et al., 2016). Second, most studies that report high correlation of ABA and BOLD response posit a negative relationship between ABA and BOLD and show decreasing post-stimulus-related ABA (Goldman et al., 2002; Hall et al., 2014; Laufs et al., 2003; Scheeringa et al., 2011, 2016; Winterer et al., 2007; Zumer et al., 2010). Some exist which report positive relationships between ABA and BOLD response (Gonçalves et al., 2006; Jann et al., 2009; Mayhew et al., 2013). For most of these studies it applies that these refer to resting state recordings (Mayhew et al., 2013). Interestingly, Liu and colleagues (Liu et al., 2012) report the relationship of deep brain (thalamic) ABA to be positive correlated to posterior BOLD responses. This evidence illustrates that both measures of the same mechanisms (expectation of the TFID) do not have to show the same spatial activation pattern, rather indicate that the measures capture a different brain signal. Considering this, the relationship between the different brain activity captured by MEG and the fMRI will shed more light into this.

Briefly, the MEG signal is mainly caused by the primary current, whereas the source of the primary current is the excitatory postsynaptic potential in pyramidal neurons of the cerebral cortex (Onozuka and Yen, 2008). Thus, the MEG signal can be interpreted as a direct signal of neuronal function. Not that simple it is for the BOLD signal.

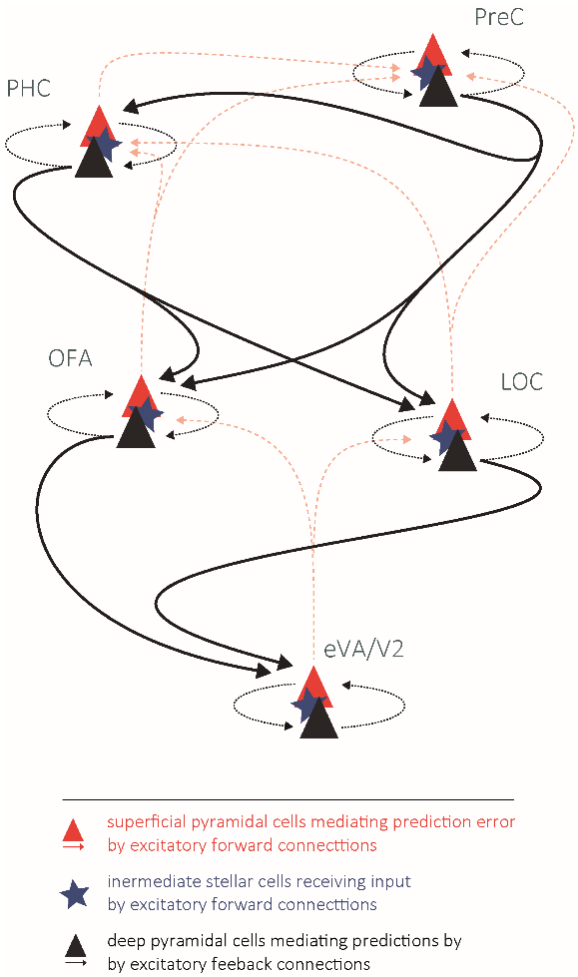

Figure 4-2: *Outline of the face-Identity-predictive (FIP) network.* The outline represents the network determined by investigating the alpha frequency band activity (ABA) in the expectation interval. Each brain area is indicated by a superficial (layer 2/3) and deep pyramid (layer 5/6) cells and intermediate stellate cells (layer 4). The layer-intrinsic wiring is abstracted by a dotted circular flow, for more details, see the Introduction and Figure 1-2. The FIP network illustrated here is proposed to represent the internal model. According to Bastos and colleagues (Bastos et al., 2012), ABA represents top-down influences, thus, upon the anatomical connections we illustrated feedback connections between the brain regions by a black arrow conveying predictions top-down. We illustrated feedforward connections by dotted pale red arrows upon anatomical evidence (Felleman et al., 1991). Feedforward connections project onto stellar cells. Feeback connections project onto superficial and deep layer neurons but terminate in the superficial layers, because deep layer pyramid cells have dendrites reaching to the superficial layers.

Seminal work was done by Logothetis and colleagues who described that the BOLD signal captures LFP and multi-unit activity (Logothetis et al., 2001) but also synaptic modulatory activity (Logothetis, 2002). Logothetis (Logothetis, 2002) explained BOLD responses in V4 during motion perception by anatomical descending connections from MT which might be of modulatory function. Thus, the BOLD response in V4 referred to synaptic activity in V4 with its origins in MT. This evidence is in line with the PCT that top-down influence is

associated with a modulatory effect in lower cortical brain regions, especially when it comes to the precision of the prediction (Kanai et al., 2015). Considering this, the BOLD response observed in the ventral stream could possibly refer to synaptic activity which originates in sources captured by brain areas located at the top of the hierarchy like the PHC and the precuneus located by the ABA. Further support for this is that early sensory brain areas receive top-down predictions to prepare for post-stimulus processing reported by Bauer and Colleagues (Bauer et al., 2014). In the case of the FIP network this preparatory function might apply to the PHC which is part of a large network connecting frontal and parietal brain areas but also temporal and occipital regions (Aminoff et al., 2013) but also preparatory function might apply to the PreC.

Alternatively, the brain areas revealed by the BOLD signal may be associated to a slightly different brain mechanism because of a much broader time window captured by fMRI compared to MEG. In other words, the differences captured by the fMRI might be due to the low time resolution of the fMRI. This is supported by the left brain activity in the occipital fusiform gyrus. Bi and colleagues (Bi et al., 2014) reported left brain posterior brain activity during learning of facial identity. They argue that the left fusiform cortex is more susceptible to perceptual learning and more plastic. As a result, the left fusiform cortex is open to changes and better able to adapt to these changes in the dynamic visual world, and in contrast the right fusiform cortex is fixed in the mature brain in its function (Golarai et al., 2007). Thus, we conclude that at least these left brain regions captured by the BOLD signal and not by the ABA may correspond to the perceptual learning mechanisms.

Summarizing this, the predictive brain sampled by the BOLD response and the ABA revealed same overlapping and not overlapping brain regions. The OFA in both measures overlaps by close voxels surrounding the peak voxels. The other brain regions do not overlap but are closely neighbouring each other; these are the left PreC, the LOC and the cuneal/V2 activity. A brain region hardly detected by the BOLD signal was the PHC. Among all six brain regions, the PHC was determined as one of the highest in the hierarchy. Because this region was considered as one of the brain areas of higher relevance, this is in line with earlier studies that the BOLD response might capture synaptic top-down modulatory activity, rather than local activity.

4.3.4 Potential Functions of the Sources of the Face-Identity-Predictive Network

The PHC is the upper part of the medial temporal lobe, located at the junction between the hippocampus and the fusiform gyrus, thus, between memory formation and high level visual processing. Accordingly, as mentioned above, the PHC is part of a large network connecting temporal (e.g., OFA, LOC), parietal (e.g., PreC) and frontal cortices. In respect to all the various memory and cognitive functions, the shared elemental function of the PHC is to build of contextual associations (Aminoff et al., 2013; Diana et al., 2007; Raslau et al., 2015). We conclude that the PHC presumably represents the main hub of the six brain areas of our FIP network. In respect to its episodic memory and associative functions and the anatomical connections, we suggest that the PHC collects the information from the ventral and dorsal stream and associates the (feature) information of previous and recent sensory information. In our experimental setting, previous and recent sensory information reveal different feature information. To bind the pieces of featural information to form a coherent internal representation, past and recent evidence must be retrieved in parallel. We propose that the PHC presumably enables hierarchically lower brains areas (like the OFA and LOC) to form a coherent representation by associating the previous and recent visual evidence. On the assumption that the OFA receives information about past evidence from the PHC, the OFA presumably is enabled to bind featural information from previous and recent evidence to form a more precise internal model and, thus, a more precise prediction about face parts constituting the face identity. Similar top-down influence of the PHC on the LOC presumably sharpens the prediction of closure solutions provided by the LOC for forthcoming closure situations by providing predictions about the 3D shape (Moore and Engel, 2001).

The PreC activity was related to various memory-related functions like episodic memory retrieval (Krause et al., 1999), memory-related imagery (Fletcher et al., 1995) and familiarity (Leveroni et al., 2000; Natu and O'Toole, 2015). In line with this, studies using perceptual closure paradigms discuss the PreC activity to be involved in memory-related closure processes (Dolan et al., 1997; Grutzner et al., 2010; Ludmer et al., 2011; Bertrand et al., 2013). Regarding the anatomy, the PreC was reported to be the most prominent

hub in the brain (Cavanna and Trimble, 2006; Tomasi and Volkow, 2010; Utevsky et al., 2014) and discussed to be a candidate for internal model representation (Land, 2014).

The perceptual closure task is solved during stimulus presentation and not during the expectation interval. We assume that the expectation interval necessarily shares mental imagery functions which is usually reported for the retrieval interval in a working memory paradigm. Therefore, we refer to the visual and mental imagery as episodic memory retrieval function of the PreC (Fletcher et al., 1995). In doing so, the PreC might function as a second main hub supporting the PHC by binding information through visual mental imagery. Further evidence for this is that the PreC is connected to higher association cortical and subcortical associative structures but not to primary sensory regions, implying no direct processing of external stimuli but being involved in elaborating highly integrated and associative information like imagery (Cavanna and Trimble, 2006).

Figure 4-2 illustrates the FIP model. In this model, we make suggestions as to how the brain areas are wired and from where information is transferred. According to the PCT, the ABA is associated with predictions sent top-down the cortical hierarchy (Bastos et al., 2012). Respecting our brain areas oscillating in the alpha frequency and regarding the anatomical evidence (Felleman et al., 1991; Maunsell and Essen, 1983), we propose a message passing via feedback connections between the five functional brain areas. According to the PCT, the gamma frequency band activity (GBA) is associated with PE sent bottom-up via feedforward connections within the cortical hierarchy. We did not investigate the GBA, because we assume no PE in the expectation interval. Therefore, we indicate feedforward connections by pale red dashed lines to highlight that this is not indicated by our measurement, but in principle we respect that the anatomical evidence for these connections exists to enable PC.

4.3.5 A Distinction Between the Alpha Frequency Band Activity Measured in the Pre- and in the Post-Stimulus Interval

A recent debate in the PCT is if ABA carries the prediction itself (Mayer et al., 2016) or if ABA refers to the precision of the prediction (Sedley et al., 2016). To get closer to answering this question, we first of all suggest a distinction between the ABA measured

in the pre- and in the post-stimulus interval. We suggest that changes in the ABA in the expectation interval (pre-stimulus) represent the prediction, thus, the internal model, because no PE is minimized and internal processing mechanisms are predominant. Especially, regarding the experimental setting we assumed according to Bubic and colleagues (Bubic, 2010) that the investigations of the expectation interval refers to the investigation of prediction related processes. In contrast, because a visual stimulus of a face is presented, in the post-stimulus interval the processing of the visual input stimulus is predominant. During that interval, the internal model should be involved in explaining the PE away (Friston, 2003, 2005), and according to the PCT, the PE in this time interval initiate an update of the internal model. Therefore, we propose that the ABA in the post-stimulus interval ought to resemble but not be identical to the ABA in the expectation interval.

Accordingly, we tested changes in the ABA in the post-stimulus interval and revealed a significant cluster with some identical sources but also additional ones. One conserved functional source is the PreC; even if it is not at the exact same location, it probably serves a similar function by representing aspects of the internal model on an abstract level.

As proposed by Cavanna (Cavanna and Trimble, 2006) and also lately by Land (Land, 2014), the PreC is a candidate for representing the internal model. Our data can be interpreted as supporting this proposal because of the ABA in the PreC in the pre- and post-stimulus interval. That means that in both time intervals we assume the internal model to be involved, and the common denominator in both networks is the PreC.

4.3.6 Potential Functions of the Sources in the Alpha Frequency Band Activity in the Post-Stimulus Interval

Furthermore, based on the ABA in the post-stimulus interval, we introduced three additional brain areas (Figure 3-14) not captured by the FIP network. The network comprised brain areas related to (1) early vision (eVA1) by activity in the occipital pole expanding into the cuneus (V1 / V2 activity), (2) the integration of shapes-from-shading by activity in the caudal inferotemporal gyrus (cITG) and (3) object recognition by activity occipital fusiform gyrus (OFG/V3).

Activity in the cITG had been reported by Georgieva and colleagues (Georgieva et al., 2008) to be associated with the extraction of 3D shape from texture and shades. This interpretation of activity in the cITG had been adopted in the Mooney face detection task (Grutzner et al., 2010) with regard to the cast and attached shadows in two-tone images which result in the 3D interpretation of a two-tone stimuli (Cavanagh, 1991; Moore and Cavanagh, 1998).

In our experiment, the ABA in the cITG in the post-stimulus interval probably indicates that the cITG provides increasing predictive information about cast and attached shadows. This could be the case, because the internal model gains information about the 3D face structure across the sequential positions. Since the cITG is reported to *extract* the 3D shape from shading cues (Georgieva et al., 2008), it is probably not part of the internal model, because it does not itself represent the abstract 3D structure, thus, no pre-stimulus activity is recorded in the cITG. Moreover, the internal model increases in abstract cues for 3D face structure, which is stored in the abstract internal model. We reviewed that pre-activation of the internal model in the ABA probably modulated hierarchically lower brain areas by tuning the gain of neurons. Respecting this, the cITG could be the target of modulated gain, and, thus, enabled to form itself an estimation of 3D extractions to send down the cortical hierarchy (V2 and V1). In doing so, the cITG increases in sensitivity and predicts more precisely the cast and attached shadows of every further stimulus by the top-down influences of the internal model (Figure 4-3).

The location of the activity of the OFG matches the location of the ventral primary visual area three (V3). The ventral V3 is sensitive to colour as V4 but also sensitive to binocular disparity and thereby contributes to stereoscopic depth processing (Nasr et al., 2016). Regarding the anatomical evidence, the OFG/V3 is compared to the cITG in a hierarchically lower brain area. Therefore, we suggest the same mechanism for the OFG/V3 as proposed for the cITG. The difference is that the origin of the top-down information presumably comes from the cITG, and therefore the prediction contains information about the stereoscopic depth. This information transfer continues until the primary visual cortex, V1, is reached.

4.3.7 Post-Stimulus Alpha Frequency Band Activity Revealed the Extended Face-Identity-Predictive Network

With these (additional) post-stimulus brain areas, we conclude with proposing an extended FIP network. Presumably the brain areas found by post-stimulus ABA are under top-down influence of the FIP network activated in the expectation interval in the ABA.

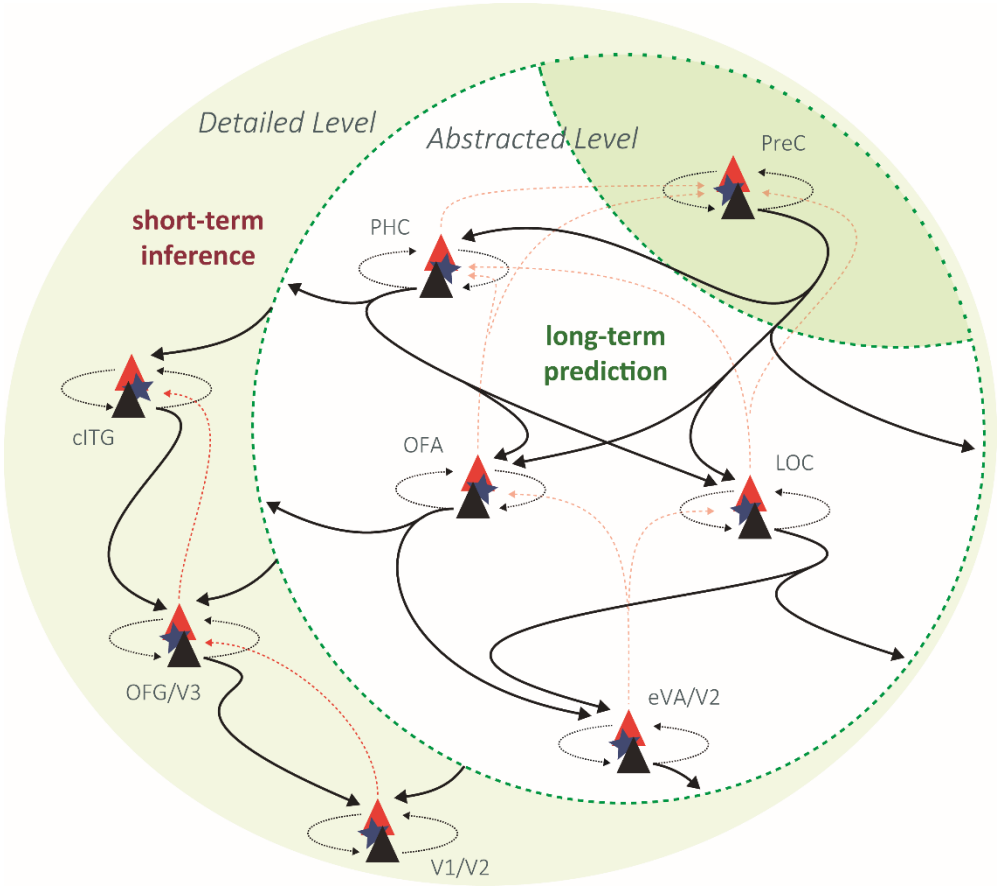

Figure 4-3: *Outline of the components and relationship of the FIP network and sources found in the post-stimulus interval.* This outline represents the sources determined by investigating ABA in pre- and post-stimulus time intervals. Hence, the network includes the FIP network introduced in Figure 4-2 (green dotted white circle). Because of the ABA in the precuneus in the pre- and post-sample stimulus interval, we propose that the precuneus (PreC) plays a central role in the representation of an abstract internal model. The brain areas outside the green circle refer to brain regions found by ABA in the post-sample stimulus interval. These brain areas are mostly early visual areas, and we refer to these brain areas to the extended subnetwork of the FIP network. Post-stimulus processes require an explanation of the input signal on a high-level of detail. Thus, according to Kwisthout (2017), we assume this subnetwork to represent the internal model on a high-level of detail which, in turn, also presumably represents short-term inference. In contrast, the core network, represented by the FIP network, represents the internal model on a low-level of detail which, in turn, also presumably represents long-term predictions. For legend, see Figure 4-2 and the list of abbrevations.

According to Kanai and colleagues (Kanai et al., 2015), the top-down influence can be modulatory by a hierarchical top-level brain area; we argue that this correspond to the FIP network previously introduced. Support for this is that brain areas of the FIP network are predominantly located higher the hierarchy. Kanai and colleagues (Kanai et al., 2015) proposed the pulvinar for neuro-modulatory gating or gain control of superficial pyramid cells transmitting the PE via feedforward connections. Although without direct evidence, we propose for our experimental setting, the case of learning a facial identity, that the PreC refers to the key player in representing the internal model. For future research, we suggest continuing with functional connectivity analysis like transfer entropy (Schreiber, 2000; Vicente et al., 2011) and storage analysis like local active storage (Lizier et al., 2012; Wibral et al., 2014) to test the proposed extended predictive model.

The FIP and extended FIP models had been proposed based on anatomical evidence and on the top-down information transfer associated with ABA according to current PCT. The recent debate about the precision of the prediction is ongoing, especially with respect to the biophysical implementation. With the following Chapters, we want to contribute to the recent debate by first reviewing recent evidence regarding the precision of predictions in PCT and second propose two interpretations of our findings with one including a new implementation of precision of prediction in PCT.

4.3.8 The Hypothesis of the Implementation of Precision in Predictive Coding Theory

The rise of a PE is due to a sensory evidence deviating from the current prediction. The consequence of the PE then is an update of the prediction to minimize the PE. We propose this update can correspond to A) *refinement* or B) *reselection* of the current prediction. The difference between *refinement* and *reselection* of a prediction is that the new prediction refers to a new (reselected) or an altered (refined) probability distribution of a current prediction. Regarding *refinement*, the probability distribution can be altered by incorporating the current evidence, because the context allows to do so (e.g., learning situation). In contrast, the probability distribution of each prediction, the previous and the current prediction, does not change when the prediction update refers to a *reselection.*

Considering the underlying probability distribution of a prediction, Feldman and Friston (Feldman and Friston, 2010) suggest the *precision of prediction* is related to the standard deviation (SD) of the probability distribution representing the prediction: a narrow distribution, i.e. a small SD, indicates a high precision. Correspondingly, a broad distribution, i.e. a high SD, indicates a low precision. Therefore, the increase of the precision is equal to the decrease in variance (smaller variance). The formalization of this uses the inverse variance, as this measure expresses a positive relationship to the precision of the prediction.

Referring the probability distribution as a dynamic function, for example, because the probabilistic structure is unknown and evidence collection is required, the probability distribution changes its shape as a function of sample size until the probabilistic structure is 'completely' known. To describe an intermediate shape of those dynamic probabilistic structure, a Gaussian distribution is not always sufficient (Kwisthout and van Rooij, 2015; Kwisthout et al., 2017).

Kwisthout and colleagues (Kwisthout et al., 2017) propose a mechanism of PE minimization which respects the precision of the prediction. The authors assume a categorical probability distribution instead of a Gaussian distribution. The authors introduce entropy as a function of the (nonuniformity) distribution and the (state space) granularity. Further, the authors introduce *level of detail* (LOD) as a concept that intuitively captures the (state space) granularity. The authors exemplify this concept by the throw of a coin in comparison to throwing a dice and only interpreting odd or even numbers. For both situations, the probability of the outcomes lies at 50%, but the granularity is higher for the throw of the dice, because we can face the one, three or five as odd numbers, and the two, four and six as even numbers. For the throw of a coin, we have two possibilities, head or tail. This simple example pictures a decrease in the LOD by concentrating only on certain information as being relevant in each outcome but also on what the uncertainty (or entropy) of the predicted outcome will be. This does not make a difference in the interpretation of a five to be odd, but in the prediction of throwing a dice with an odd number.

Kwisthout and colleagues (Kwisthout et al., 2017) proposed that PE minimization is realized by increasing the LOD of the hypothesis or decreasing the LOD of the prediction. According to the authors, hypothesis and prediction are variables of a (Bayesian) network. In this network, hypotheses jointly represent a set of working hypotheses, and predictions are based on these hypotheses. Further, a prediction is equal to a hypothesis of a node deeper in the hierarchical structure or vice versa: The hypothesis is equal to a prediction of a module higher in the hierarchical structure. Lowering the PE means to cluster or aggregate the values that the distribution can take to bring the observation and prediction closer together. Within that definition, the precision of the prediction is defined as a statistical property of the generative model at that LOD. The authors do not refer to a relationship of precision and LOD, because there is none. Furthermore, clustering the LOD has no impact on the precision of the prediction. The consequence of a 'precise' prediction is not to cluster probabilities, because the LOD of the prediction and the observation ideally match.

4.3.9 An Implementation of Precision of Prediction in Respect to the Theory by Kwisthout (2017)

Kwisthout and colleagues (Kwisthout et al., 2017) explain the proposed mechanism of PE minimization by the following example. Imagine an object in the visual field is passing by. There are two possible solutions: First, the passing object was a bird, or second, the passing by object was a robin. So, if detailed sensory information and precise knowledge of how a robin looks like was available, it is possible to call the species, i.e., it is a robin. This means that under low uncertainty (we clearly see the bird) and in a precisely predicted world (we know how a robin looks like) the minimization of the PE is on a high LOD. However, if we have less visual information, because the bird flew by quickly, existing knowledge of flying animals will be clustered (robin, nightingale and lark together are birds). To gain a unique solution of what passed by is to draw from a selection of different clusters which could be birds, butterflies and dragonflies. The answer then could be: It was a bird. The solution of the PE minimization comes at the prize of lowering the

amount of information but also of gaining a correct and at that level a more precise prediction, because the LOD of the prediction and the observation have a higher match.

Respecting this, there is a striking resemblance between the mechanism of switching the LOD for PE minimization proposed by Kwisthout and the view of representational modules across the cortical hierarchy. For instance, in the visual system the size of the receptive fields increases systematically between the visual areas up the hierarchy (Dow et al., 1981; Harvey and Dumoulin, 2011; Hubel and Wiesel, 1962). This 'dramatic' increase in receptive field size had been interpreted as leading to a successive convergence of visual information necessary for extracting invariance and abstraction (Lee and Mumford, 2003). It is suggested that the higher a cortical brain area is positioned in the cortical hierarchy the lower in detail and more abstract an object representation becomes (Lee and Mumford, 2003; Lee et al., 1998). This view is confirmed by the learning model of reverse hierarchy theory (RHT). The RHT, as proposed by Ahissar and Hochsteiner (Ahissar and Hochstein, 2004; Ahissar et al., 2009; Hochstein and Ahissar, 2002), posits that "high-level learning must precede low-level learning as it provides the essential enabling stage for the backward searching process." The authors deduce that learning begins at high visual levels and gradually progresses to low visual level (early visual) brain areas when a better signal to noise ratio is needed (Ahissar et al., 2009).

According to the proposed model by Kwisthout, for PE minimization one could tentatively propose that each brain area (at least of the sensory systems, e.g., ventral and dorsal visual pathways: V1, V2, V3 etc) could be associated with the granularity of a prediction, therefore, with the LOD. We propose an inverse relationship between the LOD and the size of receptive fields of a brain area. That means the earlier a visual area is located the higher is its LOD of a prediction.

Considering this, a shift of the LOD for PE minimization corresponds to the shift of the brain area providing the prediction which is located higher or lower in the cortical hierarchy.

4.3.10 Interpreting Our Results According to the Implementations of the Precision of Prediction

In our experimental setting, the increase of familiarity across the sequential positions was verified on the behavioural level by the discriminability and on the MEG sensor level by the ERF 250 component. This increase of familiarity we assign to a special case of increase in precision of an internal model. According to Bubic (Bubic, 2010), the internal model of the TFID becomes the prediction, as it is recalled (or retrieved) in the expectation interval. Thus, the increase in precision of the internal model could be associated with an increase in precision of prediction.

According to Sedley and colleagues (Sedley et al., 2016), precision is signalled by ABA, and the change of prediction is signalled by BBA. According to this and our experimental setting, we would not assume an effect in BBA. However, the tendency for a difference in BBA might tell that the experimental task was not exclusively solved by increasing the amount of details of a target but also by a switch of a prediction to improve in the task. This switch could refer to a recategorize of the internal model, for example the gender category first was defined to be androgynously and later features revealed the TFID to be a female. Support for this were hierarchically higher brain areas found with BBA and not with ABA. One example of this could be that the first stimuli and later stimuli differed in interpretation of the age or sex of the presented target face, therefore a different template is equipped, and the internal model updated. However, after correcting for multiple comparisons, the BBA effect remains a tendency only, and these are only speculations.

Furthermore, according to our experimental setting and the proposal of Sedley and colleagues (Sedley et al., 2016), we assumed a change in ABA. This is in line with our results: We can show a positive relationship between ABA and discriminability. Sedley and colleagues based their assumptions on investigating the PCT in the auditory domain. With our study, we show converging evidence for the visual system.

The sources activated in the alpha frequency band were in memory-related areas like the precuneus and the parahippocampal cortex, face-part detection areas like the OFA and perceptual closure-related areas like the LOC and cuneus (V2). The functional role of each

brain area was described in more details in Chapter 4.3.4. Moreover, we tested post-stimulus ABA upon the hypothesis that the precision of prediction is also a matter in the update process of the current prediction we defined as the refinement process. Corresponding to our observations in pre-stimulus ABA, we assumed an increase in ABA. The results met our assumptions, and the ABA was found in a large cluster with activity in the cuneus. In other words, the ABA distributed across the primary (V1), secondary (V2) and tertiary visual areas (V3). The different sources activated in pre- and post-stimulus interval also separate into hierarchical activity: Hierarchically higher brain areas were found in the pre-stimulus interval than in the post-stimulus interval.

In general, we interpret this finding that the ABA in the pre-stimulus interval signals the representation of the prediction and that the ABA in the post-stimulus interval is more likely to signal the refinement of the prediction. The former could be related to mechanisms of long-term learning, and the latter could be related to mechanisms of short-term inference.

Furthermore, according to the proposed implementation of the theory by Kwisthout (Kwisthout et al., 2017) of PE minimisation (Chapter 4.3.8 The Hypothesis of the Implementation of Precision in Predictive Coding) and to the finding that the ABA in pre- and post-stimulus intervals corresponds to the same internal model and its refinement, we propose that pre- and post-stimulus ABA refers to two different representations of LOD: In the pre-stimulus interval, in the absence of PE minimization, the ABA signals the precision of the internal model on an abstract LOD and in the post-stimulus interval in the presence of PE minimization the ABA signals an increase of precision of a higher LOD. Again, this is supported by the results that brain areas in the pre-stimulus interval were found on a higher hierarchical level than brain areas in the post-stimulus interval. Both LODs of the internal model are linked by an executive central which the activity of the precuneus could refer to.

If ABA in the pre-and post-stimulus intervals refer to one internal model and each represents a different LOD, both should be in direct interaction. This assumption is in line with the microcircuit theory of PCT by Bastos and colleagues (2012), who assume feedback connections to project onto layers 2 and 5 of the pyramid cells (Figure 1-2 in

Chapter 1.2 Distinctions of Low Frequency in Top-Down Predictions). Thus, top-down predictions project onto representation units of hierarchically lower brain areas, i.e. directly but also indirectly via interlaminar connections. It had been shown that pre-stimulus ABA modulates excitability in post-stimulus processes and that this mediates feedback influence (Jensen and Mazaheri, 2010; Thut et al., 2012; Weisz et al., 2011). This mechanism was interpreted to accomplish gain control and had already been associated to modulations of high frequencies band activity in post-stimulus processes signalling PE (Bauer et al., 2014; Feldman and Friston, 2010; Spratling, 2008). Accordingly, it seems obvious that the pre-stimulus ABA signalling top-down precision of predictions should influence further top-down predictions along the hierarchy, directly via projections onto layers 5 and 6 of the pyramid cells or indirectly via interlaminar connections, thus considering PE signals. Up to our knowledge, we are the first who respected the PE minimization proposed by Kwisthout and colleagues (Kwisthout et al., 2017) for neurophysiological data interpretation and further proposed an implementation of this PE minimization.

5 Zusammenfassung

In unserem Alltag begegnen uns oft dieselben Objekte wieder. Um eine valide und schnelle Objekterkennung zu gewährleisten, verlässt sich das visuelle System gerade bei häufig wiederkehrenden Objekten auf Gedächtnisinhalte. Die Predictive Coding Theory (PCT) liefert eine Erklärung, wie Erkennungsprozesse von vorhersagbaren Objekten schnell und zuverlässig ablaufen können. Die PCT schlägt vor, dass die Information, die in der Hierarchie von Hirnarealen von oben nach unten gesendet wird, kontextspezifisch und voraktiviert ist. Das heißt, diese Information hat einen Vorhersagewert, um die eintreffende sensorische Information zu erklären. Diese sensorische Information wird in der Hierarchie nach oben gesendet und mit der Vorhersage abgeglichen. Die hieraus resultierenden Restinformationen nennt man den Vorhersagefehler, welcher in der kortikalen Hierarchie weiter ausschließlich nach oben übertragen wird. Hieraus resultiert, dass der Informationsfluss zirkuliert: Der Vorhersagefehler aktualisiert die Vorhersage und die Vorhersage minimiert den Vorhersagefehler.

Das Konzept der PCT ist plausibel, und die Idee, dass die Wahrnehmung Gedächtnisinhalte verwendet, um Objekte zu erkennen, geht 150 Jahre zurück bis zu Helmholtz. Wie dieser Wahrnehmungsprozess im Gehirn realisiert wird, ist immer noch weithin ungeklärt. Allerdings schlagen Bastos und Kollegen (Bastos et al., 2012) vor, dass die neuronale Aktivität in hohen Frequenzen (> 30 Hz) die Vorhersagefehler und die in niedrigen Frequenzen (< 30 Hz) die Vorhersage repräsentiert. Dies macht die Theorie mit neurophysiologischen Methoden überprüfbar. Im Weiteren schlagen Sedley und Kollegen (Sedley et al., 2016) vor, die tieferen Frequenzen als Signale für unterschiedliche (top-down) Inhalte der Vorhersage weiter aufzutrennen.

Hieraus ergibt sich die Thematik der vorliegenden Arbeit. Diese Arbeit untersucht, wie sich das neuronale Netzwerk, welches Vorhersagen repräsentiert, räumlich und zeitlich verhält. Genauer prüfen wir, in welchen der tieferen Frequenzen die Präzision der Vorhersage repräsentiert wird. Hierfür werden visuelle Informationen für eine genauere visuelle Vorhersage schrittweise kumuliert. Wir nehmen an, dass über diese Kumulation der visuellen Information die Details eines inneren Modells zunehmen und somit auch die Präzision der Vorhersage ansteigt. Über die Beziehung von physiologischen Änderungen in tieferen Frequenzen zu einer Präzisionsänderung der Vorhersage sollte

die Vorhersage räumlich und zeitlich lokalisierbar werden. Hierfür kommen elektrophysiologische (die Magnetenzephalografie, MEG) und hämodynamische (funktionelle Magnetresonanztomografie, fMRT) Messmethoden zum Einsatz.

Für unsere Untersuchungen verwenden wir in einem Lern-Paradigma Schwarz-Weiß-Bilder von Gesichtern. Diese Bilder bestehen ausschließlich aus schwarzen und weißen Flächen und enthalten somit sehr wenige Informationen über ein Gesicht. Gerade aus dem Grund eignen sich die Schwarz-Weiß-Bilder sehr gut für unsere Untersuchung, weil wir auf Gedächtnisinhalte zurückgreifen müssen, um ein Gesicht in einem Schwarz-Weiß-Bild zu erkennen, (Dolan et al., 1997; Mooney, 1957). Wir nehmen an, dass genau aus diesen Gedächtnisinhalten in unserem Paradigma in einem Erwartungszeitfenster eine Vorhersage generiert wird. Unsere Annahme stützt sich darauf, dass nach Bubic (Bubic, 2010) das Erwarten (engl. *expectation*) ein Prozess ist, von dem man annehmen kann, dass das Gehirn eine Vorhersage generiert, wie es von der PCT beschrieben wird.

Das Erwartungszeitfenster konstruierten, wir indem wir die Studienteilnehmer instruierten, eine ihnen unbekannte Person (im Folgenden „Zielperson“ genannt) innerhalb eines definierten Zeitfensters zu erwarten. Dieses Erwartungszeitfenster beginnt mit einem Hinweisreiz, auf den nach einer kurzen Latenzzeit immer ein neues Beispielbild der Zielperson folgt. Das bedeutet, dass Probanden sich zu 100% darauf verlassen konnten, ein Beispielbild der Zielperson zu sehen. Die Bildpräsentation einer Zielperson bestand aus 48 einmaligen Bildern, von denen immer zwei Bilder zu einem Durchgang gepaart wurden (im Weiteren werden diese 48 Bilder einer Zielperson als Serie bezeichnet). In einem Durchgang entsprach das erste Bild immer einem neuen Beispielbild der Zielperson und das zweite einem Testbild. Im Testbild wurden wieder neue Bilder der Zielperson mit einer Wahrscheinlichkeit von 50% abgebildet und zu 50% eine andere Person. Über die Beispielbilder in der Serie hatten die Studienteilnehmer die Möglichkeit, die Zielperson zu erlernen, während die Studienteilnehmer mittels der Testbilder die gewonnenen Kenntnisse sozusagen „auf die Probe“ stellten.

Wir nehmen an: 1) Um die Aufgabe lösen zu können, müssen visuelle Eindrücke der Zielperson in einem inneren Modell (IM) kumuliert werden. 2) Das IM wird als eine Vorhersage verwendet, wenn die Zielperson in den Beispielbildern erwartet wird. 3) Das IM nimmt durch visuelles Lernen an Details zu. 4) Aus den ersten beiden Annahmen

schließen wir, dass die Zunahme des IM an Details mit der Zunahme der Präzision der Vorhersage in Verbindung gebracht werden kann.

Bei der Analyse des Antwortverhaltens von 41 Studienteilnehmern wurde ein positiver Lerneffekt durch die Steigerung der Erkennungsrate nachgewiesen. Unter Berücksichtigung der Effektgrößen der Erkennungsraten konnten wir bestimmen, dass der Unterschied in der Trefferquote statistisch zwischen dem ersten und dem dritten Abschnitt am größten war. Mit einem Maß aus der *Signal-Entdeckungstheorie* (SET) (Green, 1966; Macmillan and Creelman, 2005), dem Unterscheidbarkeitsmaß (d'), kann man ebenso den Lerneffekt beschreiben. Dieses Maß hat den Vorteil, dass dieses einem einen Rückschluss auf das innere Model über das zu unterscheidende „Signal“ erlaubt. Ein Signal wäre z. B., ein bestimmtes Gesicht unter vielen anderen wiederzuerkennen. Während eines Lernprozesses geht die SET davon aus, dass sich das Signal aus dem Rauschen heraushebt. Beschreibt man beides (Signal und Rauschen) jeweils als Häufigkeitsverteilung, so beschreibt das Unterscheidbarkeitsmaß, wie weit die Maxima der Verteilungen voneinander entfernt sind. Je weiter beide voneinander entfernt sind, umso besser wird das Signal entdeckt. In unserer Studie konnten wir zeigen, dass dieses Maß zum dritten Zeitabschnitt signifikant stieg. Die Trefferquote und das Unterscheidbarkeitsmaß sind Maße, die aus dem Antwortverhalten berechnet werden und die Wahrnehmung der Studienteilnehmer mittels der Zielperson im Teststimulus beschreibt. Beide Maße wiesen auf den weitesten Abstand im Kontrast ‚erster versus dritter Abschnitt‘ hin. Mittels dieses Kontrastes prüften wir für die Beispielbilder einen physiologischen Effekt.

Andere Lernstudien konnten bereits zeigen, dass eine Komponente von *Ereigniskorrelierten Feldern* (EKF) um die 250 Millisekunden im occipito-temporalen Bereich sensitiv auf vertraute Gesichter *(familiarity effect)* reagierte (Gosling and Eimer, 2011; Kaufmann et al., 2009; Saavedra et al., 2010; Tanaka and Pierce, 2009; Tanaka et al., 2006; Weibert and Andrews, 2015). In Antwort auf die Beispielbilder beobachteten wir einen Anstieg dieser Komponente. Auch wenn diese Studien hauptsächlich Fotografien von Gesichtern verwendet, nehmen wir entsprechend unserem Paradigma an, dass die M250-Komponente hier ebenso einen Lerneffekt bezüglich der Beispielbilder repräsentiert. Dieser Befund ist relativ wichtig, weil wir als Nächstes die Zeit vor und nach dem Beispielbild analysieren.

Sedley und Kollegen (Sedley et al., 2016) schlagen vor, dass die sogenannte Alphafrequenzband-Aktivität (7–13 Hz; ABA) die Präzision der Vorhersage signalisiert und die Betafrequenzband-Aktivität (14–35Hz, BBA) die Aktualisierung einer Vorhersage. Anhand der MEG-Daten der 41 Studienteilnehmer rekonstruierten wir zunächst beide Frequenzbänder im Quellenraum mit einer Auflösung von 1 cm im Erwartungszeitfenster. Über anschließende statistische Analysen konnten wir für beide Frequenzbänder unterschiedliche Hirnareale lokalisieren, die über die Serie ihr Verhalten änderten. Das Verhalten beider Frequenzbänder – in der ABA und der BBA – unterschied sich, doch nur für die ABA konnte eine signifikante Beziehung zum Unterscheidbarkeitsmaß beobachtet werden.

Das heißt, wir konnten zeigen, dass im Erwartungszeitfenster ein signifikanter Anstieg in der ABA zu beobachten war, wenn die Details in der Vorhersage zunahmen. Anhand einer zusätzlichen fMRT Studie konnten drei Quellen näher eingegrenzt werden, die im Erwartungszeitfenster von größerer Bedeutung zu sein scheinen. Dies waren der Precuneus, der occipito-temporale Bereich des *Gyrus fusiformis,* auch bekannt als das okzipitale Areal der Gesichtserkennung, kurz OFA (engl. für occipital face area), und der laterale occipitale Kortex (kurz LOC). Wir fassen diese (und zwei weitere) in einem Netzwerk zusammen, welches wir *Face-Identity-predictive* Netzwerk (FIP Network) nennen.

Als Nächstes interessierte uns, welches der Hirnareale in Beziehung mit der zuvor untersuchten EKP-Komponente steht. Tatsächlich konnten wir zeigen, dass die ABA im OFA in Beziehung zu einer etwas früheren Komponente steht, aber auch mit einer späteren, die als sensitiv für Assoziationen beschrieben wurde (Olivares et al., 2015; Schweinberger and Neumann, 2016). Mit Assoziation ist gemeint, dass im Lern- und Bestimmungsprozess Verknüpfungen zwischen verschiedenen Eigenschaften notwendig sind, wie zum Beispiel die Verbindung eines visuellen Eindrucks mit einem Namen oder einer Charaktereigenschaft.

Des Weiteren testeten wir, ob eine Änderung in der ABA auch im Post-Stimulus-Intervall zu beobachten ist, da laut der PCT die Vorhersage zum Minimieren des Vorhersagefehlers herangezogen wird. Auch hier beobachteten wir höhere ABA mit höherer Präzision des Modells, spezifischer eine geringere stimulus-induzierte Senkung der ABA für präzisere Modelle. Diese Post-Stimulus-ABA verzeichneten wir in frühen visuellen Bereichen

(V1/V2 und V3) und im Precuneus. Precuneus-Aktivität wurde schon oft mit Gedächtnisleistung, aber auch mit mentaler Vorstellungskraft assoziiert (Dolan et al., 1997; Fletcher et al., 1995). Diese Beobachtung unterstützt die Ansicht von Land (Land, 2014), dass der Precuneus die innere „Welt“ aus unserer Ich-Perspektive repräsentiert. Demnach schreiben wir dem Precuneus eine Schlüsselrolle für die Repräsentation des inneren Modells zu, und in dieser Funktion ist der Precuneus auch daran beteiligt, visuelle Vorhersagen zu generieren.

Wir nehmen an, dass sich in beiden untersuchten Zeitfenstern die Vorhersage auf dasselbe IM bezieht. Folglich gehen wir davon aus, dass die Änderung in der ABA einen Einfluss desselben IM repräsentiert. Diese Interpretation wird unterstützt durch die ähnliche und unterschiedliche Lokalisation von ABA-Effekten. Über diese Interpretation der unterschiedlichen Lokalisationen schlagen wir eine mögliche neurophysiologische Implementierung einer relativ neuen theoretischen Auseinandersetzung der PCT von Kwisthout und Kollegen (Kwisthout et al., 2017) vor. Diese Implementierung stützt sich auf die Beobachtung, dass in beiden Zeitfenstern die jeweils gefundenen Hirnareale auf zwei unterschiedlichen hierarchischen Ebenen liegen. Im Erwartungszeitfenster wird das IM durch Areale repräsentiert, die auf einer hierarchisch höheren Ebene liegen als die aus dem post-stimulus Zeitfenster. Kwisthout und Kollegen (Kwisthout et al., 2017) beschreiben die Lösung der PE-Minimierung durch eine Änderung des Detaillevels, wobei ein Detaillevel der Beschreibung einer Granularität entspricht und unabhängig von der Präzision der Vorhersage steht. Wir schlagen vor, dass dieses Detaillevel (Granularität) durch die hierarchische Anordnung der Hirnareale repräsentiert ist.

Zusammenfassend konnten wir für das visuelle System zeigen, was Sedley und Kollegen (Sedley et al., 2016) für das auditorische vorgeschlagen haben, d. h., dass die Präzision einer Vorhersage mit einer Erhöhung der ABA in Beziehung steht. Im Speziellen konnten wir zeigen, dass im Erwartungszeitfenster ein Netzwerk aktiviert wurde, welches sich aus verschiedenen Hirnarealen zusammensetzt, denen wir drei Funktionen zuordnen: die Vorhersage von fazialen Gesichtsmerkmalen (wie Auge, Nase, Mund; OFA), die Vorbereitung von Prozessen, die für die perzeptuelle Schließung notwendig sind (LOC, V2) und Die Voraktivierung von Gedächtnisprozessen (Precuneus, Parahippocampal Cortex).

6 References

Ahissar, M., and Hochstein, S. (2004). The reverse hierarchy theory of visual perceptual learning. Trends Cogn. Sci. *8*, 457–464.

Ahissar, M., Nahum, M., Nelken, I., and Hochstein, S. (2009). Reverse hierarchies and sensory learning. Philos. Trans. R. Soc. B Biol. Sci. *364*, 285–299.

Aminoff, E.M., Kveraga, K., and Bar, M. (2013). The role of the parahippocampal cortex in cognition. Trends Cogn. Sci. *17*, 379–390.

Apps, M.A.J., and Tsakiris, M. (2013). Predictive codes of familiarity and context during the perceptual learning of facial identities. Nat. Commun. *4*, 1–9.

Arnal, L.H., and Giraud, A.-L. (2012). Cortical oscillations and sensory predictions. Trends Cogn. Sci. *16*, 390–398.

Arnal, L.H., Wyart, V., and Giraud, A.-L. (2011). Transitions in neural oscillations reflect prediction errors generated in audiovisual speech. Nat. Neurosci. *14*, 797–801.

Aru, J., Rutiku, R., Wibral, M., Singer, W., and Melloni, L. (2016). Early effects of previous experience on conscious perception. Neurosci. Conscious. *1*, 1–10.

Atkinson, R.C. (1963). A variable sensitivity theory of signal detection. Psychol. Rev. *70*, 91–106.

Attal, Y., Bhattacharjee, M., Yelnik, J., Cottereau, B., Lefèvre, J., Okada, Y., Bardinet, E., Chupin, M., and Baillet, S. (2007). Modeling and detecting deep brain activity with MEG & EEG. In Engineering in Medicine and Biology Society, 2007. EMBS 2007. 29th Annual International Conference of the IEEE, (IEEE), pp. 4937–4940.

Ballard, D.H., Hinton, G.E., and Sejnowski, T.J. (1983). Parallel visual computation. Nature *306*, 21.

Bar, M. (2011). Predictions in the Brain: Using Our Past to Generate a Future (Oxford, New York: Oxford University Press).

Bastos, A.M., Usrey, W.M., Adams, R.A., Mangun, G.R., Fries, P., and Friston, K.J. (2012). Canonical microcircuits for predictive coding. Neuron *76*, 695–711.

Bastos, A.M., Litvak, V., Moran, R., Bosman, C.A., Fries, P., and Friston, K.J. (2015). A DCM study of spectral asymmetries in feedforward and feedback connections between visual areas V1 and V4 in the monkey. NeuroImage *108*, 460–475.

Bauer, M., Stenner, M.-P., Friston, K.J., and Dolan, R.J. (2014). Attentional modulation of alpha/beta and gamma oscillations reflect functionally distinct processes. J. Neurosci. *34*, 16117–16125.

Bertrand, J.-A., Tremblay, J., Lassonde, M., Vannasing, P., Khoa Nguyen, D., Robert, M., Bouthillier, A., and Lepore, F. (2013). Induced gamma-band response to fragmented images: An intracranial EEG study. Neuropsychologia *51*, 584–591.

Bi, T., Chen, J., Zhou, T., He, Y., and Fang, F. (2014). Function and Structure of Human Left Fusiform Cortex Are Closely Associated with Perceptual Learning of Faces. Curr. Biol. *24*, 222–227.

Boehm, S.G., and Paller, K.A. (2006). Do I know you? Insights into memory for faces from brain potentials. Clin. EEG Neurosci. *37*, 322–329.

Brodski, A., Paasch, G.-F., Helbling, S., and Wibral, M. (2015). The Faces of Predictive Coding. J. Neurosci. *35*, 8997–9006.

Brodski-Guerniero, A., Paasch, G.-F., Wollstadt, P., Özdemir, I., Lizier, J.T., and Wibral, M. (2017). Information-Theoretic Evidence for Predictive Coding in the Face-Processing System. J. Neurosci. *37*, 8273–8283.

Bubic (2010). Prediction, cognition and the brain. Front. Hum. Neurosci. *4*, 1–15.

Cao, L., Thut, G., and Gross, J. (2017). The role of brain oscillations in predicting self-generated sounds. NeuroImage *147*, 895–903.

Cavanagh (1991a). Representations of Vision: Trends and Tacit Assumptions in Vision Research (Cambridge, UK: Cambridge University Press).

Cavanagh, P. (1991b). What's up in top-down processing. Gorea Ed Represent. Vis. Trends Tacit Assumpt. Vis. Res. 295–304.

Cavanna, A.E., and Trimble, M.R. (2006). The precuneus: a review of its functional anatomy and behavioural correlates. Brain *129*, 564–583.

Chang, C.-C., and Lin, C.-J. (2011). LIBSVM: A library for support vector machines. ACM Trans. Intell. Syst. Technol. *2*, 1–27.

Clark, A. (2013). Whatever next? Predictive brains, situated agents, and the future of cognitive science. Behav. Brain Sci. *36*, 181–204.

Cohen, J. (1988). Statistical Power Analysis for the Behavioral Sciences (New York, NY: Taylor & Francis Inc).

Collins, D.L., Neelin, P., Peters, T.M., and Evans, A.C. (1994). Automatic 3D intersubject registration of MR volumetric data in standardized Talairach space. J. Comput. Assist. Tomogr. *18*, 192–205.

Coronel, J.C., and Federmeier, K.D. (2016). The N400 reveals how personal semantics is processed: Insights into the nature and organization of self-knowledge. Neuropsychologia *84*, 36–43.

Cowan, N. (2010). The Magical Mystery Four: How Is Working Memory Capacity Limited, and Why? Curr. Dir. Psychol. Sci. *19*, 51–57.

Dayan, P., Hinton, G.E., Neal, R.M., and Zemel, R.S. (1995). The Helmholtz Machine. Neural Comput. *7*, 889–904.

Diana, R.A., Yonelinas, A.P., and Ranganath, C. (2007). Imaging recollection and familiarity in the medial temporal lobe: a three-component model. Trends Cogn. Sci. *11*, 379–386.

Dietl, T., Trautner, P., Staedtgen, M., Vannuchi, M., Mecklinger, A., Grunwald, T., Clusmann, H., Elger, C.E., and Kurthen, M. (2005). Processing of famous faces and medial temporal lobe event-related potentials: a depth electrode study. NeuroImage *25*, 401–407.

Dolan, R.J., Fink, G.R., Rolls, E., Booth, M., Holmes, A., Frackowiak, R.S., and Friston, K.J. (1997). How the brain learns to see objects and faces in an impoverished context. Nature *389*, 596–599.

Dow, B.M., Snyder, A.Z., Vautin, R.G., and Bauer, R. (1981). Magnification factor and receptive field size in foveal striate cortex of the monkey. Exp. Brain Res. *44*, 213–228.

Durlak, J.A. (2009). How to Select, Calculate, and Interpret Effect Sizes. J. Pediatr. Psychol. *34*, 917–928.

Dürschmid, S., Edwards, E., Reichert, C., Dewar, C., Hinrichs, H., Heinze, H.-J., Kirsch, H.E., Dalal, S.S., Deouell, L.Y., and Knight, R.T. (2016). Hierarchy of prediction errors for auditory events in human temporal and frontal cortex. Proc. Natl. Acad. Sci. *113*, 6755–6760.

Eimer, M. (2000). Event-related brain potentials distinguish processing stages involved in face perception and recognition. Clin. Neurophysiol. *111*, 694–705.

Eklund, A., Nichols, T.E., and Knutsson, H. (2016). Cluster failure: Why fMRI inferences for spatial extent have inflated false-positive rates. Proc. Natl. Acad. Sci. *113*, 7900–7905.

Engel, A.K., and Fries, P. (2010). Beta-band oscillations—signalling the status quo? Curr. Opin. Neurobiol. *20*, 156–165.

Farah, M.J., Wilson, K.D., Drain, M., and Tanaka, J.N. (1998). What is “special” about face perception? Psychol. Rev. *105*, 482–498.

Feldman, H., and Friston, K.J. (2010). Attention, Uncertainty, and Free-Energy. Front. Hum. Neurosci. *4*, 1–23.

Felleman, D.J., Essen, V., and C, D. (1991). Distributed Hierarchical Processing in the Primate Cerebral Cortex. Cereb. Cortex *1*, 1–47.

Fletcher, P.C., Frith, C.D., Baker, S.C., Shallice, T., Frackowiak, R.S.J., and Dolan, R.J. (1995). The Mind's Eye—Precuneus Activation in Memory-Related Imagery. NeuroImage *2*, 195–200.

Fontolan, L., Morillon, B., Liegeois-Chauvel, C., and Giraud, A.-L. (2014). The contribution of frequency-specific activity to hierarchical information processing in the human auditory cortex. Nat. Commun. *5*, 1–10.

Friston, K. (2003). Learning and inference in the brain. Neural Netw. *16*, 1325–1352.

Friston, K. (2005). A theory of cortical responses. Philos. Trans. R. Soc. Lond. B Biol. Sci. *360*, 815–836.

Gauthier, I., and Tarr, M.J. (2002). Unraveling mechanisms for expert object recognition: bridging brain activity and behavior. J. Exp. Psychol. Hum. Percept. Perform. *28*, 431–446.

Georgieva, S.S., Todd, J.T., Peeters, R., and Orban, G.A. (2008). The Extraction of 3D Shape from Texture and Shading in the Human Brain. Cereb. Cortex *18*, 2416–2438.

Ghasemi, A., and Zahediasl, S. (2012). Normality Tests for Statistical Analysis: A Guide for Non-Statisticians. Int. J. Endocrinol. Metab. *10*, 486–489.

Golarai, G., Ghahremani, D.G., Whitfield-Gabrieli, S., Reiss, A., Eberhardt, J.L., Gabrieli, J.D.E., and Grill-Spector, K. (2007). Differential development of high-level visual cortex correlates with category-specific recognition memory. Nat. Neurosci. *10*, 512–522.

Goldman, R.I., Stern, J.M., Engel, J., and Cohen, M.S. (2002). Simultaneous EEG and fMRI of the alpha rhythm. Neuroreport *13*, 2487–2492.

Gonçalves, S.I., de Munck, J.C., Pouwels, P.J.W., Schoonhoven, R., Kuijer, J.P.A., Maurits, N.M., Hoogduin, J.M., Van Someren, E.J.W., Heethaar, R.M., and Lopes da Silva, F.H. (2006). Correlating the alpha rhythm to BOLD using simultaneous EEG/fMRI: Inter-subject variability. NeuroImage *30*, 203–213.

Gosling, A., and Eimer, M. (2011). An event-related brain potential study of explicit face recognition. Neuropsychologia *49*, 2736–2745.

Green, D.M.S., J.A. (1966). Signal Detection Theory and Psychophysics (John Wiley & Sons).

Gregory, R.L. (1997). Knowledge in perception and illusion. Philos. Trans. R. Soc. Lond. B Biol. Sci. *352*, 1121–1127.

Grill-Spector, K., Kourtzi, Z., and Kanwisher, N. (2001). The lateral occipital complex and its role in object recognition. Vision Res. *41*, 1409–1422.

Gross, J., Kujala, J., Hämäläinen, M., Timmermann, L., Schnitzler, A., and Salmelin, R. (2001). Dynamic imaging of coherent sources: studying neural interactions in the human brain. Proc. Natl. Acad. Sci. *98*, 694–699.

Grutzner, C., Uhlhaas, P.J., Genc, E., Kohler, A., Singer, W., and Wibral, M. (2010). Neuroelectromagnetic Correlates of Perceptual Closure Processes. J. Neurosci. *30*, 8342–8352.

Hall, E.L., Robson, S.E., Morris, P.G., and Brookes, M.J. (2014). The relationship between MEG and fMRI. NeuroImage *102*, 80–91.

Harrison, L.M., Duggins, A., and Friston, K.J. (2006). Encoding uncertainty in the hippocampus. Neural Netw. *19*, 535–546.

Harvey, B.M., and Dumoulin, S.O. (2011). The Relationship between Cortical Magnification Factor and Population Receptive Field Size in Human Visual Cortex: Constancies in Cortical Architecture. J. Neurosci. *31*, 13604–13612.

Heitz, R.P. (2014). The speed-accuracy tradeoff: history, physiology, methodology, and behavior. Front. Neurosci. *8*, 1–19.

Hochstein, S., and Ahissar, M. (2002). View from the top: hierarchies and reverse hierarchies in the visual system. Neuron *36*, 791–804.

Hohwy, J. (2013). The Predictive Mind (Oxford, New York: Oxford University Press).

Holm, S. (1979). A Simple Sequentially Rejective Multiple Test Procedure. Scand. J. Stat. *6*, 65–70.

Hubel, D.H., and Wiesel, T.N. (1962). Receptive fields, binocular interaction and functional architecture in the cat's visual cortex. J. Physiol. *160*, 106–154.

Jann, K., Dierks, T., Boesch, C., Kottlow, M., Strik, W., and Koenig, T. (2009). BOLD correlates of EEG alpha phase-locking and the fMRI default mode network. NeuroImage *45*, 903–916.

Jensen, O., and Mazaheri, A. (2010). Shaping Functional Architecture by Oscillatory Alpha Activity: Gating by Inhibition. Front. Hum. Neurosci. *4*, 1–8.

Joyce, C.A., and Kutas, M. (2005). Event-related potential correlates of long-term memory for briefly presented faces. J. Cogn. Neurosci. *17*, 757–767.

Kanai, R., Komura, Y., Shipp, S., and Friston, K. (2015). Cerebral hierarchies: predictive processing, precision and the pulvinar. Philos. Trans. R. Soc. B Biol. Sci. *370*, 1–13.

Kanwisher, N., and Yovel, G. (2006). The fusiform face area: a cortical region specialized for the perception of faces. Philos. Trans. R. Soc. B Biol. Sci. *361*, 2109–2128.

Kanwisher, N., McDermott, J., and Chun, M.M. (1997). The Fusiform Face Area: A Module in Human Extrastriate Cortex Specialized for Face Perception. J. Neurosci. 4302–4311.

Kaufmann, J.M., Schweinberger, S.R., and MikeBurton, A. (2009). N250 ERP correlates of the acquisition of face representations across different images. J. Cogn. Neurosci. *21*, 625–641.

van Kerkoerle, T., Self, M.W., Dagnino, B., Gariel-Mathis, M.-A., Poort, J., van der Togt, C., and Roelfsema, P.R. (2014). Alpha and gamma oscillations characterize feedback and feedforward processing in monkey visual cortex. Proc. Natl. Acad. Sci. *111*, 14332–14341.

Knight, J.L., and Kantowitz, B.H. (1974). Speed-accuracy tradeoff in double stimulation: Effects on the first response. Mem. Cognit. *2*, 522–532.

Knight, J.L., and Kantowitz, B.H. (1976). Speed-accuracy tradeoff in double stimulation: II. Effects on the second response. Mem. Cognit. *4*, 690–700.

Kok, P., Mostert, P., and de Lange, F.P. (2017). Prior expectations induce prestimulus sensory templates. Proc. Natl. Acad. Sci. *114*, 10473–10478.

Krause, B.J., Schmidt, D., Mottaghy, F.M., Taylor, J., Halsband, U., Herzog, H., Tellmann, L., and Müller-Gärtner, H.-W. (1999). Episodic retrieval activates the precuneus irrespective of the imagery content of word pair associates. Brain *122*, 255–263.

Kwisthout, J., and van Rooij, I. (2015). Free energy minimization and information gain: The devil is in the details. Cogn. Neurosci. *6*, 216–218.

Kwisthout, J., Bekkering, H., and van Rooij, I. (2017). To be precise, the details don't matter: On predictive processing, precision, and level of detail of predictions. Brain Cogn. *112*, 84–91.

Lambert, N.A., Swain, M.A., Miller, L.A., and Caine, D. (2006). Exploring the neural organization of person-related knowledge: lateralization of lesion, category specificity, and stimulus modality effects. Neuropsychology *20*, 346–354.

Land, M.F. (2014). Do we have an internal model of the outside world? Philos. Trans. R. Soc. B Biol. Sci. *369*, 1–6.

Laufs, H., Kleinschmidt, A., Beyerle, A., Eger, E., Salek-Haddadi, A., Preibisch, C., and Krakow, K. (2003). EEG-correlated fMRI of human alpha activity. NeuroImage *19*, 1463–1476.

Lee, T.S., and Mumford, D. (2003). Hierarchical Bayesian inference in the visual cortex. J. Opt. Soc. Am. A *20*, 1434.

Lee, T.S., Mumford, D., Romero, R., and Lamme, V.A.F. (1998). The role of the primary visual cortex in higher level vision. Vision Res. *38*, 2429–2454.

Leleu, A., Caharel, S., Carré, J., Montalan, B., Snoussi, M., Vom Hofe, A., Charvin, H., Lalonde, R., and Rebaï, M. (2010). Perceptual interactions between visual processing of facial familiarity and emotional expression: An event-related potentials study during task-switching. Neurosci. Lett. *482*, 106–111.

Leube, D.T., Erb, M., Grodd, W., Bartels, M., and Kircher, T.T. (2003). Successful episodic memory retrieval of newly learned faces activates a left fronto-parietal network. Cogn. Brain Res. *18*, 97–101.

Leveroni, C.L., Seidenberg, M., Mayer, A.R., Mead, L.A., Binder, J.R., and Rao, S.M. (2000). Neural Systems Underlying the Recognition of Familiar and Newly Learned Faces. J. Neurosci. *20(2)*, 878–886.

Levine, T.R., and Hullett, C.R. (2002). Eta squared, partial eta squared, and misreporting of effect size in communication research. Hum. Commun. Res. *28*, 612–625.

Lewis, A.G., Wang, L., and Bastiaansen, M. (2015). Fast oscillatory dynamics during language comprehension: Unification versus maintenance and prediction? Brain Lang. *148*, 51–63.

Liu, Z., de Zwart, J.A., Yao, B., van Gelderen, P., Kuo, L.-W., and Duyn, J.H. (2012). Finding thalamic BOLD correlates to posterior alpha EEG. NeuroImage *63*, 1060–1069.

Lizier, J.T., Prokopenko, M., and Zomaya, A.Y. (2012). Local measures of information storage in complex distributed computation. Inf. Sci. *208*, 39–54.

Lobmaier, J.S., Klaver, P., Loenneker, T., Martin, E., and Mast, F.W. (2008). Featural and con¢gural face processing strategies: evidence from a functional magnetic resonance imaging study. Brain Imaging *19*, 287–291.

Logothetis, N.K. (2002). The neural basis of the blood-oxygen-level-dependent functional magnetic resonance imaging signal. Philos. Trans. R. Soc. B Biol. Sci. *357*, 1003–1037.

Logothetis, N.K., Pauls, J., Augath, M., Trinath, T., and Oeltermann, A. (2001). Neurophysiological investigation of the basis of the fMRI signal. Nature *412*, 150-157.

Ludmer, R., Dudai, Y., and Rubin, N. (2011). Uncovering Camouflage: Amygdala Activation Predicts Long-Term Memory of Induced Perceptual Insight. Neuron *69*, 1002–1014.

Lupyan, G. (2015). Cognitive penetrability of perception in the age of prediction: Predictive systems are penetrable systems. Rev. Philos. Psychol. *6*, 547–569.

Macmillan, N.A., and Creelman, C.D. (2005). Detection theory: a user's guide (Mahwah, N.J: Lawrence Erlbaum Associates).

Maris, E., and Oostenveld, R. (2007). Nonparametric statistical testing of EEG- and MEG-data. J. Neurosci. Methods *164*, 177–190.

Marr, D. (1982). Vision: A Computational Investigation into the Human Representation and Processing of Visual Information by Marr, David (2010) Taschenbuch (W.H. Freeman, New York).

Martinez, A., Moses, P., Frank, L., Buxton, R., Wong, E., and Stiles, J. (1997). Hemispheric asymmetries in global and local processing: evidence from fMRI. Neuroreport *8*, 1685–1689.

Mattout, J., Henson, R.N., and Friston, K.J. (2007). Canonical Source Reconstruction for MEG. Comput. Intell. Neurosci. *2007*, 1–10.

Maunsell, J.H., and Essen, D. van (1983). The connections of the middle temporal visual area (MT) and their relationship to a cortical hierarchy in the macaque monkey. J. Neurosci. *3*, 2563–2586.

Mayer, A., Schwiedrzik, C.M., Wibral, M., Singer, W., and Melloni, L. (2016). Expecting to See a Letter: Alpha Oscillations as Carriers of Top-Down Sensory Predictions. Cereb. Cortex *26*, 3146–3160.

Mayhew, S.D., Ostwald, D., Porcaro, C., and Bagshaw, A.P. (2013). Spontaneous EEG alpha oscillation interacts with positive and negative BOLD responses in the visual–auditory cortices and default-mode network. NeuroImage *76*, 362–372.

Michalareas, G., Vezoli, J., van Pelt, S., Schoffelen, J.-M., Kennedy, H., and Fries, P. (2016). Alpha-Beta and Gamma Rhythms Subserve Feedback and Feedforward Influences among Human Visual Cortical Areas. Neuron *89*, 384–397.

Mizumori, S.J.Y. (2013). Context Prediction Analysis and Episodic Memory. Front. Behav. Neurosci. *7*, 1–10.

Mooney, C.M. (1957). Age in the development of closure ability in children. Can. J. Psychol. *11*, 219–226.

Moore, C., and Cavanagh, P. (1998). Recovery of 3D volume from 2-tone images of novel objects. Cognition *67*, 45–71.

Moore, C., and Engel, S.A. (2001). Neural Response to Perception of Volume in the Lateral Occipital Complex. Neuron *29*, 277–286.

Nakagawa, S., and Cuthill, I.C. (2007). Effect size, confidence interval and statistical significance: a practical guide for biologists. Biol. Rev. *82*, 591–605.

Nasr, S., Polimeni, J.R., and Tootell, R.B.H. (2016). Interdigitated Color- and Disparity-Selective Columns within Human Visual Cortical Areas V2 and V3. J. Neurosci. *36*, 1841–1857.

Natu, V.S., and O'Toole, A.J. (2015). Spatiotemporal changes in neural response patterns to faces varying in visual familiarity. NeuroImage *108*, 151–159.

Niessing, J., Ebisch, B., Schmidt, K.E., Niessing, M., Singer, W., and Galuske, R.A. (2005). Hemodynamic signals correlate tightly with synchronized gamma oscillations. Science *309*, 948–951.

Nolte, G. (2003). The magnetic lead field theorem in the quasi-static approximation and its use for magnetoencephalography forward calculation in realistic volume conductors. Phys. Med. Biol. *48*, 3637–3652.

Nowotny, T. (2014). Two Challenges of Correct Validation in Pattern Recognition. Front. Robot. AI *1*, 1–5.

Nunez, P.L., and Srinivasan, R. (2006). A theoretical basis for standing and traveling brain waves measured with human EEG with implications for an integrated consciousness. Clin. Neurophysiol. *117*, 2424–2435.

Olivares, E.I., Iglesias, J., Saavedra, C., Trujillo-Barreto, N.J., and Valdés-Sosa, M. (2015). Brain Signals of Face Processing as Revealed by Event-Related Potentials. Behav. Neurol. *2015*, 1–16.

Oostenveld, R., Fries, P., Maris, E., and Schoffelen, J.-M. (2011). FieldTrip: Open Source Software for Advanced Analysis of MEG, EEG, and Invasive Electrophysiological Data. Comput. Intell. Neurosci. *2011*, 1–9.

van Pelt, S., Heil, L., Kwisthout, J., Ondobaka, S., van Rooij, I., and Bekkering, H. (2016). Beta- and gamma-band activity reflect predictive coding in the processing of causal events. Soc. Cogn. Affect. Neurosci. *11*, 973–980.

Percival, D.B., and Walden, A.T. (1993). Spectral Analysis for Physical Applications (Cambridge: Cambridge University Press).

Pierce, L.J., Scott, L.S., Boddington, S., Droucker, D., Curran, T., and Tanaka, J.W. (2011). The N250 Brain Potential to Personally Familiar and Newly Learned Faces and Objects. Front. Hum. Neurosci. *5*, 1–13.

Pinto, Y., Sligte, I.G., Shapiro, K.L., and Lamme, V.A.F. (2013). Fragile visual short-term memory is an object-based and location-specific store. Psychon. Bull. Rev. *20*, 732–739.

Pinto, Y., van Gaal, S., de Lange, F.P., Lamme, V.A.F., and Seth, A.K. (2015). Expectations accelerate entry of visual stimuli into awareness. J. Vis. *15*, 1–13.

Pitcher, D., Walsh, V., and Duchaine, B. (2011). The role of the occipital face area in the cortical face perception network. Exp. Brain Res. *209*, 481–493.

Rao, R.P., and Ballard, D.H. (1997). Dynamic model of visual recognition predicts neural response properties in the visual cortex. Neural Comput. *9*, 721–763.

Rao, R.P., and Ballard, D.H. (1999). Predictive coding in the visual cortex: a functional interpretation of some extra-classical receptive-field effects. Nat. Neurosci. *2*, 79–87.

Raslau, F.D., Mark, I.T., Klein, A.P., Ulmer, J.L., Mathews, V., and Mark, L.P. (2015). Memory Part 2: The Role of the Medial Temporal Lobe. Am. J. Neuroradiol. *36*, 846–849.

Saavedra, C., Iglesias, J., and Olivares, E.I. (2010). Event-related potentials elicited by the explicit and implicit processing of familiarity in faces. Clin. EEG Neurosci. *41*, 24–31.

Sagiv, N., and Bentin, S. (2001). Structural encoding of human and schematic faces: holistic and part-based processes. J. Cogn. Neurosci. *13*, 937–951.

Scheeringa, R., Fries, P., Petersson, K.-M., Oostenveld, R., Grothe, I., Norris, D.G., Hagoort, P., and Bastiaansen, M.C.M. (2011). Neuronal Dynamics Underlying High- and Low-Frequency EEG Oscillations Contribute Independently to the Human BOLD Signal. Neuron *69*, 572–583.

Scheeringa, R., Koopmans, P.J., van Mourik, T., Jensen, O., and Norris, D.G. (2016). The relationship between oscillatory EEG activity and the laminar-specific BOLD signal. Proc. Natl. Acad. Sci. *113*, 6761–6766.

Schreiber, T. (2000). Measuring Information Transfer. Phys. Rev. Lett. *85*, 461–464.

Schultz, W., and Dickinson, A. (2000). Neuronal coding of prediction errors. Annu. Rev. Neurosci. *23*, 473–500.

Schulz, C., Kaufmann, J.M., Walther, L., and Schweinberger, S.R. (2012). Effects of anticaricaturing vs. caricaturing and their neural correlates elucidate a role of shape for face learning. Neuropsychologia *50*, 2426–2434.

Schweinberger, S.R., and Neumann, M.F. (2016). Repetition effects in human ERPs to faces. Cortex *80*, 141–153.

Sedley, W., Gander, P.E., Kumar, S., Kovach, C.K., Oya, H., Kawasaki, H., Howard, M.A., and Griffiths, T.D. (2016). Neural signatures of perceptual inference. ELife *5*, 1–13.

Skrandies, W. (1990). Global field power and topographic similarity. Brain Topogr. *3*, 137–141.

Sligte, I.G., Scholte, H.S., and Lamme, V.A.F. (2008). Are There Multiple Visual Short-Term Memory Stores? PLOS ONE *3*, 1–8.

Spaak, E., Fonken, Y., Jensen, O., and de Lange, F.P. (2016). The Neural Mechanisms of Prediction in Visual Search. Cereb. Cortex *26*, 4327–4336.

Spratling, M.W. (2008). Reconciling predictive coding and biased competition models of cortical function. Front. Comput. Neurosci. *2*, 1–8.

Tacikowski, P., Jednoróg, K., Marchewka, A., and Nowicka, A. (2011). How multiple repetitions influence the processing of self-, famous and unknown names and faces: An ERP study. Int. J. Psychophysiol. *79*, 219–230.

Tanaka, J.W., and Farah, M.J. (1993). Parts and Wholes in Face Recognition. Q. J. Exp. Psychol. Sect. A *46*, 225–245.

Tanaka, J.W., and Pierce, L.J. (2009). The neural plasticity of other-race face recognition. Cogn. Affect. Behav. Neurosci. *9*, 122–131.

Tanaka, J.W., Curran, T., Porterfield, A.L., and Collins, D. (2006). Activation of preexisting and acquired face representations: the N250 event-related potential as an index of face familiarity. J. Cogn. Neurosci. *18*, 1488–1497.

Thut, G., Miniussi, C., and Gross, J. (2012). The Functional Importance of Rhythmic Activity in the Brain. Curr. Biol. *22*, 658–663.

Tomasi, D., and Volkow, N.D. (2010). Functional connectivity density mapping. Proc. Natl. Acad. Sci. *107*, 9885–9890.

Trenner, M.U., Schweinberger, S.R., Jentzsch, I., and Sommer, W. (2004). Face repetition effects in direct and indirect tasks: an event-related brain potentials study. Cogn. Brain Res. *21*, 388–400.

Utevsky, A.V., Smith, D.V., and Huettel, S.A. (2014). Precuneus Is a Functional Core of the Default-Mode Network. J. Neurosci. *34*, 932–940.

Vicente, R., Wibral, M., Lindner, M., and Pipa, G. (2011). Transfer entropy—a model-free measure of effective connectivity for the neurosciences. J. Comput. Neurosci. *30*, 45–67.

Von Helmholtz, H. (1867). Handbuch der physiologischen Optik (Voss).

Wang, X.-J. (2010). Neurophysiological and Computational Principles of Cortical Rhythms in Cognition. Physiol. Rev. *90*, 1195–1268.

Weibert, K., and Andrews, T.J. (2015). Activity in the right fusiform face area predicts the behavioural advantage for the perception of familiar faces. Neuropsychologia *75*, 588–596.

Weisz, N., Hartmann, T., Müller, N., and Obleser, J. (2011). Alpha Rhythms in Audition: Cognitive and Clinical Perspectives. Front. Psychol. *2*, 1–14.

Wibral, M., Lizier, J.T., Vögler, S., Priesemann, V., and Galuske, R. (2014). Local active information storage as a tool to understand distributed neural information processing. Front. Neuroinformatics *8*, 1–11.

Wiese, H., and Schweinberger, S.R. (2015). Getting connected: Both associative and semantic links structure semantic memory for newly learned persons. Q. J. Exp. Psychol. *68*, 2131–2148.

Winterer, G., Carver, F.W., Musso, F., Mattay, V., Weinberger, D.R., and Coppola, R. (2007). Complex relationship between BOLD signal and synchronization/desynchronization of human brain MEG oscillations. Hum. Brain Mapp. *28*, 805–816.

Yonelinas, A.P. (1994). Receiver-operating characteristics in recognition memory: evidence for a dual-process model. J. Exp. Psychol. Learn. Mem. Cogn. *20*, 1341–1354.

Yonelinas, A.P., Aly, M., Wang, W.-C., and Koen, J.D. (2010). Recollection and familiarity: Examining controversial assumptions and new directions. Hippocampus *20*, 1178–1194.

Zimmermann, F.G.S., and Eimer, M. (2013). Face learning and the emergence of view-independent face recognition: An event-related brain potential study. Neuropsychologia *51*, 1320–1329.

Zumer, J.M., Brookes, M.J., Stevenson, C.M., Francis, S.T., and Morris, P.G. (2010). Relating BOLD fMRI and neural oscillations through convolution and optimal linear weighting. NeuroImage *49*, 1479–1489.

Onozuka, M., and Yen, C.-T. (2008). Novel trends in brain science: brain imaging, learning and memory, stress and fear, and pain (Tokyo; New York: Springer).

7 Supplementary Information

Pathways related to the MEG data

Path of the RAW DATA [***_MooneyIDs_YYYYMMDD_0#.ds]
//data/MEGArchive/data/meg/CTF_Data/pool/…

Path of the trl data [*.mat]

//[...]/NewMooney/BrainDataMooneyIDs/MEG/DataRaw/PredDynAnalysis/LvL1-4/qCleaned2017JAN/

Path of data used for sensor level analysis

//[...]/NewMooney/BrainDataMooneyIDs/MEG/ERFAnalysis/20170203_ValidSet/SampleStimulus/
//[...]/NewMooney/BrainDataMooneyIDs/MEG/TimeFreqAnalysis/20170203_ValidSet/…
…SampleStimulus/

//[...]/NewMooney/BrainDataMooneyIDs/MEG/SpectraAnalysis/20170203_ValidSet/SampleStimulus/

Path of data used for source level analysis

//[...]/NewMooney/BrainDataMooneyIDs/MEG/SourceLocalization/Headmodels
//[...]/NewMooney/BrainDataMooneyIDs/MEG/SourceLocalization/Beamf_PrePro_PredDyn/…
…BI-0.400_-0.090s/7-13Hz
//[...]/NewMooney/BrainDataMooneyIDs/MEG/SourceLocalization/Beamf_PrePro_PredDyn/…
…BI-0.400_-0.090s/14-19Hz

Pathways related to the MRI data

functional data

//[...]/NewMooney/BrainDataMooneyIDs/MRI/ALH20/xrawdat/dcmfiles

anatomical T1 data

//[...]/NewMooney/BrainDataMooneyIDs/MRI/ALH20/anatomy/dcmfiles

fieldmap data set

//[...]/NewMooney/BrainDataMooneyIDs/MRI/ALH20/fieldmaps

behavior log-files

//[...]/NewMooney/BrainDataMooneyIDs/MRI/ALH20/behav.LOG

Recording Management

No.	Identifier	Recording date		Valid blocks of rec		Match response		Within final analysis	
		MEG	MRI	MEG	MRI	MEG	fMRI	MEG	fMRI
1	'AHH02'	24.06.2014		[2,3,4,5,6]		left	n.a.	n.a.	n.a.
2	'ALH20'	31.07.2014	20.01.2016	[2,3,4,5,6]	anat	right	right	X	+bh
3	'AME02'	31.10.2016	18.10.2016	[2,3,4,5,6]	anat	left	right	X	+bh
4	'AMN27'	03.09.2014	14.07.2015	[2,3,4,5,6]	anat	left	n.a.	n.a.	n.a.
5	'ATE26'	30.06.2014	25.06.2015	[2,3,4,5,6]	anat	left	n.a.	X	n.a.
6	'BLD19'		14.07.2015		anat	n.a.	right	n.a.	n.a.
7	BMA05'	12.01.2016	13.01.2016	[2,3,4,5,6]	[4,7,10]	right	right	X	X
8	'BME09'	08.08.2014	22.01.2016	[1,2,3,4,5]	[4,8,11]	left	left	X	X
9	'CFS02'	02.09.2015	01.07.2015	[3,4,5,6,7]	[5,8,11]	right	right	X	X
10	'CLA25'	12.09.2016	22.09.2016	[2,3,4,5,6]	[4,7,10]	left	right	X	X
11	'DWA02'	20161107	18.11.2016	[1,2,3,4,5]	[4,7,10]	right	right	X	X
12	'ECM29'	28.10.2016	05.10.2016	[2,3,4,5,6]	[6,9,12]	right	left	X	X
13	ECN16'	08.11.2016	18.102016	[2,3,4,5,6]	[5,9,12]	right	right	X	X
14	'EHE16'	08.09.2015	02.07.2015	[2,3,4,5,6]	anat	right	right	X	n.a.
15	'EST28'	17.09.2015	17.07.2015	[2,3,4,5,6]	[4,7,11]	left	left	X	X
16	'ETO07'	16.09.2015	16.07.2015	[2,3,4,5,6]	[5,8,13]	left	left	X	X
17	'GMK03'		14.07.2015		[7,10,13]	n.a.	right	n.a.	X
18	'GSK21'	11.09.2014	16.03.2016	[2,3,4,5,6]	anat	left	left	X	+bh
19	'GSS25'	23.06.2014	18.06.2015	[4,5,6,7,8]	anat	right	left	X	n.a.
20	'HEA16'	23.09.2016	05.10.2016	[2,3,4,5,6]	[4,7,12]	right	right	X	X
21	'EKR22'	12.09.2015		[2,3,4,5,6]		right	n.a.	X	-
22	'HKE09'	21.09.2015	18.08.2015	[2,3,4,5,6]	[4,9,12]	right	left	X	X
23	'HRS06'	09.03.2016	02.03.2016	[2,3,4,5,6]	[4,7,10]	left	right	X	X
24	'HSL12'	30.11.2016	24.11.2016	[2,3,4,5,6]	[5,8,11]	left	left	X	X
25	'JHA13'	04.09.2014	20.01.2016	[2,3,4,5,6]	[5,8,11]	right	left	X	X
26	'JSO14'	01.07.2014	25.02.2016	[2,3,4,5,6]	[6,9,12]	right	left	X	X
27	'KRA30'	07.07.2014	19.02.2016	[2,3,4,5,6]	[4,7,10]	right	left	X	X
28	'LBA18'	08.07.2014	27.01.2016	[2,3,4,5,6]	[4,7,10]	left	right	X	X
29	'MAE14'	10.09.2015	15.07.2015	[2,3,4,5,6]	[4,7,10]	left	left	X	X
31	'MPT30'	28.08.2015	17.08.2015	[2,3,4,5,6]	[5,8,11]	right	left	X	X
32	'MRL02'	01.09.2015	04.09.2015	[2,3,4,5,6]	[4,7,10]	right	right	X	X
33	'MTA15'	04.11.2016	16.11.2016	[1,2,3,4,5]	[4,7,10]	left	left	X	X
34	'MWG16'	26.08.2015	15.07.2015	[3,4,5,6,7]	[4,7,10]	right	left	X	X
35	'NAO14'	19.08.2014		[3,4,5,6,7]		left	n.a.	n.a.	n.a.
36	'NAS28'	22.07.2014		[2,3,4,5,6]		right	n.a.	n.a.	n.a.
37	'OKM06'	22.09.2016	12.10.2016	[2,3,5,6,7]	[4,7,10]	right	left	X	X
38	'OZL24'	14.08.2014	08.09.2015	[2,3,4,5,7]	anat	left	right	X	-
39	'PER09'	05.02.2016	17.07.2015	[2,3,4,5,6]	[4,7,11]	right	right	X	X
40	'PWA23'	01.11.2016	18.11.2016	[2,3,4,5,6]	[4,7,10]	left	left	X	+bh
41	'RNA06'	26.09.2016	05.10.2016	[2,3,4,5,6]	[5,9,12]	left	right	X	X
42	'RSA06'	03.09.2015	06.07.2015	[3,4,5,6,7]	[4,7,10]	right	right	X	X
43	'RSE18'	08.09.2015	01.07.2015	[2,3,4,5,6]	[4,7,11]	left	right	X	X
44	'RWA14'	21.07.2014		[2,3,4,5,6]		left	n.a.	n.a.	n.a.
45	'SKO14'	01.09.2014	11.09.2015	[2,3,4,5,6]	[4,8,11]	right	right	X	n.a.
46	'SON11'	18.08.2014	21.01.2016	[2,3,4,5,6]	[5,8,11]	right	right	X	X
47	'SRA25'	28.08.2014		[2,3,4,5,6]		left	n.a.	n.a.	n.a.
48	'SWL11'	10.09.2014		[2,3,4,5,6]		right	n.a.	n.a.	n.a.
49	'UBS14'	11.08.2014		[2,3,4,5,7]		right	n.a.	n.a.	n.a.
50	'UFA27'	15.02.2016	18.02.2016	[2,3,4,5,6]	[5,8,12]	left	right	n.a.	X
51	'UNN30'	02.03.2016	18.03.2016	[2,3,4,5,6]	[4,7,10]	right	left	X	X
52	'UWA18'	15.09.2015	16.09.2015	[2,3,4,5,6]	[4,7,10]	left	left	X	n.a.
53	'VTA21'	09.09.2014		[2,3,4,5,6]		left	n.a.	n.a.	n.a.
54	'XCN02'	26.08.2014	18.09.2015	[2,3,4,5,6]	anat	right	left	X	n.a.

8 Ehrenwörtliche Erklärung

Ich erkläre hiermit ehrenwörtlich, dass ich die vorliegende Arbeit entsprechend den Regeln guter wissenschaftlicher Praxis selbstständig und ohne unzulässige Hilfe Dritter angefertigt habe.

Sämtliche aus fremden Quellen direkt oder indirekt übernommenen Gedanken sowie sämtliche von Anderen direkt oder indirekt übernommenen Daten, Techniken und Materialien sind als solche kenntlich gemacht.

Die Arbeit wurde bisher bei keiner anderen Hochschule zu Prüfungszwecken eingereicht.

Ort, Datum _____

Unterschrift _____

9 Curriculum Vitae

Academic education with degree

10/2005 - 09/2012	Biology studies, Darmstadt University of Technology; majors in: cell and developmental biology, neurobiology, animal ecology; animal physiology

Scientific degree

09/2012	Dipl.-Biol. (Diploma in Biology) Title of the Thesis "*The use of implicit prior knowledge in perceptual closure*"; supervised by Prof. M. Wibral from the Brain Imaging Centre, J.W. Goethe University Frankfurt: and Prof. R. Galuske and Prof. B. Laube from the Technical University of Darmstadt.

Professional education

Since 01/2014	PhD Student at the Technical University of Darmstadt, Supervised by Prof. R. Galuske and Prof. M. Wibral from the J. W. Goethe University Frankfurt Working title: *'Predictive coding investigated by violations of visual priors in perceptual closure'*.
02/2016 – 12/2016	Resarch assistant at the MPI for empirical Aesthetics at the Working group of David Poepl, in a research project by Dr. A. Tavano.
11/2012 – 12/2013	Research assistant at the MEG Unit of the Brain Imaging Center, J.W. Goethe University Frankfurt
01/2011 – 03/2011	Research internship: MEG-Unit at Brain Imaging Centre, J. W. Goethe University Frankfurt; Supervisor: Prof. M. Wibral;
09/2010 – 12/2010	Research internship: Max Planck Institute for Brain Research (MPIH), Department of Neurophysiology (Dr. L. Melloni and Prof. R Singer); Supervisor: Dr. C. Schwiedrzik;
06/2003 – 01/2004	Certificate in paramedic (Rettungssanitäter), State-accepted vocational school for paramedic, ASB Hamburg (Staatlich anerkannte Berufsfachschule für Rettungsassistenten, ASB Hamburg)

Scholarship

2014/2016 PhD Scholarship by the Federal Ministry of Education and Research (*Bundesministerium für Bildung und Forschung, BMBF*) via the foundation Evangelisches. Studienwerk Villigst

2012/2013 Study sponsorship of the foundation: *Schönbecksche Stiftung*

Publications

Paasch, G.-F.*; Brodski, A.*; Helbling, S.; Wibral, M. "The faces of predictive coding" J.Neurosci. 2015 Jun 17;35(24):8997-9006;
DOI 10.1523/JNEUROSCI.1529-14.2015

Brodski-Guerniero, A., Paasch, G. F., Wollstadt, P., Oezdemir, I., Lizier, J. T., & Wibral, M. „Information-theoretical evidence for predictive coding in the face-processing system". J.Neurosci. 2017 Aug 23;37(34):8273-8283.
DOI: 10.1523/JNEUROSCI.0614-17.2017.

IN PREP: Paasch, G.-F.; Brodski, A.; Eisenhauer, S.; Wibral, M. "Investigating the *Predictive Code* of Predictive Coding Theory via Face Identity Expectation in a Learning Task". 2018.

Teaching

05/2015 Lecture: ‚*Bildgebung in den nicht-invasiven Neurowissenschaften'* at the University of Arts and Media (Berlin) during the Workshop *BILD-GEBUNG, Technologien, Epistemologie und Ästhetik wissenschaftlicher Bilder*

2014–2015 Supervised Master theses: '*Internal models of face identity in predictive coding'* by Susanne Eisenhauer

03/2014 Supervised Master Course of the Master Program 'Technical Biology' at the Technical University of Darmstadt: Module 'Neurobiology': *Introduction in MRI, MEEG and Psychophysics"*

12/2012 Supervised Master Course of the Master program 'Interdisciplinary Neuroscience' at the Goethe University Frankfurt am Main: *Studying human cognition with Magnetoencephalography*

Talks and Presentations

2016/11 Talk at Neuro-Conference Villigst in Heidelberg for undergraduate and graduate Students: *"Who is Up" investigating Predictive Coding by Identity anticipation.*

2016/9 Poster presentation at 'MEG Symposium 2016 Tübingen', Title: *"Who is Up" investigating Predictive Coding by Identity anticipation.*

2015/6 Poster presentation at 'Psychologie und Gehirn 2015 Frankfurt', Title: *Internal Models of face Identities in Predictive Coding,* rewarded with one of seven equal poster prizes

2014/6 Poster presentation at 'The Rhine-Main Neuroscience Network Biennial Meeting' Title: *Neural correlates of prediction errors in visual perception,* rewarded with the second poster prize.

2013/5 Poster presentation at the 10th Göttingen Meeting of the German Neuroscience Society; Title: *Neural Correlates Underlying the Use of Prior Information in Perceptual Closure*

2012/4 Talk at the Cognitive Neuroscience Lab a research group at the 'Centre for Behavioral Brain Science' Magdeburg: *Neuroelectromagnetic correlates of violated priors in perceptual closure processes*

Languages

German: native speaker

English: fluent in speaking and writing

Voluntary Activities

Member of the Preselection Commitee for Student Schoolarships (2014 and 2015)

Member of ORGA Team to realize a 4 days conference for 80 Phd-Studentes (Nov.2014)

Student representative of the vocational committee (Berufungskomitee)

Member of the student council (Fachschaft)

Trainer in university sports program Silat (Indonesian Martial art) (2010-2016)